Dear Prof. Dr. Jack Middelburg,

please find enclosed our revised manuscript with the revised title "**Do degree and rate of silicate weathering depend on plant productivity?**" (bg-2020-69) by Oeser and von Blanckenburg.

We would like to thank you and the reviewers for the lively and interactive discussion in *Biogeosciences*, allowing us to design a better structured and much more accessible manuscript.

From the reviews, we identified several priority revision items (see also our final response submitted on May 28th) that we addressed in this revised version of the manuscript. These are:

(1) The text was strongly revised for clarity and logic.

(2) We addressed the misunderstandings arising from possibly contrasting, but not contradictory viewpoints emerging from different scientific disciplines. A new section called "2 *Conceptual perspectives*" describing the different models of soil development and weathering was added. In this section, we focus on the continuous evolution model and the steady state model of soil development and weathering, and put emphasis on the relevant timescales over which the different metrics integrate.

(3) We were convinced by the reviewers' concerns regarding the over-interpretation of our data on plant stoichiometry. This section has been removed from the manuscript without loss for the conclusions of the manuscript.

(4) We strongly clarified that we never suggested that plants do not contribute to silicate weathering.

(5) We tested the main question, whether plants accelerate weathering more so than other drivers, by a statistical analysis. We first performed an ANOVA to statistically test for significant differences in expressions of weathering (i.e. degree and rate of weathering) between the sites. We then determined Pearsons's correlation coefficients between denudation rate D, mean annual precipitation MAP, and net primary productivity NPP, respectively, on the one hand, and the metrics quantifying weathering on the other hand, to single out the possible biogenic weathering driver from confounding effects. This statistical

analysis was further complemented by an assessment of possible confounding effects of differences in bedrock mineralogy on weathering.

(6) The section dealing with the impact of plants on weathering has been revised. We amended the analysis presented in the previous version by a concept in which plants actively discriminate for or against silicon, hence setting the solubility limits of silicates – the main constituents in regolith on granitoid substrate.

(7) Figures were checked for readability for color-blind readers using the software Color Oracle (http://colororacle.org). The color schemes were changed in a way that they are now readable in grayscale and by readers affected by Deuteranopia.

(8) Appendix B was added. Here we provide information on sample replication and the applied statistical methods. The Tables A1 – A3 show these statistical evaluations.

(9) We toned down our main conclusion – essentially asking whether plant activity might dampen and not necessarily accelerate silicate weathering, depending on overall setting.

(10) To reflect this change in thrust we have changed the title from "**Decoupling silicate weathering from primary productivity – how ecosystems regulate nutrient uptake along a climate and vegetation gradient"** to "**Do degree and rate of silicate weathering depend on plant productivity?"**

We do note that we here do not response point by point to the reviewers' comments which we have already done in our author responses (AC1: May 05; AC2: May 08; AC3: May 17; and AC4: May 19). Instead we summarize the changes in the manuscript below:

Revision notes

L90 – 95: We explicitly address the challenge in disentangling biotic from abiotic weathering drivers caused by confounding effects in a dedicated paragraph.

L185 – 395: We added a section "*2 Conceptual perspectives*" describing the fundamental different concepts that describe the relationship between regolith formation and time. In this section we compare the continuous evolution model with the steady-state model and highlight the different timescales over which the various metrics integrate. The subsequent sections' numbering has been changed accordingly.

L516 – 521: A paragraph was added to point out that our study sites do indeed cross of several pedogenic thresholds along the north-south transect.

L551 – 561: Additional description of *vegetation sampling* has been added.

L678: Text was added to clarify the use of one 10^{12} Ω resistor instead of a 10^{11} Ω resistor to detect the intensities of the ion beams measuring to ^{82}Kr. However, whether a 10^{11} Ω or a 10^{12} Ω resistor is used has no effect on the $^{87}Sr/^{86}Sr$ isotope composition

L682: We added text to describe how the correction for a session offset were performed.

L690: Text was added to refer to Appendix B (statistical analysis)

L713 – 720: We emphasized that whether a mineral nutrient is beneficial or essential to plants is, to a certain extent, species-dependent.

L758 – 761: We added a paragraph describing the range in soil weathering rates W along the north-south transect. Further, elemental weathering fluxes in this section do include associated uncertainties.

L810: In the section's header, "*ecosystems"* has been replaced by "*plants"*.

L810 – 829: Further text on the total inventories in saprolite, soil and bulk regolith was added.

L881 – 891: Text that explains the high elemental Al and Na concentration in the northernmost site that was formerly contained in section "Nutrient recycling as buffering mechanism" was moved into this section.

L892 – 898: Uncertainties of nutrient uptake fluxes were added.

L903 – 905: We rectified that the radiogenic Sr composition in Pan de Azúcar indeed differs between the single regolith profiles.

L1004 – 1146: Text formerly contained in the section "*Are nutrient sources setting plant stoichiometry*" was included in this section and toned down. We use the X:P ratio in plants and the bio-available fraction (Fig. 6), respectively, and the $^{87}Sr/^{86}Sr$ ratio in the bio-available fraction to locate the nutrient pool of plants rather than inferring nutrient limitation.

L1147 ff: The section's header was changed from "*Nutrient recycling as buffering mechanism*" to "*An increase in nutrient recycling with NPP*". We link the fluxes of the geogenic nutrient pathway and the organic nutrient cycle and describe the increasing recycling rates along the north-south transect, and how increasing recycling affects he X:P ratio in the bio-available fraction.

L1287: This section's header was changed from "*How the organic and the geogenic nutrient pathway set the size of the bioavailable pool*" to "*Processes that set the size of the bio-available pool.*"

L1287 – 1349: This section was strongly revised and now discusses the main processes that set the size of the bio-available pool at conceptual steady state. We further tuned down the importance of CEC_{eff} in setting the size of that pool and conclude that retention capacity and water flow ultimately set its size.

L1350 – 1551: This section's header was changed from "*How the organic and the geogenic nutrient pathway set the size of the bioavailable pool"* to "*Concepts for biotas role in setting fluxes in the geogenic and the organic nutrient cycle*". The section was strongly revised. Here we discuss the role of biota in setting the delicate balance between the organic and geogenic nutrient pathway. We discuss how recycling and biogenic weathering can in general contribute towards this balance.

L1552ff: This section's header was changed from "*Is weathering modulated by biota?*" to "*Is weathering modulated by biota? A statistical approach.*" In this section, we discuss correlational statistical methods to single out the possible biogenic weathering driver from the confounding factors. We define three hypothesis on the potential drivers of weathering and its potential drivers: (1) Where denudation rate D is high bulk weathering fluxes are high… (2) At sites at which MAP and hence runoff is high, weathering fluxes are high… (3) If NPP is high the degree and rate of weathering will be high… . Using this statistical approach, we found that neither MAP nor NPP have a significant effect of rate and degree of weathering. Instead, denudation rate the is the main driver. We further expand the analysis of confounding factors to include the differences in initial bedrock composition and mineralogy that exist between Santa Gracia and Nahuelbuta, and the resulting effects of weathering. In summary, we discuss that in Santa Gracia the mineral suite is more susceptible to weathering than in Nahuelbuta and might result in the observed similarities in weathering fluxes between the two sites despite massive differences in vegetation cover, NPP, and MAP.

L1613ff: A subsection named "*Do negative feedbacks decouple biomass growth from weathering rate and degree?*" was added and returns to the analysis of the suite of processes how plants and their associated biota directly and indirectly impact weathering. We particularly focus in point (D) on how plants can increase or decrease solubility of silicate minerals by Si accumulation or by discriminating against Si during uptake. The Si-uptake flux is minor compared to its release by weathering. The ecosystems at the EarthShape sites can be regarded to be below the threshold considered for Si accumulators. We thus conclude that Si uptake by plants does not contribute towards increasing weathering rates. Given this

observation together with the analysis of pedogenic oxides, we argue that in the humid-temperate site of Nahuelbuta, Si weathering rates are subdued despite the elevated solubility of primary minerals due to increased CO_2 respiration by roots in regolith.

L1771 – 1779: We toned down the summary of this section. We state that we did not find evidence for coupling of silicate weathering fluxes with the nutrient demands of biota to an extent that exceeds other controlling factors of weathering.

L1812 – 1820: We toned down our main conclusion so as to direct the reader at possibly rethinking common views, which is the aim of our study.

Best regards,

Ralf Oeser and Friedhelm von Blanckenburg

Do degree and rate of silicate weathering depend on plant productivity?

Ralf A. Oeser[1], Friedhelm von Blanckenburg[1,2]

[1] GFZ German Research Centre for Geosciences, Section Earth Surface Geochemistry, Potsdam, D-14473, Germany
[2] Freie Universität Berlin; Institute of Geological Science, Berlin, D-12249, Germany

Correspondence to: Ralf A. Oeser (oeser@gfz-potsdam.de)

Abstract. Plants and their associated below-ground microbiota possess the tools for rock weathering. Yet the quantitative evaluation of the impact of these biogenic weathering drivers relative to abiogenic parameters, such as the supply of primary minerals, of water, and of acids is an open question in Critical Zone research. Here we present a novel strategy to decipher the relative impact of these drivers. We quantified the degree and rate of weathering and compared these to nutrient uptake along the "EarthShape" transect in the Chilean Coastal Cordillera. These sites define a substantial north-south gradient in precipitation and primary productivity but overlie granitoid rock throughout. We present a substantial dataset of the chemistry of Critical Zone compartments (bedrock, regolith, soil, and vegetation) to quantify the relative loss of soluble elements (the "degree of weathering") and the inventory of bio-available elements. We use $^{87}Sr/^{86}Sr$ isotope ratios to identify the sources of mineral nutrients to plants. With rates from cosmogenic nuclides and biomass growth we determined fluxes ("weathering rates"), meaning the rate of loss of elements out of the ecosystems, averaged over weathering timescales (millennia), and quantified mineral nutrient recycling between the bulk weathering zone and the bulk vegetation cover. We found that neither the degree of weathering nor the weathering rates increase systematically with precipitation from north to south along the climate and vegetation gradient. Instead, the increase in biomass nutrient demand is accommodated by faster nutrient recycling. In the absence of an increase in weathering rate despite a five-fold increase in precipitation and NPP, we hypothesize that plant growth might in fact dampen weathering rates. Because plants are thought to be key players in the global silicate weathering - carbon feedback, this hypothesis merits further evaluation.

hat gelöscht: Decoupling
hat gelöscht: from primary
hat gelöscht: – how ecosystems regulate nutrient uptake along a climate and vegetation gradient
hat gelöscht: 3.3
hat gelöscht: In addition to the supply of primary minerals and water flow the presence and growth rate of land plants are thought to drive rock weathering. While doubtlessly plants
hat gelöscht: considerable
hat gelöscht: work,
hat gelöscht: their
hat gelöscht: the common
hat gelöscht: weathering processes remains poorly known. Here we report on a
hat gelöscht: two
hat gelöscht: did so by quantifying
hat gelöscht: rates
hat gelöscht: where landscapes are subjected to
hat gelöscht: to
hat gelöscht: vegetation growth, whereas rock type is
hat gelöscht: and tectonic process rates do not differ much along
hat gelöscht: gradient. We quantified the bio-available fraction of nutritive elements in regolith and we measured $^{87}Sr/^{86}Sr$ isotope ratios in the different
hat gelöscht: of the Earth's Critical Zone
hat gelöscht: bio-available fraction in saprolite and
hat gelöscht: We thereby budgeted inventories, gains,
hat gelöscht: losses
hat gelöscht: nutritive
hat gelöscht: in and
hat gelöscht: these
hat gelöscht: .
hat gelöscht: do not
hat gelöscht: simultaneous
hat gelöscht: growth rate
hat gelöscht: The
hat gelöscht: in spite of
hat gelöscht: leads us to
hat gelöscht: the presence of plants can negatively impact weathering through inducing secondary-mineral formation and by fostering a microbial community that is adapted for nutrient-recycling rather than nutrient-acquisition through weathering.

1 Introduction

Ever since the emergence of land plants, their dependence on mineral-derived nutrients has impacted rock weathering, used here to mean the combined processes of primary mineral dissolution, secondary solid formation, and the loss of elements in aqueous solution. This impact results from three types of interaction. The first is mechanical processes, that weaken rock or change the depth of the weathering zone through roots and microbial symbionts (e.g. mycorrhizal fungi; Blum et al., 2002; Brantley et al., 2017; Hasenmueller et al., 2017; Minyard et al., 2012; Quirk et al., 2014; van Schöll et al., 2007). The second is a variety of biogeochemical processes that alter the susceptibility of minerals to weathering. These mechanisms include root respiration that releases protons and CO_2, lowering soil pH, the exudation of organic ligands through roots that increases the solubility of nutrients through complexation, and the uptake, uplift, and recycling of pore fluids and nutrients from solution (e.g. Berner et al., 2003; Brantley et al., 2012; Drever, 1994; Kump et al., 2000; Lee and Boyce, 2010; Jobbágy, 2001; Giehl and von Wiren, 2014). The third interaction affects the water cycle which is impacted by rooting depth and seasonal water storage in saprolite and evapotranspiration (Kleidon et al., 2000; Ibarra et al., 2019). All of these interactions impact weathering, either directly by aiding plant acquisition of mineral nutrients from rock, or indirectly by modifying the water cycle (e.g. Brantley et al., 2011; Porder, 2019; Moulton et al., 2000). This means the presence and growth rate of land plants is commonly thought to have strongly impacted the evolution of Earth's atmosphere over geologic time by strengthening the negative feedback between silicate weathering rates and atmospheric CO_2 concentrations (Beerling and Berner, 2005; Doughty et al., 2014; Lenton et al., 2012; Pagani et al., 2009; Porada et al., 2016).

While biota in general and plants in particular are undoubtedly key players in weathering and pedogenesis, a quantitative evaluation of their impact remains elusive. The reason is our inability to disentangle abiotic from biotic processes in field observations (Amundson et al., 2007). Almost all mass transfer in the weathering zone can have biotic and abiotic causes. An additional challenge is the difficulty in accounting for confounding effects. Environmental state variables shaping the Critical Zone (the zone of the Earth surface that extends from the top of unweathered bedrock to the top of the vegetation cover; the zone in which most biogeochemical reactions take place) can obscure or amplify the effects of biology, making the attribution of cause and effect challenging. Another reason for our inability to directly attribute

hat gelöscht: . This impact results from mechanical weakening of rock…

hat gelöscht: , and from

hat gelöscht: weatherability

hat gelöscht: .

hat gelöscht: releasing

hat gelöscht: which lowers the

hat gelöscht: hence increasing

hat gelöscht: by

hat gelöscht: A

hat gelöscht: . The subsurface water cycle

hat gelöscht: , whereas the surface water cycle is affected by

hat gelöscht: Because all

hat gelöscht: either directly

hat gelöscht:

hat gelöscht: to acquire

hat gelöscht: affect weathering

hat gelöscht: ,

hat gelöscht: providing a

hat gelöscht: on

hat gelöscht: the

hat gelöscht: in these processes is a topic still widely open.

hat gelöscht: for this

hat gelöscht: during

hat gelöscht: (Amundson et al., 2007).

hat gelöscht: taking place in the weathering zone can have biotic and abiotic causes. Thus, field studies rely on exploring ecosystem functioning and weathering

weathering to plant growth arises from the ability of ecosystems to recycle nutrients through microbial mineralization from plant litter and organic matter, rather than acquiring fresh nutrient from rock (Chaudhuri et al., 2007; Lang et al., 2016; Lucas, 2001; Spohn and Sierra, 2018; Wilcke et al., 2002). Given the ability of ecosystems to buffer changes in nutrient fluxes (Spohn and Sierra, 2018) the dependence of weathering on plant growth and biomass distribution can be expected to be a highly non-linear one.

A classical strategy in field studies that aim to decipher how ecosystem functioning and weathering shape the Critical Zone relies on exploring the interactions along natural environmental gradients. Studies along a Hawaiian chronosequence (soils of variable discrete initial formation age) have evaluated the role of soil age in weathering and the distribution and cycling of cations through plants. These studies revealed the dependency of nutrient cycling on the degree of weathering (e.g. Bullen and Chadwick, 2016; Chadwick et al., 1999; Laliberte et al., 2013; Porder and Chadwick, 2009; Vitousek, 2004). Studies along a climosequence (gradients in climate whilst minimizing other environmental differences) have evaluated the effect of climate on ecological and pedogenic processes (Bullen and Chadwick, 2016; Calmels et al., 2014; Dere et al., 2013; Egli et al., 2003; Ferrier et al., 2012). These studies generally show an increase in weathering rates with increasing mean annual temperature (MAT) and mean annual precipitation (MAP), while vegetation plays a significant role in pedogenesis. Studies across different rock substrates have evaluated the availability of nutrients and the dissolution kinetics of minerals for ecosystem nutrient budgets (Hahm et al., 2014; Uhlig and von Blanckenburg, 2019) and indicate a 'bottom-up' lithological and mineralogical control on nutrient availability to ecosystems. Studies along gradients in erosion rates explored the supply of minerals to ecosystems and discovered an increase in nutrient supply through weathering with increasing erosion rates (Chadwick and Asner, 2016; Eger et al., 2018; Porder et al., 2007; Schuessler et al., 2018). Studies that have tried to isolate just the role of vegetation cover show that the weathering fluxes in adjacent areas in which only vegetation differs showed higher fluxes with more vegetation (Moulton et al., 2000). All these studies differ widely in their methodology, time scale, spatial scale, conceptual framework and even discipline. We return to this topic below by comparing our conceptual perspective to other approaches.

hat gelöscht: on
hat gelöscht: mobile
hat gelöscht: , and discovered a strong
hat gelöscht: such
hat gelöscht: effects
hat gelöscht: combined
hat gelöscht: rate
hat gelöscht:
hat gelöscht: along a lithogradient (gradients in
hat gelöscht: substrate)
hat gelöscht: nutrients
hat gelöscht: up lithologic
hat gelöscht: mineralogic
hat gelöscht: . A challenge faced in many such field-based studies are the confounding effects, as environmental state variables and ecosystem properties often shift simultaneously along the gradient

In this study we explore weathering, nutrient uptake, and nutrient recycling along one of the Earth's impressive climate and vegetation gradient, located in the Chilean Coastal Cordillera (Oeser et al., 2018). The study was conducted within the framework of the priority program of the Deutsche Forschungsgemeinschaft "EarthShape: Earth Surface Shaping by Biota" (DFG-SPP 1803). Along this gradient we quantify the degree of weathering, (using chemical analyses of rock and regolith, Oeser et al., 2018) and rates of weathering (using cosmogenic ^{10}Be, Schaller et al., 2018) and nutrient uptake (using net primary productivity, NPP and the chemical composition of the major plant species at each site). Sequential extraction protocols applied to bulk regolith were used to identify the stoichiometry of the main plant-available elements in the regolith. Radiogenic $^{87}Sr/^{86}Sr$ isotope ratios in bulk rock, regolith, the bio-available fraction in regolith, and plant biomass were used to identify the sources of mineral nutrients. We were thus able to identify gains and losses of nutritive elements in and out of these ecosystems and to quantify the efficiency of nutrient recycling. We applied the conceptual framework and parameterization of Uhlig and von Blanckenburg (2019) to place quantitative constraints on the "organic nutrient cycle" and the "geogenic nutrient pathway" as detailed in the next section.

Specifically, we evaluated the following questions: (1) Do weathering rates increase along the north-south precipitation gradient because runoff, the main driver of weathering flux, increases? (2) Do the variations in NPP along the climate and vegetation gradient correlate with nutrient supply rates from weathering? We find that neither is the case. Rather than the expected increase in weathering rate, the recycling efficiency of nutrients increases instead along the north – south transect.

2. Conceptual perspectives

Two fundamentally different concepts describe the relationship between regolith formation and time, and their relationship to different geomorphic regimes (Lin, 2010; Smeck et al., 1983): the continuous evolution model and the steady-state model. The continuous evolution model describes regolith or soil evolution with time from an initial point and describes chronosequences, where soils evolve on stable (non-eroding) surfaces. These soils have a distinct age and undergo several phases of soil development (e.g. Chadwick et al., 1999; Vitousek and Chadwick, 2013). In contrast, the steady-state model assumes all regolith state variables are independent of an initial point. In this concept, regolith is constantly

hat gelöscht: Another reason for our inability to directly attribute weathering to plant growth arises from ecosystems' ability to recycle (i.e. nutrient re-utilization through microbial mineralization from plant litter and organic matter), rather than acquiring fresh nutrients (Chaudhuri et al., 2007; Lang et al., 2016; Lucas, 2001; Spohn and Sierra, 2018; Wilcke et al., 2002). Given this ability to buffer changes in nutrient fluxes (Spohn and Sierra, 2018) the dependence of weathering on plant growth and biomass distribution would be a highly non-linear one. ¶
Previous conceptual models of the relationship between weathering and ecosystem functioning emphasized the role of erosion, and hence landscape and nutrient supply by landscape rejuvenation for ecosystem nutrition (Buendía et al., 2010; Porder et al., 2007). Another class of models accounted for the coupled weathering – recycling – uptake systems by linking the short-term, biological cycle with the long-term, largely geological and hydrological driven cycle fostering nutrient inputs to and outputs from terrestrial ecosystems (Powers et al., 2015; Vitousek et al., 1998). Such models have recently been adapted by geochemistry (Uhlig and von Blanckenburg, 2019). In these, the so-called "organic nutrient cycle" comprises a set of strategies for efficient nutrient re-utilization through microbial mineralization from plant litter and organic matter and entails rapid nutrient turnover. However, ecosystems in sloping landscapes permanently lose these organic-derived nutrients by plant-litter erosion

hat gelöscht: Heartsill Scalley

hat gelöscht: 2012; Scatena

hat gelöscht: Lugo, 1995

hat gelöscht: as well as litter and root decomposition and their subsequent export in solution (Baskaran et al., 2017; Chaudhuri et al., 2007; Moore et al., 2005; Silver and Miya, 2001). Atmospheric wet and dry deposition serves as a potential replacement in tropical

rejuvenated by production at depth and its removal through erosion from above (e.g. Heimsath et al., 1997). In other words, the regolith is continuously turned over and has no distinct age, but rather a residence time. This concept applies to all sloping landscapes on Earth, on which typical regolith residence times ($\leq 10^4$ yrs) are often less than or equal to the timescales over which tectonics and climate vary ($\geq 10^4$ yrs). This suggests that much of the Earth surface operates in a manner that is consistent with the steady-state model of soil formation (Dixon et al., 2009; Ferrier et al., 2005; Riebe and Granger, 2013). The state variables do not necessarily vary linearly with age (in the continuous evolution model) or residence time (in the steady-state model). Thus, in the continuous evolution model, pedogenic thresholds have been deduced based on certain soil properties (Dixon et al., 2016; Vitousek and Chadwick, 2013). These have also been described to exist and strongly vary along the eroding surfaces in Chile explored in this study (Bernhard et al., 2018).

Although ecosystems respond over shorter time scales to environmental change, ranging from seasonal to decadal or longer climate cycles, their evolution can nevertheless be linked to the two regolith evolution models (Brantley et al., 2011). In the continuous evolution model, ecology and soil development are linked via progressive increases in soil stability and water retention capacity and a unidirectional decrease in mineral nutrient availability (Vitousek and Farrington, 1997). In contrast, in the steady-state model, regolith replenishment by uplift and erosion sets the upward advection of mineral nutrients (Buendía et al., 2010; Porder et al., 2007; Vitousek et al., 2003; Uhlig and von Blanckenburg, 2019) and availability of regolith moisture (Rempe and Dietrich, 2018). Thus, the combination of regolith residence time and mineral weathering rates determines whether an ecosystem is limited in a specific mineral nutrient which in turn is thought to set plant diversity and nutrient acquisition strategies. For example, ecosystems on strongly mineral nutrient-depleted soils seem to be characterized by high plant diversity (Laliberte et al., 2013; Lambers et al., 2008).

The methods employed to explore these processes span a range of time scales that are discipline specific. Plant ecology typically works on (sub-)annual timescales for ecosystem fertilization or manipulation experiments (Tielbörger et al., 2014; Tipping et al., 1999), while instrumental monitoring of water, gas, and nutrient fluxes between Critical Zone compartments in hydrology, soil ecology, and biogeochemistry can reach decadal timescales (Joos et al., 2010; Kelly and Goulden, 2016; Lang et al., 2016; Sprenger et

hat gelöscht: e.g. Boy and Wilcke, 2008; Chadwick

hat gelöscht: 1999; Dosseto

hat gelöscht: 2012

hat gelöscht: , and desert (Wang et al., 2014) ecosystems which are subject to slow erosion rates and high atmospheric input. However, in most sloping landscapes, the dominant nutrient-replacing mechanism is provided by the "geogenic nutrient pathway" which counterbalances losses by a slow but steady release of nutrients through chemical weathering of rock

hat gelöscht: (Buendía et al., 2010; Cleveland et al., 2013; Uhlig and von Blanckenburg, 2019)

hat gelöscht: . Even though these geogenic fluxes are minor compared to the organic nutrient cycle they sustain ecosystem nutrition over the long-term (millennial) time scales. The importance of this geogenic nutrient source to sustain ecosystem nutrition with macronutrients (e.g. Ca, K, Mg, and P) over longer time scales has recently been demonstrated by several studies across a variety of biomes

hat gelöscht: (Hahm et al., 2014; Schuessler et al., 2018; Uhlig et al., 2017; Uhlig and von Blanckenburg, 2019)

hat gelöscht: . Uhlig and von Blanckenburg (2019) found that long-term ecosystem nutrition is ensured by the adjustment of the nutrient re-utilization loop towards higher efficiency that compensates for a lower nutrient supply from chemical weathering.¶ However, whether the geogenic nutrient pathway is sufficiently effective to prevent development of nutrient limitation over the millennial scale depends on the supply of fresh rock into the weathering zone, the bio-availability of the nutrients released, and whether plant roots and the associated mycorrhizal fungi can access them. Thus, any exploration of these links remains inconclusive without constraining the loci of nutrient source in regolith and its stoichiometry in comparison to plant demand.¶
¶
In this study, we explored weathering, nutrient uptake, and nutrient recycling along the "EarthShape" (Oeser et al., 2018) climate and vegetation gradient in the Chilean Coastal Cordillera. The four sites range from ~26°S to ~38°S and while lithology (granitoid), tectonic uplift, and erosion rates (10 to 40 t km^{-2} yr^{-1}; Schaller et al., 2018) are broadly similar, precipitation forms a gradient from 10 mm yr^{-1} in the north to 1100 mm yr^{-1}in the south (Ministerio de Obras Públicas, 2017). Similarly, net primary productivity (NPP) increases from 30 to 520 g_C m^{-2} yr^{-1} (Werner et al., 2018). Along this gradient we quantified the degree (using chemical analyses of rock and regolith, Oeser et al., 2018) and rates (using cosmogenic ^{10}Be, Schaller et al., 2018) of weathering and nutrient uptake (using NPP and the chemical composition of the major plant species at each site). Sequential extraction on bulk regolith was used to identify the stoichiometry of the main plant-available elements in the regolith (sum of saprolite and soil) in addition to phosphorus (Brucker and Spohn, 2019). We further utilized radiogenic $^{87}Sr/^{86}Sr$ isotope ratios in bulk rock, regolith, and plant samples along with those in the bio-available fraction to identify the sources of mineral nutrients. Thus, we were able to identify gains and losses of nutritive elements in and out of these ecosystems and to quantify the efficiency of nutrient recycling. We applied the conceptual framework and parameterization of Uhlig and von Blanckenburg (2019) to place quantitative constraints onto the "organic nutrient cycle" and the "geogenic nutrient pathway". ¶ We evaluated the following questions. (1) Does weathering increase from north to south along the along the EarthShape precipitation... [1]

al., 2019; Sohrt et al., 2019; Wilcke et al., 2017). Geochemical estimates of rock weathering or evolution of plant-available nutrient inventories typically integrate over millennial timescales (Buendía et al., 2010; Porder et al., 2007; Riebe and Granger, 2013; Uhlig and von Blanckenburg, 2019; Vitousek et al., 2003). To integrate these different time scales, some soil ecological models account for the coupled weathering – recycling – uptake systems by linking the short-term, biological cycle with the long-term, largely geological and hydrological-driven cycle (Porder and Chadwick, 2009; Powers et al., 2015; Vitousek et al., 1998). Such models have recently been complemented by concepts and methods from geochemistry (Uhlig and von Blanckenburg, 2019) that we pursue in this study. In this conceptual framework, the so-called "organic nutrient cycle" comprises a set of strategies for efficient nutrient re-utilization through microbial mineralization from plant litter and organic matter and entails rapid nutrient turnover. The "geogenic nutrient pathway" compensates the loss of nutrients by erosion and in solution through the slow but steady supply of nutrients from chemical weathering of rock (Buendía et al., 2010; Cleveland et al., 2013; Uhlig and von Blanckenburg, 2019). This concept is particularly relevant where atmospheric wet and dry deposition (e.g. Boy and Wilcke, 2008; Chadwick et al., 1999; Dosseto et al., 2012) do not suffice to balance the losses. These geogenic input fluxes are often minor compared to those in the organic nutrient cycle and may even be undetectable over the annual to decadal scales of ecosystem monitoring experiments. However, they sustain ecosystem nutrition over longer (decadal to millennial) time scales because they prevent nutrient deficiency that may otherwise develop (Hahm et al., 2014; Schuessler et al., 2018; Uhlig et al., 2017; Uhlig and von Blanckenburg, 2019). Whether the geogenic nutrient pathway is sufficient to prevent development of nutrient limitation over the millennial scale depends on the rate of supply of fresh rock into the weathering zone, the bioavailability of the nutrients released, and whether plant roots and the associated mycorrhizal fungi can access them. Thus, any exploration of these links must constrain where nutrients are released in regolith relative to where plants obtain them. The aim of this study is to illustrate how these methods from geochemistry can be employed to assess the flux balances between the top of bedrock and the top of the vegetation canopy as integrated over millennia, and how plant growth affects these in comparison to the geologic drivers like uplift and erosion or climatic drivers like precipitation and runoff.

3 Study area and previous results

The four study sites are part of the EarthShape study area which is located along the Chilean Coastal Cordillera. Three sites are located in national parks and one in a nature reserve, so human impact is minimized. The sites are located on the plutonic rocks of the Chilean Coastal Cordillera and are close to the Pacific coast (less than 80 km; Oeser et al., 2018) and are detailed in two previous studies that introduced the field area, its pedogenic and weathering characteristics, and a substantial set of new soil- and geochemical data (Oeser et al., 2018; Bernhard et al., 2018).

The sites define a vegetation gradient controlled by climate, ranging over 1300 km. From north to south, they cover arid (Pan de Azúcar National Park, ~26°S), semi-arid (Santa Gracia Nature Reserve, ~30°S), mediterranean (La Campana National Park, ~33°S), and humid-temperate (Nahuelbuta National Park, ~38°S) climate conditions. The mean annual precipitation (MAP) increases from 10 mm yr^{-1} in Pan de Azúcar, 89 mm yr^{-1} in Santa Gracia, 440 mm yr^{-1} in La Campana, to 1100 mm yr^{-1} in Nahuelbuta, respectively. The mean annual air temperature (MAT) ranges from 18.1°C in the northernmost site in Pan de Azúcar to 14.1°C in the southernmost site in Nahuelbuta (Fig. 1, Table 1; Ministerio de Obras Públicas, 2017).

Net primary productivity (NPP), derived from a dynamic vegetation model (LPJ-GUESS) that simulates vegetation cover and composition during the Holocene (Werner et al., 2018), ranges from 30 g_C m^{-2} yr^{-1} and 150 g_C m^{-2} yr^{-1} in the arid shrubland of Pan de Azúcar and Santa Gracia, respectively, to 280 g_C m^{-2} yr^{-1} in the sclerophyllous woodland of La Campana, and is highest (520 g_C m^{-2} yr^{-1}) in the humid-temperate forests of Nahuelbuta (Fig. 1, Table 1). The vegetation cover (< 5%) in Pan de Azúcar consists only of small shrubs, geophytes and annual plants (Armesto et al., 1993), which are mainly present in small ravines. The vegetation in Santa Gracia belongs to the "Interior Mediterranean desert scrub of *Heliotropium stenophyllum* and *Flourensia thurifera*" formation (Luebert and Pliscoff, 2006). Plants are affected by livestock grazing (mostly goats; Bahre, 1979), and vegetation cover is generally sparse. In La Campana the vegetation (almost 100% ground cover) is part of the "Coastal Mediterranean sclerophyllous forest of *Lithraea caustica* and *Cryptocarya alba*" formation (Luebert and Pliscoff, 2006). The dominant vegetation in Nahuelbuta is associated with the "Coastal temperate forest of *Araucaria araucana*" formation (Luebert and Pliscoff, 2006) and covers 100% of ground area.

hat gelöscht: They form a sequence from
hat gelöscht: covering
hat gelöscht: simulating
hat gelöscht: (Werner et al., 2018)
hat gelöscht: Fig. 1
hat gelöscht: Table 1).
hat gelöscht: consist
hat gelöscht: (Armesto et al., 1993)
hat gelöscht: Ecosystems at all sites are primarily nitrogen-limited (Stock et al., 2019).

The basement at those sites is mainly composed of granitoid intrusions of late Carboniferous to Cretaceous age. The compositional variation ranges from monzo- to syenogranites in Pan de Azúcar (199 Ma; Berg and Breitkreuz, 1983; Berg and Baumann, 1985; Parada et al., 2007), pyroxene and hornblende-bearing diorites and monzodiorites in Santa Gracia (98 – 89 Ma; Moscoso et al., 1982), as well as tonalites and granodiorites in Nahuelbuta (Nahuelbuta complex, 294 Ma; Parada et al., 2007) and in the Caleu Pluton in La Campana with an intrusion age of 130 Myr (Molina et al., 2015; Parada and Larrondo, 1999; Parada et al., 2002).

For the soil pits studied here, denudation rates inferred from cosmogenic nuclides (*in situ* ^{10}Be), interpreted as soil production rates, are 8 – 11 t km^{-2} yr^{-1} in Pan de Azúcar, 16 – 22 t km^{-2} yr^{-1} in Santa Gracia, 54 – 69 t km^{-2} yr^{-1} in La Campana and 18 – 48 t km^{-2} yr^{-1} in Nahuelbuta (Schaller et al., 2018b). Catchment-wide denudation rates broadly agree with these soil-scale rates, except in La Campana. Here, they are higher, attributed to debris flows in valley tops due to the higher channel steepness than elsewhere (e.g. mean slope 23° in La Campana, 9° in Nahuelbuta; van Dongen et al., 2019). The relative consistency of these rates along the climate gradient is ascribed to consistent tectonic forces acting along the whole gradient (e.g. Blanco-Chao et al., 2014; Melnik, 2016), with the moderate increase in denudation rates at the two southern sites explainable with the combined effect of higher precipitation and increasing shielding by vegetation (Schaller et al., 2018b).

The architecture of the regolith profiles, their chemistry, mineralogy, and the physical properties of soils, saprolite, and the rocks beneath have been extensively described for four soil pits at each site by Bernhard et al. (2018), Dal Bo et al. (2019), Oeser et al. (2018) and Schaller et al. (2018b). The regolith profiles in Pan de Azúcar are located between 330 and 340 m above sea level (asl) on steep (25 – 40°; Table 1) hill slopes. The soils on the north- and south-facing slopes were classified by Bernhard et al. (2018) as Regosols with only shallow A and B horizons of ~20 – 30 cm thickness, lacking any kind of organic and litter layer. In this area, the processes disintegrating rock and developing regolith are mainly physical weathering, specifically a combination of insolation- and salt weathering (Oeser et al., 2018). The regolith profiles in Santa Gracia are situated at almost 700 m asl on gently sloping hills (15 – 25°; Table 1). The soils on the north- and on the south-facing slope are a Leptosol and a Cambisol, respectively (Bernhard et al., 2018). Distinct O-horizons and a litter layer are not apparent. The Ah horizons in both profiles

hat gelöscht: Cretaceous to

hat gelöscht: (98 – 89 Ma; Moscoso et al., 1982)

hat gelöscht: Catchment-wide denudation rates inferred from cosmogenic nuclides (*in situ* ^{10}Be) are lowest in Pan de Azúcar (7.7 ± 0.7 t km^{-2} yr^{-1}) and Santa Gracia (9.2 ± 0.8 t km^{-2} yr^{-1}), highest in La Campana (200 ± 22 t km^{-2} yr^{-1}), and intermediate in Nahuelbuta (27.4 ± 2.4 t km^{-2} yr^{-1}) is lower (van Dongen et al., 2019). At the soil pit scale, Schaller et al. (2018) report a trend in total soil denudation rates, interpreted as soil production rates, from Pan de Azúcar (8 – 11 t km^{-2} yr^{-1}) to Santa Gracia (16 – 22 t km^{-2} yr^{-1}) with a peak in La Campana (54 – 69 t km^{-2} yr^{-1}) and 18 – 48 t km^{-2} yr^{-1} in Nahuelbuta. The elevated catchment-wide rates at La Campana are attributed to faster erosion processes dominating the entire catchment that is characterized by higher hill slopes than in the other areas (e.g. mean slope 23° in La Campana, 9° in Nahuelbuta; van Dongen et al., 2019). They are thus towards the lower end of global cosmogenic nuclide-derived soil production rates (Dixon et al., 2012). The relative consistency of these rates along the climate gradient are ascribed to uniform tectonic forces acting in the whole study area

hat gelöscht: (e.g. Blanco-Chao

hat gelöscht: ., 2014; Melnik, 2016

hat gelöscht: . ¶
The architecture of the regolith profiles, their chemistry, mineralogy, and the physical properties of soils, saprolite, and the rocks beneath have been extensively described by Bernhard et al. (2018)

hat gelöscht: Dal Bo et al. (2019)

hat gelöscht: Oeser et al. (2018) and Schaller et al. (2018).¶

hat gelöscht: a.s.l.

hat gelöscht: Table 1

hat gelöscht: on the

hat gelöscht: slope

hat gelöscht: attributed to

hat gelöscht: (Oeser et al., 2018).

hat gelöscht: a.s.l.

hat gelöscht: mild

hat gelöscht: Table 1).

hat gelöscht: soul

reach depths of 10 cm and the transition from the mineral soil (Bw) into saprolite occurs at 25 – 30 cm depth. Oeser et al. (2018) attribute this sites' high degree of elemental depletion (50% loss relative to bedrock as quantified by the CDF; Fig. A1; Table S2) despite low precipitation to the low abundance of quartz and the high abundance of readily weatherable plagioclase and mafic minerals. The regolith profiles in La Campana, located at 730 m asl and on gently sloping hills (12 – 23°), are classified as Cambisols. The O-horizon is ~5 cm thick and is followed by a Ah horizon, extending up to 40 cm depth (Bernhard et al., 2018). Here, the mineral-soil layer turns into saprolite at approximately 110 cm in both profiles (Table 1). The elemental depletion of Ca relative to bedrock increases from ~45% at the profiles' bottom towards ~70% at their top and can be classified as depletion (north-facing) or depletion and enrichment profiles (south-facing, Fig. A1; Table S2; Brantley and Lebedeva, 2011), respectively. The regolith profiles in Nahuelbuta are situated on gently sloping hills (~15°) at about 1200 m asl (Table 1). Bernhard et al. (2018) have classified the soils on the north- and south-facing slope as umbric Podsols and orthodystric Umbrisols, respectively. Here, the Ah horizons measure up to 50 cm (greater thickness on the south-facing slope) and are overlain by an organic horizon of 5.5 cm thickness. In the two regolith profiles, the soil-saprolite transition is at 100 and 120 cm depth, respectively. The coarse-grained saprolite disaggregates readily. These two profiles are characterized by highly heterogeneous weathering patterns caused by the incorporation of the metamorphic basement at various parts (e.g. Oeser et al., 2018; Hervé, 1977). Along the EarthShape north-south transect, many of the soil properties indicate crossing of several distinct pedogenic thresholds (Bernhard et al., 2018). We note that while the detailed geochemical work reported in this study is based on two profiles per site, the soil properties (Bernhard et al., 2018) and bulk geochemical data (Oeser et al., 2018) of these profiles are corroborated by two additional replicates per site as reported in these previous studies. A comprehensive summary of the characteristics of the eight regolith profiles and major plant types is given in Table 1.

hat gelöscht: Oeser et al. (2018)
hat gelöscht: study
hat gelöscht: i.e. τ, almost 60
hat gelöscht: of Ca and Na
hat gelöscht: a.s.l.
hat gelöscht: mild
hat gelöscht: Table 1).
hat gelöscht: for example
hat gelöscht: accordingly
hat gelöscht: (south-facing, Fig. A1; Table S2; Brantley and Lebedeva, 2011)
hat gelöscht: a.s.l.
hat gelöscht: Table 1).
hat gelöscht: Podsol
hat gelöscht: Umbrisol
hat gelöscht: ¶
hat gelöscht: eight regolith profiles'
hat gelöscht: Table 1

4 Methods

4.1 Sampling

Regolith samples were collected in a continuous sequence of depth increments from bottom to top. Increments amount to a thickness of 5 cm for the uppermost two samples, 10 cm for the 3rd sample from top, and increase to 20 cm thickness for the 4th sample onwards. To account for the dependence on solar radiation, two regolith profiles on adjacent hillslopes (north- and south-facing) were sampled at each study site (see Appendix B for further information on sample replication).

The underlying unweathered bedrock was not reached in any of the regolith profiles and the depth to bedrock remains unknown. Thus, bedrock samples were collected from nearby outcrops. This sample set comprises the 20 bedrock samples already reported in Oeser et al. (2018) and 15 additional bedrock samples (in total 12 in Pan de Azúcar, 8 in Santa Gracia, 10 in La Campana, and 5 in Nahuelbuta).

Vegetation samples from representative shrubs and trees (grasses have been excluded) of each study site were sampled in the austral summer to autumn 2016. The sample set comprises material from mature plants of the prevailing species: *Nolana mollis* (Pan de Azúcar), *Asterasia* sp., *Cordia decandra*, *Cumulopuntia sphaerica*, and *Proustia cuneifolia* (Santa Gracia), *Aristeguietia salvia*, *Colliguaja odorifera*, *Cryptocarya alba*, and *Lithraea caustica* (La Campana), *Araucaria araucana*, *Nothofagus antarctica*, and *Chusquea coleu* (Nahuelbuta). From each sampled plant (n = 20), multiple samples of leaves, twigs and stem were collected, pooled together, and homogenized prior to analysis. These samples were either taken using an increment borer (stem samples) or plant scissors (leaf and twig samples) equipped with a telescopic arm to reach the higher parts of trees. As is commonly the case in field studies, roots could not be sampled in a representative manner though we account for their influence on plant composition (see Appendix A). The litter layer in La Campana and Nahuelbuta was also sampled.

4.2 Analytical methods

4.2.1 Chemical composition of regolith and bedrock

The concentration of major and trace elements in bedrock and regolith samples were determined using a X-Ray Fluorescence spectrometer (PANalytical AXIOS Advanced) at the section for “Inorganic and

hat gelöscht: 3
hat gelöscht: 3
hat gelöscht: .
hat gelöscht: has
hat gelöscht: been
hat gelöscht: either
hat gelöscht: Oeser et al. (2018)
hat gelöscht:) from within the respective study sites.
hat gelöscht: have been
hat gelöscht: .
hat gelöscht: stem-, twig-, and leaf-samples
hat gelöscht:), respectively.
hat gelöscht: In addition,
hat gelöscht: 3
hat gelöscht: 3

Isotope Geochemistry", GFZ German Research Centre for Geosciences. A detailed description of the analytical protocols and sample preparation is given in Oeser et al. (2018).

4.2.2 Chemical composition of vegetation

Major and trace element concentrations of vegetation samples were determined using a Varian 720-ES axial ICP-OES at the Helmholtz Laboratory for the Geochemistry of the Earth Surface (HELGES), GFZ German Research Centre for Geosciences (von Blanckenburg et al., 2016) with relative uncertainties smaller than 10%. Prior to analysis, all samples were oven-dried at 120°C for 12 hrs. Subsequently, leaves were crushed and homogenized. About 0.5 g of leaf and 1 g of woody samples were digested in PFA vials using a microwave (MLS start) and ultra-pure concentrated acid mixtures comprising H_2O_2 and HNO_3, HCl and HNO_3, and HF. In some plant samples Si-bearing precipitates formed upon evaporation after digestion. These sample cakes were redissolved in a mixture of concentrated HF and HNO_3 to ensure complete dissolution of Si prior to analysis. As some Si might have been lost by volatilization as SiF_4 in this process, we do not include these samples (indicated by a * in Table S5) for the compilation of the plants' Si budget. With each sample batch, the international reference material NIST SRM 1515 Apple leaves and a procedural blank were processed.

4.2.3 Extraction of the bio-available fraction and its chemical analyses

The bio-available fraction of regolith samples was extracted using a sequential extraction procedure adapted from Arunachalam et al. (1996), He et al. (1995), and Tessier et al. (1979). The sequential extraction was performed in parallel on two regolith aliquots, and the supernatants were pooled together for analyses. About 2 g of dried and sieved (< 2 mm) sample material were immersed in 14 ml 18 MΩ Milli-Q H_2O (water-soluble fraction) and then in 1M NH_4Oac (exchangeable fraction; maintaining a sample/reactant ratio of ca. 1:7), and gently agitated. After each extraction, the mixture was centrifuged for 30 min at 4200 rpm and the supernatant was pipetted off. The remaining sample was then rinsed with 10 ml Milli-Q H_2O and centrifuged again (4200 rpm, 30 min), and the rinse solution added to the supernatant. Subsequently, the supernatants were purified using a vacuum-driven filtration system (Millipore®; 0.2 µm acetate filter), evaporated to dryness, and redissolved with ultra-pure concentrated

hat gelöscht: 3
hat gelöscht: (von Blanckenburg et al., 2016)
hat gelöscht: redissoled
hat gelöscht: evaporation
hat gelöscht: have
hat gelöscht: included
hat gelöscht: plant
hat gelöscht: was
hat gelöscht: 3
hat gelöscht: Arunachalam et al. (1996)
hat gelöscht: He et al. (1995)
hat gelöscht: Tessier et al. (1979)
hat gelöscht: of which
hat gelöscht: either
hat gelöscht: or
hat gelöscht:), thus
hat gelöscht: to
hat gelöscht: about
hat gelöscht: . Each extraction step was performed with mild agitation…
hat gelöscht:). This
hat gelöscht: was

acid mixtures comprising H_2O_2, HNO_3, and HCl. With each sample batch, international reference materials (NIST SRM 2709a San Joaquin soil, CCRMP TILL-1) along with a procedural blank were processed.

The water-soluble fraction is comprised of elements contained in soil water in the form of free ions and ions which form complexes with soluble organic matter. It represents the most labile soil compartment and thus is most accessible to plants (e.g. He et al., 1995). This fraction was accessed by suspending the samples for 24 hrs in Milli-Q H_2O at room temperature. The exchangeable fraction comprises elements that form weak electrostatic bonds between the hydrated surfaces of phyllosilicates (i.e. clays and micas), oxyhydroxide minerals (e.g. boehmite, diaspore, goethite, lepidocrocite, ferrihydrite), and organic matter. This fraction was extracted by suspending the samples in a mechanical end over end shaker at room temperature in 1 M NH_4OAc for 2 hrs at 60 rpm. Note that none of the further extraction steps described in Tessier et al. (1979) have been applied to the regolith samples as they are believed to make a negligible contribution to the bio-available fraction.

The element concentrations of the water-soluble and exchangeable fraction were determined using a Varian 720-ES axial ICP-OES at HELGES, following the analytical procedures described in Schuessler et al. (2016) with relative uncertainties estimated at smaller than 10%. Soil-P fractions were determined by Brucker and Spohn (2019). In this case, the bio-available fraction refers to the inorganic products of the modified Hedley sequential P fractionation method of Tiessen and Moir (1993), specifically the water-extractable P_i and labile P_i which was extracted by using 0.5 M $NaHCO_3$.

4.2.4 $^{87}Sr/^{86}Sr$ isotope ratios

The radiogenic Sr isotope ratio was determined on bulk bedrock and regolith, the bio-available fractions of saprolite and soil, and on the different plant organs at each study site.

After sample digestion (bulk samples) or sequential extraction (bio-available fraction), Sr was separated from matrix elements using 200 µl Sr-Spec resin. Matrix elements were removed by elution with 2.5 ml 3 M and 2 ml 7.5 M HNO_3. Subsequently, Sr was eluted with 4 ml of 18 Ω Milli-Q H_2O. Any organic crown-ether which has been released from the Sr-spec resin was removed after evaporation and subsequent redissolution of the Sr fraction in 1 ml of a 1:1 mixture of concentrated H_2O_2 and HNO_3. This

hat gelöscht: (e.g. He et al., 1995)
hat gelöscht: constitutes of
hat gelöscht: Tessier et al. (1979)
hat gelöscht: has
hat gelöscht: in this study
hat gelöscht: Schuessler et al. (2016)
hat gelöscht: ¶
The soil
hat gelöscht: Brucker and Spohn (2019).
hat gelöscht: 3
hat gelöscht: Upon

mixture was cooked in a tightly closed beaker at 150°C for at least 12 hrs. Within each sample batch, a minimum of one standard reference material and a procedural blank were processed.

$^{87}Sr/^{86}Sr$ was measured in a 50-ng g^{-1} pure Sr solution in 0.3 M HNO_3 using a multi collector inductively coupled plasma mass spectrometer (MC-ICP-MS, Thermo Neptune) in medium mass resolution. The MC-ICP-MS was equipped with an APEX-Q (ESI) desolvater and a nebulizer with an uptake rate of 70 µl min^{-1} and a nickel sampler cone. Radiogenic Sr isotope ratios were determined over one block of 20 cycles with an integration time of 16 seconds each. The sequence of a sample run was comprised of 10 to 12 blocks, where each block comprised a blank, four samples, and five SRM 987 which were not processed through chemistry. Blank correction of samples and reference material during the sequence was less than 0.4% of the sample signal. The intensities of the ion beams on the masses ^{82}Kr (L4), ^{83}Kr (L3), ^{84}Sr (L2), ^{85}Rb (L1), ^{86}Sr (central Cup), ^{87}Sr (H1) and ^{88}Sr (H2) were monitored using Faraday collectors equipped with 10^{11} Ω and one 10^{12} Ω (connected to L4 cup) resistors. Isobaric interference on the masses 84, 86, and 87 were corrected for with the Kr and Rb isotope ratios measured prior to the sequence run. To correct for any natural and instrumental isotope fractionation, the measured $^{87}Sr/^{86}Sr$ ratio was normalized to a $^{88}Sr/^{86}Sr$ ratio of 8.375209 (Nier, 1938's value) by using an exponential law. Finally, the $^{87}Sr/^{86}Sr$ ratios were corrected for a session offset that account for the differences between the certified and measured $^{87}Sr/^{86}Sr$ ratio of the SRM 987 reference material, which in any case where smaller than ±0.00006 (2SD).

4.3 Parameterizing geogenic and biogenic element fluxes in a terrestrial ecosystem

The parameterization of the "geogenic nutrient pathway" and the "organic nutrient cycle" (Fig. 2) to characterize element fluxes into, within, and from the Critical Zone and its ecosystem components is thoroughly described in Uhlig and von Blanckenburg (2019). Here, we only briefly summarize the metrics, which are shown in Table 2. Calculations and parameters used for these metrics are presented in Appendix A, including the propagation of uncertainties. A statistical analysis (i.e. ANOVA, Pearson correlation coefficients) of the weathering parameters is presented in Appendix B.

hat gelöscht: desolvating
hat gelöscht: rates
hat gelöscht: Faraday
hat gelöscht: the
hat gelöscht: (Nier, 1938's value)
hat gelöscht: .
hat gelöscht: 3
hat gelöscht: Fig. 2
hat gelöscht: , including the derivation of the corresponding equations has been
hat gelöscht: Uhlig and von Blanckenburg (2019)
hat gelöscht: Because throughout this article we make use of this framework
hat gelöscht: Table 2
hat gelöscht: Calculation

5 Results

We structure the presentation of our results in the following sequence: (1) the element fluxes of the geogenic nutrient pathway; (2) the availability of elements in regolith to plants; and (3) the plant chemical composition along with the element fluxes that couple the geogenic nutrient pathway to the organic nutrient cycle. The fluxes are presented as study-site averages, with the full dataset available in an associated open access data publication (Oeser and von Blanckenburg, 2020).

We focus the detailed presentation of these results on P and K, the two most important mineral nutrients to plants. Further data is provided for other plant-beneficial and plant-essential elements. Whether an element is considered as beneficial or essential to plants, however, is species-dependent (Marschner, 1983). Following Marschner (1983) we refer to the elements Al, Na, and Si as plant-beneficial elements and include the micronutrient Fe in this group. We refer to the elements Ca, K, Mg, and Mn as plant-essential elements. In this presentation, we treat Sr as a plant-essential element due to its similar (bio-)chemical behavior to Ca (e.g. Blum et al., 2012; Faure and Mensing, 2005; Faure and Powell, 1972; Poszwa et al., 2002). All metrics are defined in Table 2.

5.1 Element fluxes contributing to the geogenic nutrient pathway

5.1.1 Degree of weathering and elemental gains and losses

The chemical depletion fraction (CDF; Table 2, Eq. 5 and Appendix A) and elemental mass transfer coefficient (τ; Table 2, Eq. 6 and Appendix A) disclose the total and the element-specific loss, respectively, of soluble elements relative to bedrock. Thus, both metrics quantify the degree of weathering. The average CDF of the shallowest mineral soil (combined analysis of north- and south-facing profiles) in Pan de Azúcar, Santa Gracia, La Campana, and Nahuelbuta amounts to 0.03, 0.54, 0.50, and 0.25, respectively (Fig. 3; Table S2). At all four sites, the elemental losses (Fig. A1; Table S2) can be attributed to a "kinetically limited weathering regime" (Brantley and Lebedeva, 2011). This means that the erosion rate is at a sufficient level to continuously replenish the weatherable primary minerals that transit vertically through the weathering profile.

hat gelöscht: 4

hat gelöscht:

hat gelöscht: plants'

hat gelöscht: link

hat gelöscht: We focus the detailed presentation of these results on the two most important mineral nutrients to plants P and K, and further provide data on the plant-essential elements Ca, K, Mg, and Mn as well as plant-beneficial elements Al, Fe, Na, and Si (Marschner, 1983). In this presentation, we treat both Sr and Ca as plant-essential elements due to their similar (bio-) chemical behavior (e.g. Blum et al., 2012; Faure and Mensing, 2005; Faure and Powell, 1972; Poszwa et al., 2002). ¶ 4

hat gelöscht: 4

hat gelöscht: 6

hat gelöscht: (Fig. 3

hat gelöscht: (Brantley and Lebedeva, 2011).

hat gelöscht: nutrient stock held in

Systematic differences in chemical depletion (i.e. CDF and τ) are not discernible between north- and south-facing slopes. Anomalously high Zr concentrations throughout the entire north-facing profile at La Campana cause one exception to this rule. Moreover, we found that neither CDF nor τ^X differ significantly between Santa Gracia, La Campana, and Nahuelbuta, despite both increasing precipitation and increasing biomass growth.

A comprehensive presentation of these data can be found as Appendix in Fig. A1 and in the supplementary Table S2 (Oeser and von Blanckenburg, 2020).

5.1.2 Elemental chemical weathering fluxes

The soil weathering rate W quantifies the bulk weathering flux from rock and regolith. This flux is lowest in Pan de Azúcar (0 – 0.9 t km^{-2} yr^{-1}) and highest in La Campana (53.7 – 69.2 t km^{-2} yr^{-1}). In Santa Gracia (7.2 – 11.9 t km^{-2} yr^{-1}) and Nahuelbuta (3.5 – 7.5 t km-2 yr-1, Table 1; Oeser et al., 2018; Schaller et al., 2018b), these fluxes are at a similarly intermediate level.

$W^X_{regolith}$ (Table 2, Eq. 3 and Appendix A) quantifies elemental-specific release fluxes from rock and regolith by weathering. It thus assesses the maximum possible weathering supply of nutrients to plants by the "geogenic pathway", as some of this flux is potentially lost into groundwater before being accessible to roots. The weathering-release fluxes for phosphorus ($W^P_{regolith}$) amount to 1.3 ± 0.4, 12 ± 3, 19 ± 6, and 11 ± 4 mg m^{-2} yr^{-1} and of potassium ($W^K_{regolith}$) to 30 ± 30, 80 ± 50, 840 ± 220, and 100 ± 120 mg m^{-2} yr^{-1} (Fig. 4, Table 3) in Pan de Azúcar, Santa Gracia, La Campana, and Nahuelbuta, respectively. Similar trends are seen for the plant-beneficial elements Al, Na, and Si along with Fe and Sr. The rates of supply of P, K, and the plant-beneficial elements are thus similar at both Santa Gracia and Nahuelbuta despite the differences in MAP, NPP, and vegetation cover. $W^{Ca}_{regolith}$ and $W^{Mg}_{regolith}$ deviate from this general pattern; the highest Ca and Mg weathering-release fluxes occur in Santa Gracia followed by La Campana, Nahuelbuta, and Pan de Azúcar. These elevated fluxes in Santa Gracia are attributed to the initial bedrock mineralogy, with their high Ca and Mg concentration (Table S1).

hat gelöscht: pattern
hat gelöscht: that arose from different combinations of (micro-) climate and biota
hat gelöscht: are not discernible or, as is the case of La Campana, caused by anomalous
hat gelöscht: .
hat gelöscht: τ systematically
hat gelöscht: .
hat gelöscht: 4
hat gelöscht: the
hat gelöscht: and
hat gelöscht: ecosystems. The weathering release for
hat gelöscht: most plant-essential rock-derived mineral nutrient
hat gelöscht: $W^P_{regolith}$ in Pan de Azúcar, Santa Gracia, La Campana, and Nahuelbuta amounts to 1.3
hat gelöscht: , respectively, and those of the similarly plant-essential element
hat gelöscht:
hat gelöscht: Fig. 4
hat gelöscht: Table 3). $W^X_{regolith}$ of
hat gelöscht: follow the trend described for K and P. The weathering …
hat gelöscht: fluxes
hat gelöscht: both
hat gelöscht: K as well as
hat gelöscht: in Santa Gracia and Nahuelbuta
hat gelöscht: in a
hat gelöscht: range
hat gelöscht: severe
hat gelöscht: do
hat gelöscht: such that these elements'
hat gelöscht: are attained
hat gelöscht: weathering release
hat gelöscht: of Ca and Mg
hat gelöscht: bedrocks'
hat gelöscht: and

5.2 Availability of mineral nutrients to plants

The maximum amount of nutrients present can be assessed by determining their inventory in bulk regolith (I^{X}_{bulk}; Table 2, Eq. 8 and Appendix A). For most elements I^{X}_{bulk} is by far greatest in Santa Gracia (apart from K and Si; Table 4). I^{X}_{bulk} at the other three study sites are at similar levels. Element concentrations in the bio-available fraction are orders of magnitude lower than in the bulk regolith (Fig. A2 & A3, Table S3). Bio-available P in saprolite ($I^{P}_{bio\text{-}av,\ sap}$) is virtually absent in Pan de Azúcar and amounts to 21, 39, and 23 g m^{-2} in Santa Gracia, La Campana, and Nahuelbuta, respectively (Table 4). $I^{K}_{bio\text{-}av,\ sap}$ equals 253 in the northernmost, and 23, 70, and 19 g m^{-2} at the sites progressively southwards. The inventory of the remaining mineral nutrients in saprolite generally decreases from north to south. Accordingly, the total inventory (i.e. the sum of all determined inventories) is highest in Pan de Azúcar (5100 g m^{-2}), intermediate in Santa Gracia (2100 g m^{-2}) and La Campana (1600 g m^{-2}), and lowest in Nahuelbuta (140 g m^{-2}; Table 4). Note that $I^{X}_{bio\text{-}av,\ sap}$ was calculated over the uppermost 1 m of saprolite, whereas in fact the zone of mineral nutrient extraction might extend deeper. Bio-availability in soil features a similar trend. The total inventory is highest in Pan de Azúcar (2100 g m^{-2}), on par in Santa Gracia (960 g m^{-2}) and La Campana (1000 g m^{-2}), and despite featuring the thickest soils, lowest in Nahuelbuta (200 g m^{-2}). P deviates from this general trend: $I^{P}_{bio\text{-}av,\ soil}$ amounts to 3.3 g m^{-2} in Pan de Azúcar, 22 g m^{-2} in Santa Gracia, 28 g m^{-2} in La Campana, and 31 g m^{-2} and Nahuelbuta (Table 4). $I^{K}_{bio\text{-}av,\ soil}$ behaves differently, and amounts to 53, 38, 90, and 38 g m^{-2} in Pan de Azúcar, Santa Gracia, La Campana, and Nahuelbuta, respectively. Thus, K is almost equally available to plants in all four study sites.

5.3 Plant element composition and nutrient-uptake fluxes

Average elemental concentrations in bulk plants generally decrease from Pan de Azúcar towards Nahuelbuta. For example, the Al and Na concentrations in the plants of Pan de Azúcar reach 2700 and 34600 µg g^{-1}, respectively, compared with minima of 70 and 80 µg g^{-1} in Nahuelbuta. However, element specific deviations from this pattern exist (Table 5). The most prominent exceptions are those of P and K. Average P concentration increases from 290 µg g^{-1} in Pan de Azúcar to 1400 µg g^{-1} in Nahuelbuta. The average K concentration amounts to 6900, 6400, 12000, and 5400 µg g^{-1} along the north-south

hat gelöscht: 4
hat gelöscht: ecosystems
hat gelöscht: Table 2
hat gelöscht: , apart from K and Si, the inventory of potentially available elements
hat gelöscht: (
hat gelöscht: in
hat gelöscht: mostly
hat gelöscht: a
hat gelöscht: level. Note that only a minor fraction of this bulk nutrient inventory is readily bio-available. ¶ The element concentration
hat gelöscht: some
hat gelöscht: below
hat gelöscht: concentrations in
hat gelöscht: in
hat gelöscht: other study
hat gelöscht: further south, respectively. Bio-availability
hat gelöscht: is high
hat gelöscht: ,
hat gelöscht: low
hat gelöscht: Pan de Azúcar and
hat gelöscht: (
hat gelöscht: $I^{K}_{bio\text{-}av,\ sap}$
hat gelöscht: of most elements
hat gelöscht: , bar
hat gelöscht: few exceptions, increase from
hat gelöscht: to
hat gelöscht: . However,
hat gelöscht: bio-availability is
hat gelöscht: . Exceptions
hat gelöscht: are P and K.
hat gelöscht: and
hat gelöscht: and is as high as
hat gelöscht: in La Campana
hat gelöscht: , respectively
hat gelöscht:
hat gelöscht: the
hat gelöscht: 4
hat gelöscht: The exception is P, whose average concentration ... [2]
hat gelöscht: Azúcar to 1400

gradient. Thus, in Pan de Azúcar, Santa Gracia, and Nahuelbuta, average K concentrations are in a similar range, whereas in La Campana, K concentration in plants is almost 2x higher than in the other sites (Table 5). In Pan de Azúcar and Santa Gracia some elemental concentrations in plants are exceptionally high. This elevated mineral-nutrient storage is typical for plants growing in infertile habitats (Chapin III et al., 2011). Accumulation of such an internal nutrient pool allows for plant growth when conditions improve, e.g. during rare rain events (e.g. Chapin III, 1980; Chapin III et al., 2011; Vitousek et al., 1998). For example, high amounts of Al and Na are incorporated into plants tissues, though they may hinder plant growth at high concentrations (e.g. Delhaize and Ryan, 1995; Kronzucker and Britto, 2011). However, Al-toxicity is prevented in these plants by accumulation of correspondingly high amounts of Si that compensates the effects of Al (Liang et al. (2007). The exceptional high Na concentration in *N. mollis* in Pan de Azúcar is typical of the metabolism of *N. mollis* which is known to be covered with salt glands on their leaves, aiding to retrieve water by directly condensing moisture from unsaturated air (Rundel et al., 1980; Mooney et al., 1980).

The nutrient-uptake fluxes (U^{X}_{total}; Table 2, Eq. 4 and Appendix A) of P and K increase from north to south, such that U^{P}_{total} amounts to 5 ± 2, 70 ± 20, 170 ± 90, and 350 ± 100 mg m^{-2} yr^{-1} and U^{K}_{total} to 110 ± 40, 500 ± 200, 2000 ± 1000, and 1400 ± 400 mg m^{-2} yr^{-1} in Pan de Azúcar, Santa Gracia, La Campana, and Nahuelbuta, respectively (Table 3). U^{X}_{total} of the plant-essential elements Ca, K, Mg, Mn, P, and Sr exceed $W^{X}_{regolith}$ up to several times. U^{X}_{total} and $W^{X}_{regolith}$ are similar for Mg, Mn, and Sr in La Campana (Fig. 4; Table 3). U^{X}_{total} of the remaining plant-beneficial elements are, with the exception of Fe and Na in Pan de Azúcar, always lower than their release by weathering.

5.4 $^{87}Sr/^{86}Sr$ isotope ratios

Radiogenic Sr isotope ratios on bulk bedrock and regolith samples disclose mineral-weathering reactions and the incorporation of external sources into the regolith profiles. Moreover, $^{87}Sr/^{86}Sr$ in the bio-available fraction and plants reveal the plants' mineral nutrient sources.

In Pan de Azúcar, the $^{87}Sr/^{86}Sr$ ratio of average bedrock is 0.726 ± 0.002 (Fig. 5, Table 6). In regolith, $^{87}Sr/^{86}Sr$ differs significantly between the two profiles (0.728 ± 0.003 and 0.733 ± 0.003 on the north- and south-facing regolith profile, respectively) which can be attributed to varying degrees of atmospheric

hat verschoben (Einfügung) [1]

hat gelöscht:). The average K concentration amounts to 6900, 6400, 12000, and 5400 µg g^{-1} along the EarthShape climate and vegetation gradient from north to south. Thus, in Pan de Azúcar, Santa Gracia, and Nahuelbuta, average K concentrations are in a similar range, whereas in La Campana, K concentration in plants is almost twice as high compared to the other three sites. ¶
The nutrient-uptake fluxes of the two most important rock-derived mineral nutrients to plants, P and K,

hat gelöscht: steadily

hat gelöscht: Table 3). ¶

hat gelöscht: close to identical

hat gelöscht: Fig. 4

hat gelöscht: Table 3

hat gelöscht: apart from

hat gelöscht: 4

hat gelöscht: bulk regolith ranges from 0.723 to 0.737 and is distinct from

hat gelöscht: (

hat gelöscht: ; Fig. 5

hat gelöscht: The Sr isotope ratios differ

hat gelöscht: regolith

hat gelöscht: the

deposition ($^{87}Sr/^{86}Sr_{seaspray}$ = 0.7092; Pearce et al., 2015). The $^{87}Sr/^{86}Sr$ ratios in the bio-available fraction of saprolite and soil deviate by 0.02 from those of bulk bedrock and regolith but do not vary considerably between saprolite and soil, or between the north- and south-facing slopes. Bulk plant samples yield $^{87}Sr/^{86}Sr$ ratios of 0.710 and are thus indistinguishable from the $^{87}Sr/^{86}Sr$ ratio in the bio-available fraction (0.710 ± 0.001; Fig. 5, Table 6).

In Santa Gracia, the $^{87}Sr/^{86}Sr$ ratios in both bedrock and the regolith profiles do not differ significantly ($^{87}Sr/^{86}Sr_{rock}$ = 0.7039 ± 0.0004, $^{87}Sr/^{86}Sr_{regolith}$ = 0.7043 ± 0.0003; Fig. 5, Table 6). The radiogenic Sr composition of the bio-available fractions in saprolite and soil are identical within uncertainty, and no differences in $^{87}Sr/^{86}Sr$ between the north- and south-facing regolith profile are apparent. Plants yield an average $^{87}Sr/^{86}Sr$ ratio of 0.7062 ± 0.0001 and are thus indistinguishable from the bio-available fractions in saprolite and soil (Fig. 5, Table 6).

The bulk regolith $^{87}Sr/^{86}Sr$ ratio in La Campana ranges from 0.7051 in the north-facing to 0.7055 in the south-facing regolith profile. These ratios are lower than bedrock (0.7063 ± 0.0003; Fig. 5, Table 6) which can be attributed to the loss of a mineral with a high $^{87}Sr/^{86}Sr$ isotope ratio (e.g. biotite) beneath the sampled regolith profiles. The radiogenic Sr composition of the bio-available fraction in saprolite and soil amounts to 0.7051 and 0.7053, in the north- and south-facing slopes, respectively, and is within the range of bulk regolith. The average $^{87}Sr/^{86}Sr$ ratio in plants is 0.7059 and can be as high as 0.7063 in *Cryptocaria alba* (Table S7) and is thus higher than the soil and saprolite bio-available fractions. All these ratios are lower than in bulk bedrock.

In Nahuelbuta the radiogenic Sr isotope ratio in bedrock (0.716 ± 0.007) is in good agreement to those reported by Hervé et al. (1976) for the granitoid basement (0.717). However, the large spread among the bedrock samples implies petrological and geochemical heterogeneity of the Nahuelbuta mountain range (e.g. Hervé, 1977). Thus, $^{87}Sr/^{86}Sr$ in regolith is also variable (Fig. 5, Table 6 & S2). The $^{87}Sr/^{86}Sr$ ratios in both bio-available fractions in Nahuelbuta are restricted to a relatively narrow range in both regolith profiles, equal to 0.711 ± 0.002 and are indistinguishable from the mean ratio in plants (Fig. 5, Table 6). Individual plants' radiogenic Sr signature are distinct from each other and reflect the slope's bio-available fraction they grow on.

hat gelöscht:).
hat gelöscht: and
hat gelöscht: , respectively
hat gelöscht: ± 0.001; Fig. 5
hat gelöscht: deviate
hat gelöscht: from each other
hat gelöscht: Fig. 5
hat gelöscht: Fig. 5
hat gelöscht: N
hat gelöscht: This ratio is a substantially
hat gelöscht: in
hat gelöscht: 7061
hat gelöscht: Fig. 5
hat gelöscht:
hat gelöscht: depth of the
hat gelöscht: Here, the difference in the $^{87}Sr/^{86}Sr$ ratio between the north- and the south-facing regolith profile increases from bulk regolith to the bio-available fraction in saprolite and is highest in the soil bio-available fraction.
hat gelöscht: slightly
hat gelöscht: in
hat gelöscht: fraction
hat gelöscht: is remarkable and denotes to the high
hat gelöscht: chemical variability
hat gelöscht: subject to a high variability as well
hat gelöscht: Fig. 5
hat gelöscht: and amount
hat gelöscht: thus
hat gelöscht: ratios
hat gelöscht: Fig. 5

6 Discussion

6.1 The source of mineral nutrients

Comparing the radiogenic Sr composition of the bio-available fractions in saprolite and soil with that of bulk plant serves as a proxy for the nutrient sources of plants. At all four sites, the $^{87}Sr/^{86}Sr$ ratio in plants is largely indistinguishable within uncertainty to the bio-available fraction they grow on (Table 6), and no differences in $^{87}Sr/^{86}Sr$ between leaves, to twig, or stem are apparent (Table S5). Neither the plant $^{87}Sr/^{86}Sr$ ratio nor the $^{87}Sr/^{86}Sr$ ratio of the bio-available fraction is identical to that of bedrock or of bulk regolith. We conclude that plants obtain their Sr from the bio-available fraction rather than directly from primary minerals or from the atmosphere through leaves. Only La Campana showed evidence for a deep nutrient source (i.e. somewhere between the bottom of the regolith profile and unweathered rock) in the elemental-depletion pattern (Fig. A1). Here, deep-rooting plants (e.g. *Lithraea caustica*; Canadell et al., 1996) bypass the bio-available fraction of saprolite and soil and take up Sr with a higher proportion of radiogenic ^{87}Sr which has been released through biotite weathering beneath the regolith profiles. We can also use the $^{87}Sr/^{86}Sr$ ratio to identify the ultimate source of bio-available Sr. In the southernmost mediterranean and humid-temperate sites of La Campana and Nahuelbuta, the bio-available Sr is supplied by release from rock and regolith through weathering, albeit from specific minerals rather than bulk rock. In arid Pan de Azúcar the Sr pool in the bio-available fraction is formed by deposition from atmospheric sources (up to 93% seaspray contribution; Table 6). In semi-arid Santa Gracia, we found a possible combination of both sources (up to 43% seaspray contribution; Table 6).

Expanding our analysis of the source of mineral nutrients to include other plant-essential (P, K, Ca, Mg, Mn) and plant-beneficial (Al, Fe, Na, Si) elements, we normalized both the mineral nutrient concentrations in plants (Table 5) and those in the bio-available fraction in saprolite and soil (Table S3) by the most-demanded mineral nutrient P (Fig. 6). This removes differences in concentrations induced by the very different matrices of regolith and plant. In this analysis, an element X that plots on the 1:1 line would have the same X:P ratio in plants and in the bio-available fraction. In turn, any deviation from that line would indicate positive or negative discrimination of an element contained in the regolith bio-available fraction by plants relative to P. We find a good correlation in the X:P ratios for all elements,

hat gelöscht: 5

hat gelöscht: 5

hat gelöscht: The

hat gelöscht: along

hat gelöscht: those

hat gelöscht: plants'

hat gelöscht: . In all four study sites,

hat gelöscht: take up

hat gelöscht: . In the arid site Pan de Azúcar this Sr pool is formed by Sr deposition from atmospheric sources (e.g. up to 93% seaspray contribution; Table 6). In the mediterranean and humid sites of La Campana and Nahuelbuta, respectively, the bio-available Sr is supplied by release from rock and regolith through weathering. In semi-arid Santa Gracia, we found a combination of both sources (up to 43% seaspray contribution; Table 6). In La Campana we found evidence for a deep nutrient source (located

hat gelöscht: (e.g. *Lithraea caustica*; Canadell et al., 1996)

hat gelöscht: **5.2 Are nutrient sources setting plant stoichiometry?**¶
We expand the analysis of the source and demand of mineral nutrients, which in the preceding section was based solely on Sr as plant-essential element, to all other plant-essential (P, K, Ca, Mg, Mn) and plant-beneficial (Al, Fe, Na, Si) elements. We note that the ecosystems in the EarthShape study sites are mostly N-limited (Stock et al., 2019), yet we consider the essential mineral nutrients to be potentially co-limiting. To do so, we first evaluate whether "ecological stoichiometry" has been attained by the plants. Ecological stoichiometry suggests that, similar to ocean microbial biomass, an optimum C:N:P ratio is attained – the "Redfield ratio" (e.g. Redfield, 1934). However, it is less clear whether such stoichiometrical pattern is also valid for terrestrial ecosystems, and for other elements besides C, N, and P (Cleveland and Liptzin, 2007; Sardans et al., 2011). As pointed out by several authors (e.g. Elser et al., 2010; Geider and La Roche, 2002; Hillebrand et al., 2014; White et al., 2006), photoautotrophs only exploit a weak stoichiometric homeostasis. Hence, the elemental composition in plants (i.e. ecological stoichiometry; Sterner and Elser, 2003) is mainly set by the nutrient-supplying reservoirs ('you are what you root in model'; Elser et al., 2010), and only to a second order by homeostasis. Evidence for this suggestion was provided by Uhlig and von Blanckenburg (2019) for a large number of mineral nutrients. In that study, it was shown that the plant-available fraction in saprolite and soil is well correlated with the ecological stoichiometry in two forested ecosystems and that deviations from that trend may have been driven by demand.¶
As an evaluation of the hypothesis that the nutrient reservoir sets plant stoichiometry we normalized both the mineral nutrient concentrations in plants (Table 5) and those in the bio-available fraction in saprolite and soil (Table S3) by the most plant-essential mineral nutrient P (Fig. 6). In this analysis, an element X that plots on the 1:1 line would fulfill the entirely hypothetical condition of being perfectly co-limited and that its relative composition is set by the relative composition in the plant-available fraction (i.e. "optimum" stoichiometric range). Such pattern would be similar to an ocean Redfield ratio in which a C:N:P ratio is identical between seawater and marine micro-biota (Capek et al., 2018; Moore et al., 2013). Elements that plot beneath the 1:1 line are available in excess in the ... [3]

and the ratios found in plants reflect those in the bio-available regolith fraction to within one order of magnitude. We interpret this correlation to confirm nutrient uptake mainly from the bio-available fraction. We also note that the X:P ratios increasingly approach the 1:1 line with increasing NPP from Pan de Azúcar to Nahuelbuta and the agreement is more pronounced in soil than in saprolite. We interpret these shifts to denote the increasing significance of recycling, a topic we return to in the next section.

6.2 An increase in nutrient recycling with NPP

In Section 5.1.2 we established that neither total weathering rate W, nor elemental weathering rates $W^X_{regolith}$, correlate with NPP. Only at La Campana weathering rates are elevated, as expected from the higher denudation rate. Santa Gracia and Nahuelbuta, have similar denudation rates and element release rates by weathering $W^X_{regolith}$, yet elemental uptake rates U^X_{total} of the plant-essential nutrients P, K, and Ca increase between a factor of two and five (Figure 4). We examine these correlations in more detail in Section 6.5. Here we first focus on the question: How is nutrient demand satisfied at the more vegetated sites?

Recycling of mineral nutrients is the key mechanism enabling differences in NPP. We quantified recycling by the nutrient recycling factor Rec^X (Table 2, Eq. 7 and Appendix A; Table 7; note that in this discussion we use the Rec^X calculated for $W^X_{regolith}$ from rock weathering, whereas in Table 7 and Fig. A4 we also show Rec^X including atmospheric inputs in Pan de Azúcar). The amplitude of recycling varies from nutrient to nutrient and site to site. In the arid Pan de Azúcar, nutrients are primarily recycled via photodegradation of shrubs (e.g. Gallo et al., 2006; Day et al., 2015). In the remaining sites Rec^X increases from Santa Gracia to Nahuelbuta and is highest for the plant-essential elements Ca (increasing from 1 to 6), K (increasing from 6 to 15), and P (increasing from 5 to 30; Table 7). Thus, despite having the smallest nutrient inventory of bio-available nutrients (Table 4) but the highest NPP, Nahuelbuta can at least partially satisfy its nutrient requirements through efficient nutrient recycling. In contrast, in the (semi-) arid sites, where the bio-available pool is larger, plants forage nutrients by deep rooting from depth (McCulley et al., 2004).

The Rec^X metric reflects a mass balance between the total weathering zone and the total vegetation cover but does not yield insight to the mechanisms of recycling. The elemental stochiometric considerations

hat gelöscht: of the most plant-essential mineral nutrients is the key mechanism enabling differences in NPP despite near-constant

hat gelöscht: . As seen in Figure 4 elemental uptake rates U^X_{total} of the most plant-essential nutrients P, K, and Ca increase in spite of rather uniform release rates from

hat gelöscht: to

hat gelöscht:

hat verschoben (Einfügung) [2]

hat gelöscht: by the

hat nach oben verschoben [2]: recycling factor Rec^X (Table 2, Eq.

hat gelöscht: 7

hat gelöscht: ; note that in this discussion we use the Rec^X calculated for $W^X_{regolith}$ from weathering only. In Table 7 and Fig. A4 we also show Rec^X including atmospheric inputs). For example, K is recycled 3 times through biomass after release by weathering at the arid site and 15 times at the humid site. P is recycled 4 times in the arid site, and 30 times in the humid site. Ca shows a similar, albeit weaker difference. Moreover, we found evidence that recycling of K through plants (Fig. 4) increases its availability in soil relative to saprolite over the entire climate gradient (Fig. 6). ¶
Furthermore, with increasing recycling efficiency (Table 7) the nutrient pools in the bio-available fraction are increasingly dominated by the pool of recycled nutrients, thus shifting the stoichiometry in the bio-available fraction with increasing proportion of recycling successively towards the stoichiometry in vegetation (Fig. 6). In other words, over the course of several recycling loops, the chemical composition of the bio-available fraction and biota eventually approaches a ratio close to the relative requirement of the ecosystem for the different nutrients (Vitousek et al., 1998), ultimately resulting in a virtually almost perfect stoichiometric yield (Sterner and Elser, 2003). P also obtains an increasingly biocycled speciation where the total organic P fractions increase strongly along the gradient (Brucker and Spohn, 2019). In Nahuelbuta Ca, K, Mg, and Sr are taken up in excess over P. Here, organic-bound P is not as easily available, whereas the plant-availability of these elements might increase due to the higher potential for solubilization at the lower pH in soil (soil pH = 4 – 4.5; Bernhard et al., 2018). Thus, the amplitude of recycling varies from nutrient to nutrient and site to site (Table 7). In the arid Pan de Azúcar, nutrients are primarily being recycled after photodegradation of shrubs (e.g. Gallo et al., 2006; Day et al., 2015). In the remainder sites Rec^X increases from Santa Gracia to Nahuelbuta and is highest for the plant-essential elements Ca, K, and P (Table 7). Thus, despite having the smallest nutrient inventory of bio-available nutrients but highest NPP of these sites, the ecosystem of Nahuelbuta can at least partially maintain its nutrient requirements through efficient nutrient recycling. ¶
Particular conditions of plant nutrition prevail at the arid sites. In Pan de Azúcar and Santa Gracia elemental concentrations in plants are exceptionally high (bar P and K; Table 5), even though these sites' nutrient-availability through weathering and water availability is generally low (Table 3 & S2). This elevated mineral-nutrient storage is typical for plants growing in infertile habitats. Through such intermediate storage, plants accumulate an internal nutrient pool that is available for homeostasis when growth conditions eventually improve during, for example, rare rain events (e.g. Chapin III, 1980; Chapin III et al., 2011; Vitousek et al., 1998). High amounts of Al [4]

presented above show that recycling is indeed fed from plant material accumulated in soil (Lang et al., 2017). With increasing recycling the nutrient pools in the soil bio-available fraction are increasingly dominated by the pool of recycled nutrients, thus shifting the X:P ratio in the bio-available fraction successively towards the X:P ratio in vegetation (Fig. 6). In other words, over the course of several recycling loops, the chemical composition of the bio-available fraction and biota eventually approaches a ratio close to the relative requirement of the ecosystem for the different nutrients (Vitousek et al., 1998).

6.3 Processes that set the size of the bio-available pool

In none of our sites is the bio-available nutrient pool entirely depleted (Table 4), but its elemental concentrations strongly shift along the gradient. The concentrations of the plant-essential mineral nutrients K, Ca, and Mg in saprolite are highest in the arid site, lower in the semi-arid and mediterranean site, and lowest in the humid-temperate site. The element concentration in the bio-available fraction translates into the size of the inventory, quantifying the pool size (note, however, that the true inventory can in fact be larger than the 1 m inventory that we have used for its calculation. This is suggested by the elevated $^{87}Sr/^{86}Sr$ ratios in plants at La Campana suggesting extraction of a pool beneath the bio-available upper saprolite). The bio-available pool represents the link between the organic and the geogenic pathway. That is because weathering in the geogenic pathway supplies elements that plants take up and recycle in the organic pathway (Uhlig and von Blanckenburg, 2019). We thus briefly review the potential processes that may set the pool size.

If a bio-available pool is in conceptual steady state, input fluxes and loss fluxes balance. Over millennial time scales or longer, we consider that such a balance must exist, as otherwise a pool might become depleted. In this case the inventory of the pool is set by the input fluxes of an element and a first-order rate constant that describes the relationship between the loss flux as a function of element inventory and thus the retention capacity. Essentially it is the inverse of the turnover time of an element. Biotic processes likely contribute towards setting this retention capacity directly or indirectly, a topic we return to below. Given that elemental weathering fluxes $W^{X}_{regolith}$ do not correlate with pool size we assume that retention capacity sets the pool size.

hat nach oben verschoben [1]: be covered with salt glands on their leaves, aiding to retrieve water by directly condensing moisture from unsaturated air (Rundel et al., 1980; Mooney et al., 1980). ¶

hat gelöscht: **5.4 How the organic and the geogenic nutrient pathway**

hat gelöscht: **bioavailable**

hat gelöscht: Both our data on ecological stoichiometry and the radiogenic Sr isotopic composition suggest that the bio-available pool in saprolite and soil feeds plants.

hat gelöscht:).

hat gelöscht: most

hat gelöscht: and bio-available

hat gelöscht:

hat gelöscht: calculated to allow a comparison.

hat gelöscht: Regardless, given that neither these pool sizes nor the concentrations of the bio-available elements correlate with elemental release rates $W^{X}_{regolith}$, gradients in pool sizes cannot solely be explained by differences in weathering rate. Further, the differences in the pool size cannot be explained by the lack of fresh primary minerals. All four sites represent kinetically limited weathering regimes (Oeser et al., 2018) such that primary minerals are permanently available for dissolution and in turn for replenishing the bio-available pool. We thus consider next pedogenic properties as pool size-controlling factors.

A first potential control over element retention capacity are pedogenic properties. The decrease of soil pH from 8 at the arid site to 4 at humid-temperate site (Bernhard et al., 2018) might cause the decrease in the bio-available divalent base cations Mg, Ca, and Sr. Conversely, the decrease in pH could be the result of the loss of these elements and thus their pH buffering capacity. Another possibility is the degree of complexing of elements to organic molecules. Such complexing might lead to either higher retention, or higher loss, depending on the element. Organic complexing is likely more pronounced in the mediterranean and humid-temperate sites where soil organic carbon concentrations are higher compared to the (semi-) arid sites (Bernhard et al., 2018). However, elements like Al and P, which are readily complexed, are available in higher concentration in the humid-temperate and mediterranean sites than in the other two sites. Differences in water flow is the third cause we discuss. Where fluid residence times are long, concentrations of solutes are more likely to be at equilibrium with secondary minerals (Maher and Chamberlain, 2014) and the bio-available fraction, formed by precipitation and sorption from pore fluids, can build up. We consider this to be the case in the low-precipitation sites. At sites with high MAP regolith fluids may be diluted, and thus desorb elements from the bio-available pool. Such a dilution effect might be in effect at Nahuelbuta for elements like Mg and Ca. At Nahuelbuta these are also the elements with the lowest bio-available inventory. We thus consider water flow to be the main factor governing the size of the bio-available pool.

6.4 Concepts for biotas role in setting fluxes in the geogenic and the organic nutrient cycle

Even if negligible on ecological timescales, ecosystems experience losses of nutrients through erosion (e.g. Heartsill Scalley et al., 2012) and as solutes (e.g. Chaudhuri et al., 2007). To prevent bio-available nutrients becoming depleted over longer timescales, the pool must be replenished (Uhlig and von Blanckenburg, 2019). Biological mechanisms comprise two means to regulate this delicate balance between nutrient replenishment by weathering and plant uptake. The first is by adjusting the recycling of nutrients, as shown in Section 6.2. At Nahuelbuta, where the bio-available pool is smallest, nutrient recycling rates are the highest. If the bio-available pool is small, plants may invest energy into re-using P and other elements from leaf litter, rather than foraging P at depth which is associated with higher energy expenditure (Andrino et al., 2019). This is a component of the organic nutrient cycle. The biochemical

hat gelöscht: However

hat gelöscht: in turn

hat gelöscht: are

hat gelöscht: concentrations of

hat gelöscht: at the mediterranean and the humid sites compared to the arid sites. We regard this cause as unlikely as those elements like Al, Fe(III), and P that are readily complexed and thus lost as organic complexes are higher in the humid and mediterranean sites than the other two sites. The cation exchange capacity CEC_{eff} (Table 1; Bernhard et al., 2018) exceeds the element concentration in the bio-available fraction in the semi-arid (85 $\mu mol_C\ g^{-1}$ vs. 35 $\mu mol\ g^{-1}$), mediterranean (80 $\mu mol_C\ g^{-1}$ vs. 40 $\mu mol\ g^{-1}$), and humid-temperate (30 $\mu mol_C\ g^{-1}$ vs. 6 $\mu mol\ g^{-1}$) site. Thus, exchange sites are available in excess and do not set the maximum pool size. As a result where fluid residence times are long the bio-available fraction, formed by precipitation and sorption from pore fluids, is likely close to equilibrium with regolith fluid (Maher and Chamberlain, 2014). Only at sites with high MAP regolith fluids might be diluted and deviate from a chemostatic behavior (e.g. Godsey et al., 2019), and these fluid concentrations will be below equilibrium concentrations. No discharge data is available for the EarthShape sites, but with MAP slightly > 1000 mm yr^{-1} a dilution effect might be in effect at Nahuelbuta for elements like Mg and Ca that tend to switch from chemostatic to dilution behavior at high discharge (e.g. Godsey et al., 2019). At Nahuelbuta these are also the elements with the lowest bio-available inventory and are thus possibly present in concentrations below equilibrium there.¶
The third possibility is that the inventory of a bio-available nutrient pool is set by the rate at which an element is extracted into plants from regolith relative to its replenishment by weathering. For a given bio-available reservoir an increase in uptake rate (Fig. 4; Table 3) will decrease the turnover time, or residence time of mineral-derived nutrients in the soil bio-available fraction ($T^X_{bio-av.soil,U}$; Table 8). For all important mineral nutrients, we see a decrease in turnover time of the bio-available soil pool with respect to uptake from the arid to the humid sites. Short turnover times with respect to uptake also reflect fast recycling. The humid-temperate ecosystem in the south of our ecological gradient is dominated by this "organic nutrient cycle".¶
Yet the organic nutrient cycle alone cannot be separated from its geogenic counterpart, because as discussed above the regolith nutrient pool is subject to losses by desorption and runoff, and these we consider to be quantified by the elemental weathering release flux $W^X_{regolith}$. Another loss trajectory not included in $W^X_{regolith}$ might be erosion of solid plant matter (Uhlig et al., 2017). To prevent the bio-available nutrient stocks from eventually running into depletion over longer timescales, the pool needs to be replenished. This replenishment takes place either by exogenous inputs

mechanisms of nutrient-recycling are beyond the scope of this paper, but are thought to be related to leaf litter quality (Hattenschwiler et al., 2011), soil fungal and bacterial communities (Fabian et al., 2017; Lambers et al., 2008), and plant diversity (Lambers et al., 2011; Oelmann et al., 2011; van der Heijden et al., 1998).

The second means for biota to influence the bio-available pool is via the geogenic pathway. Nutrient replenishment may take place either by exogenous inputs (e.g. Boy and Wilcke, 2008; Porder et al., 2007; Vitousek, 2004; Vitousek et al., 2010), or by weathering of primary minerals (Uhlig et al., 2017; Uhlig and von Blanckenburg, 2019). In arid Pan de Azúcar, where weathering-release fluxes are low, these pools are being replenished by the deposition of atmospheric sources (up to 93%; Table 6). In the other study sites the bio-available pools are replenished by weathering of rock and regolith. The timescales $T^{X}_{bio-av,W}$ of replenishment from weathering are long, and typically orders of magnitude longer than their turnover times with respect to plant uptake $T^{X}_{bio-av,U}$. For example, the inventory of K in the bio-available soil pool at Nahuelbuta is turned over every 30 years between soil and plants, but it takes 400 years to be replenished in its entirety by weathering (Table 8). Previous models in ecosystem science (e.g. Bormann et al., 1969; Vitousek and Reiners, 1975; Vitousek et al., 1998) suggest that increasing nutrient demand will eventually lead to tightly coupled recycling loops such that nutrient losses will be minimized, and plant nutrition is sustained. Our data is also consistent with a relationship between demand (i.e. NPP) and recycling efficiency.

If recycling indeed exerts the dominant role in the supply of mineral nutrients, then we need to revisit the significance of biogenic weathering towards the nutrition of plants. The direct and indirect impacts of plants and their associated microbiota on weathering is well-documented and can be categorized into four suites of processes: (*A) Direct primary mineral dissolution by ectomycorrhizal fungi.* Ectomycorrhizal fungi can directly extract nutrients such as P, K, Ca, Mg, and Fe from minerals distant from the root, even under dry conditions, and thereby actively increase mineral dissolution kinetics. Laboratory dissolution experiments (Balogh-Brunstad et al., 2008b; Gerrits et al., 2020; Kalinowski et al., 2000), plant growth mesocosms (Bonneville et al., 2011; Smits et al., 2012), and deployment of minerals within the soil of natural ecosystems (Balogh-Brunstad et al., 2008a) all show either evidence for mineral dissolution by mycorrhiza, or quantify an increase in mineral dissolution over abiotic controls. Whether these short-term

hat gelöscht: , or by weathering of primary minerals at depth (Uhlig et al., 2017; Uhlig and von Blanckenburg, 2019). This replenishment is the "geogenic nutrient pathway". In the arid Pan de Azúcar, where weathering-release fluxes are low, these pools are being substantially replenished by the deposition of atmospheric sources (up to 93%;

hat gelöscht: being

hat gelöscht: $T^{X}_{bio-av.soil,W}$ over which this

hat gelöscht: occurs do not deviate much between semi-arid, mediterranean

hat gelöscht: humid-temperate climates, bar a few exceptions (Table 8). For Ca, Mg, and Sr these turnover times are within the same range as turnover times with respect to plant uptake, meaning these elements reflect a delicate balance between supply and nutrient demand. For P and K they are sometimes

hat gelöscht: .

hat gelöscht: replenish their external losses

hat gelöscht: . The turnover times of the bio-available fraction in saprolite with respect to weathering (calculated here for an inventory of the uppermost meter), decrease from the semi-arid, mediterranean, to the humid-temperate site for the elements Ca, Mg, K, and Sr (but not for P). The weathering turnover times

hat gelöscht: the south are lower because of the lower bio-available inventories, given

hat gelöscht: supply rates by weathering do not differ as much as the inventories.¶
A key observation of these considerations is the decrease in the saprolites' bio-available pool in K, Mg, and Ca from the dry to wet sites, the increase in the organic nutrient cycle as reflected by decreasing turnover times with respect to plant uptake and

hat gelöscht: ratios, all in the face of similar weathering supply rates of nutrients. We speculate

hat gelöscht: soil chemical properties and water discharge are of subordinate importance in setting the size of the bio-available regolith pool. Instead, we consider plants and their nutrient demands to primarily control its size. If true, biological mechanisms need to be in place that regulate this delicate balance between nutrient replenishment by weathering and plant uptake in the ecosystems of Santa Gracia, La Campana, and Nahuelbuta, in order to prevent the nutrient pools from entire depletion

hat gelöscht: **5.5 Is weathering modulated by biota?**¶ ... [5]

hat gelöscht: e.g. Godsey

hat gelöscht: 2019; Maher and Chamberlain, 2014

hat gelöscht: . High NPP is thought to raise $W^{X}_{regolith}$ as well

hat gelöscht: e.g. Berner

hat gelöscht: 2003; Brantley

hat gelöscht: 2011; Buss et al., 2005; Kelly et al., 1998; Porder, 2019; Schwartzmann, 2015

hat gelöscht: . Indeed, plants and their associated micro-biota do enhance weathering rates in a direct and indirect way. (1) Deep plant ... [6]

experiments can be extrapolated to the millennial time scales of the geogenic nutrient pathway is not obvious (review by Finlay et al., 2020). Over these time scales, mineral dissolution is often slowed by the development of nanoscale layers at the interface (Gerrits et al., 2020) or coatings by secondary precipitates (Oelkers et al., 2015). Slowing of mineral dissolution with time, known from weathering zone studies, has also been attributed to coating by secondary precipitates (White and Brantley, 2003), or to chemical saturation of pore fluids (Maher, 2010). *(B) Roots deepening regolith thickness*. Tree roots can physically penetrate and biogeochemically alter the immobile regolith underlying mobile soil (Brantley et al., 2017). They can take water up from depth, recycle water to depth for storage, or provide pathways in which water bypasses rather than infiltrating the shallow regolith (Fan et al., 2017). Deep roots aid nutrient transfer from the subsoil to shallow levels (Jobbágy and Jackson, 2004). *(C) Canopy and roots converting precipitation into evapotranspiration* (Drever and Zobrist, 1992). In sites with higher vegetation cover, water vapor is recycled and does not immediately enter runoff. By providing canopy, trees both modulate infiltration while turning water back into transpiration (Ibarra et al., 2019). For example Ibarra et al. (2019) have shown that total runoff can decrease by up to 23% as vegetation cover increases from barely vegetated to highly vegetated sites. Water recycling hence decreases total runoff and potentially reduces weathering-release fluxes in the highly vegetated sites. (D) *Increasing mineral solubility by release of soil CO_2 and organic complexing agents.* Through the respiratory release of soil CO_2 and excretion of organic complexing agents, plants, hyphae, and their associated microbiota can increase the solubility limits of primary and secondary minerals by a factor of up to <10 (Perez-Fodich and Derry, 2019; Winnick and Maher, 2018). If dissolution is not kinetically limited, we would indeed expect higher solute concentrations with higher soil CO_2, and hence higher dissolution rates of primary minerals (Winnick and Maher, 2018).

Studies of biogenic weathering in natural Critical Zone systems struggle to disentangle expressions of these biogenic drivers of weathering rates from various competing drivers of weathering. Although the sites were selected to minimize potential confounding effects, this study also faces this challenge. We turn to a statistical approach in isolating any potential biogenic weathering signal.

6.5 Is weathering modulated by biota? A statistical analysis

To single out the possible biogenic weathering driver from the confounding factors at the EarthShape sites we used correlational statistics between indicators of weathering and metrics for its potential drivers along the EarthShape gradient. We determined Pearson correlation coefficients to determine how the degree of weathering (CDF, τ^X) and the flux of weathering (W, $W^X_{regolith}$) depend on denudation rate D, water availability (approximated by mean annual precipitation, MAP), and biomass growth as quantified by net primary productivity (NPP). See Appendix B for a detailed description on statistical analysis and Table A1, A2, and A3 for the results. We used these statistics to evaluate three starting hypotheses that reflect the basic confounding factors: (1) Where denudation rate D is high bulk weathering fluxes are high, since minerals with fast dissolution kinetics, such as plagioclase and P-bearing apatite, are supply limited (Dixon et al., 2012; Porder et al., 2007). Where D is high, regolith residence times are low such that τ^X for elements not mostly contained in rapidly dissolving minerals are not depleted. (2) At sites at which MAP and hence runoff is high, weathering fluxes are high. This is because weathering rate is proportional to runoff for the chemostatic elements that comprise the bulk of the weathering flux, amongst them Si that contributes roughly half of the flux (e.g. Godsey et al., 2019; Maher and Chamberlain, 2014). As a result, CDF and τ^X will also be high. τ^X of soluble elements (e.g. Na) will be higher at higher runoff than τ^X of elements that strongly partition into secondary phases. (3) If NPP is high the degree (CDF, τ^X) and rate of weathering (W, $W^X_{regolith}$) will be high (e.g. Berner et al., 2003; Brantley et al., 2011; Buss et al., 2005; Kelly et al., 1998; Porder, 2019; Schwartzmann, 2015), for the reasons predicted in Section 6.4. In support of hypothesis (1) we find that total and elemental weathering rates correlate well with D (the average of the correlation coefficients is r (10) ~ .88, p < .01; Table A1) and only a weak correlation relates denudation rate with the degree of weathering and elemental depletion. Thus, denudation rate is the predominant driver of weathering rate. However, D itself is also correlated with MAP and NPP. To evaluate whether D is nevertheless the main driver we exclude the La Campana site of unusually high D. The correlations between W, $W^X_{regolith}$, and D are still significant (the average of the correlation coefficients is r (7) ~ .72, p < .05; Table A2) confirming that D is the main driver of weathering rate. Concerning hypothesis (2), neither the degree nor rates of weathering correlate with MAP. Only the

soluble element Na becomes more depleted (τ^{Na}: r (7) = .73, p < .05; Table A2) at higher MAP. Thus, a competing effect seem to counteract the expected increase in weathering rate with precipitation. As NPP is an output of the LPJ-GUESS model for which MAP is the basis, it is no surprise that both parameters are strongly correlated (r (7 – 10) ~ 1.00, p < .01; Table A1 & A2). We would thus expect the same strong relationship between the degree and rates of weathering and NPP as with MAP. This is indeed the case. However, weathering release rates $W^{X}_{regolith}$ for elements like Na, P, and Si correlate slightly more strongly with NPP (the average of the correlation coefficients is r (7) ~ .62, p < .05; Table A2) than with MAP (the average of the correlation coefficients is r (7) ~ .51, p > .05; Table A2). This is the only indication that biomass growth exerts any control over weathering at all. In summary, neither MAP nor NPP seem to have a major impact on the degree and rates of weathering, and D is the main driver of total and elemental weathering rate at the EarthShape sites.

In this analysis we have not evaluated the potential confounding effects of differences in bedrock mineral composition. Because of the lack of an unequivocal metric allowing a statistical evaluation of the resulting differences in rock weatherability we focus on a comparison between the two study sites in semi-arid (Santa Gracia) and humid-temperate climate (Nahuelbuta). At these two sites, denudation rates (15 – 48 t km^{-2} yr^{-1}) and soil residence times (22 – 28 kyr; Schaller et al., 2018b) are similar. Although both granitoid, bedrock between the two sites differs. Santa Gracia is underlain by diorite, a mafic rock, while Nahuelbuta is underlain by granodiorite (Oeser et al., 2018). Thus, the suite of primary minerals in Santa Gracia is more prone to weathering than in Nahuelbuta. Specifically, this means a higher amount of plagioclase and amphibole, and less unreactive quartz, at Santa Gracia. These differences in predominantly Ca- and Mg-bearing minerals are reflected in higher Ca and Mg inventories in bulk regolith in Santa Gracia (Table 4) , that also translate into higher Ca and Mg weathering fluxes (Table 3). Total soil weathering rates (5 – 10 t km^{-2} yr^{-1}; Table 1), and differences in weathering properties are not statistically significant (Table A3). The weathering-release fluxes (Fig. 4, Table 3) for K, Na, P, and Si are similar despite massive differences in vegetation cover, NPP, and even MAP (Table 1 & A3). These similarities, and the higher weathering fluxes of Ca and Mg at Santa Gracia can be explained with the confounding effects of higher rock weatherability at Santa Gracia and the higher precipitation at Nahuelbuta. A comparison of concentration-discharge relationships between catchments underlain by

mafic (basaltic) and granitoid rock (Ibarra et al., 2016) shows higher solute concentrations for all major elements in the basaltic catchments at a given runoff, and the preservation of chemostatic solute concentrations to higher runoff than in granitoid catchments. As a result, weathering fluxes in mafic catchments at low runoff are similar to fluxes from granitoid rock subjected to high runoff, as we observe at Santa Gracia and Nahuelbuta. Regardless, an increase in either weathering rate or degree of weathering at Nahuelbuta resulting from the 3.5 times higher NPP at Nahuelbuta is not discernible.

6.6 Do negative feedbacks decouple biomass growth from weathering rate and degree?

Why do neither the degree nor the rate of weathering increase with NPP or MAP, nor does higher biomass growth overwhelm differences in rock mineralogy? Nutrient recycling may be the mechanism that decouples weathering from NPP, as shown in Section 6.2. Even so, the higher runoff results in a greater loss of nutrients from the bio-available pool and thus requires higher weathering rate to balance the loss. We thus speculate that the increased vegetation cover might even counteract a potential increase in weathering that would be caused by the increase in MAP, essentially damping the geogenic pathway. We return to the four suites of processes as outlined in Section 6.4 on the direct and indirect impacts of plants and their associated microbiota on weathering and discuss their potential operation at the EarthShape sites.

(A) Direct primary mineral dissolution by ectomycorrhizal fungi. As yet we have no direct observations on nutrient foraging by fungi and other microbes in regolith from the EarthShape sites as obtained on other mountain sites in Chile (Godoy and Mayr, 1989). Proxies for total microbial biomass in saprolite do not increase along the gradient: total gene copy numbers have similar ranges from Santa Gracia to Nahuelbuta, and DNA amounts even decrease slightly (Oeser et al., 2018). Common strategies of microbial symbionts with tree roots suggest that energy investment into nutrient recycling from leaf litter is more advantageous than dissolving primary minerals (Andrino et al., 2019). Thus, we would expect that mycorrhiza predominantly aid recycling in Nahuelbuta. In Santa Gracia, however, the absence of a litter layer may prompt the subsurface fungal network to invest in primary mineral dissolution, adding microbial weathering to total weathering at that that site.

(B) Roots deepening regolith thickness. A detailed survey of rooting depth along the gradient has not been completed, but deep roots were not observed in Santa Gracia whereas in Nahuelbuta and La Campana, individual roots reach several meters into the saprolite. A and B horizons in Santa Gracia are shallow (20 – 40 cm), whereas they are deep in Nahuelbuta (80 – 100 cm; Bernhard et al., 2018; Oeser et al., 2018). We do not know the depth of the weathering front which appears to be at least a dozen of meters depth or more at both sites. Thus, deep rooting can benefit plant growth by increasing the size of the bio-available pool.

(C) Canopy and roots converting precipitation into evapotranspiration. Along the EarthShape transect the potential 23% reduction in runoff predicted by Ibarra et al. (2019) is minor considering the 100-fold increase in precipitation over the entire gradient. A larger effect may occur if roots provide preferential flow paths such that infiltrating water bypasses the regolith matrix available for weathering (Brantley et al., 2017). However, given the deep weathering fronts - likely beneath rooting depth - we consider this effect to be minor, or even acting to increase deep weathering. Thus, we consider the hydrological impact of plants on weathering to be minor along the gradient.

(D) Increasing solubility by release of soil CO_2 and organic complexing agents. Although with increasing NPP soil respiration of CO_2 should lead to increased primary mineral dissolution, plants potentially impose a negative feedback onto this dependence by influencing the silicon cycle. Because silicon is the most abundant element in felsic rock and regolith (besides oxygen), it exerts a major control on the total weathering fluxes. The Si concentration in the bio-available pool is key in setting the saturation with respect to the various dissolving and precipitating minerals in regolith. Plants can impact this pool in both directions. Some plant species accumulate Si by active transporter-mediated uptake or through passive uptake within the transpiration stream, whole others exclude Si and avoid accumulation (Ma and Yamaji, 2008; Schaller et al., 2018a). Enhanced Si uptake from soil solution by Si accumulating plants would result in Si undersaturation of solutions with respect to secondary minerals and would thus result in an increase in weathering rates. However, this increase may be damped. That is because these plants would also convert silicon into biosilica (e.g. phytoliths). If returned to soil in plant debris this biosilica becomes a key factor in the stability of secondary minerals (e.g. kaolinite; Lucas, 2001). However, neither factor seems to be the case: In the EarthShape sites, the average Si concentration in the above-ground living

hat gelöscht: While a
hat gelöscht: EarthShape
hat gelöscht: done,
hat gelöscht: (La Campana and)
hat gelöscht: reached up to
hat gelöscht: depth
hat gelöscht: Oeser et al., 2018;
hat gelöscht: making a higher nutrient inventory
hat gelöscht: .
hat gelöscht: *(2) Canopy and roots converting precipitation into evapotranspiration*. In sites with higher vegetation cover, water vapor is being recycled and does not immediately enter runoff. By providing canopy, trees can modulate infiltration whereas they turn water back into transpiration (Ibarra et al., 2019). For example Ibarra et al. (2019) have shown that total runoff can decrease by up to 23% as vegetation cover raise from barely vegetated towards highly vegetated sites. Such an effective water recycling hence decreases total runoff and potentially reduces weathering-release fluxes in the highly vegetated sites of La Campana and Nahuelbuta. However, along the EarthShape transect this potential total 23% reduction is a minor effect when considering the 100-fold increase in precipitation over the entire gradient. A larger effect might be presented by roots if they provide preferential flowpaths such that infiltrating water either bypasses the regolith matrix available for weathering (Brantley et al., 2017). However, given the deep weathering front at the EarthShape sites that is likely beneath rooting depth we consider this effect to be minor too, or in the contrary might even increase deep weathering. Thus, we consider the impact of plants on the hydrology that is relevant to weathering to be minor along the EarthShape gradient.¶ *(3) Increase in primary mineral dissolution by ectomycorrhizal fungi*. As yet we have no direct observations on nutrient foraging by fungi and other microbes in regolith from the EarthShape sites as obtained on other mountain sites in Chile (Godoy and Mayr, 1989). Parameters of total microbial biomass in saprolite show no increase along the gradient: total gene copy have similar ranges from Santa Gracia to Nahuelbuta, and DNA amounts even decrease slightly (Oeser et al., 2018). Common strategies of microbial symbionts by tree roots suggest that energy investment into nutrient recycling from leaf litter is more advantageous than dissolving primary mineral (Andrino et al., 2019). Thus, we would expect that mycorrhiza predominantly aids recycling in La Campana and Nahuelbuta. In Santa Gracia, ... [7]
hat gelöscht: Process (4) mainly increases the equilibrium limit of elemental solubility. If dissolution is not kinetically limited, we ... [8]
hat gelöscht: , and hence higher dissolution rates of primary minerals (Winnick and Maher, 2018). Plants
hat gelöscht: interfering into
hat gelöscht:)
hat gelöscht: the
hat gelöscht: conversion of dissolved silicon into biosilica by
hat gelöscht: formation of e.g. phytoliths would aid kaolinite formation (Lucas, 2001). However, the Si
hat gelöscht: flux at all sites is negligible compared to the Si weathering flux: $W^{Si}_{regolith}$ amounts to 2100 and 2000 mg m^{-2} yr^{-1} in ... [9]

ecosystems ranges from 110 µg g^{-1} in Nahuelbuta to 2500 µg g^{-1} in Pan de Azúcar (Table 5). Thus, the Si weathering flux $W^{Si}_{regolith}$ exceeds the Si uptake flux U^{Si}_{total} throughout (Table 3) and uptake from soil solution by plants equates to only 5%, 0.2%, and 2% of the Si release flux in Santa Gracia, La Campana, and Nahuelbuta, respectively. Only in Pan de Azúcar, relative uptake of Si is higher (25%).The ecosystems at our sites can thus be regarded to be below the threshold considered for Si accumulators (Schaller et al., 2018a). We can therefore exclude plant Si uptake and recycling of Si as a factor that increases weathering rates substantially. Rather, if plants in these ecosystems are discriminating against Si uptake whilst taking up water, the residual pore waters will get oversaturated with respect to secondary minerals. In this regard a key observation is provided by the analysis of pedogenic oxides (i.e. dithionite-extractable Al, Si extracted by oxalate, dithionite, and pyrophosphate; Oeser et al., 2018) and cation exchange capacity (Bernhard et al., 2018). These analyses suggest high amounts of amorphous precipitates and secondary minerals in the regolith of Nahuelbuta. We thus argue that Si is effectively captured in these barely soluble secondary minerals after initial dissolution from rock and regolith. In turn, $W^{Si}_{regolith}$ in Nahuelbuta is subdued despite elevated solubility of primary minerals due to increased CO_2 respiration by roots.

Ecosystems thus exert substantial control over weathering by both directly and indirectly modulating processes. These processes can either enhance or reduce weathering fluxes and result, in combination with effective recycling loops of plant-litter material, in well-balanced nutrient cycles. From our field data, we did not find evidence for coupling of silicate weathering fluxes with the nutrient demands of biota to an extent that exceeds other controlling factors of weathering. Our data suggests that the combination of recycling and negative feedbacks on weathering by secondary mineral formation within the regolith decrease weathering rates in areas of high vegetation cover and net primary productivity from what they would be in the absence of high biomass density.

hat gelöscht: ecosystem of Santa Gracia (1400 µg g^{-1})

hat gelöscht: concentration in Nahuelbuta (110 µg g^{-1}; Table 5). This leads to an uptake of Si from soil solution (U^{Si}_{total}) of 100 mg m^{-2} yr^{-1} in Santa Gracia and 30 mg m^{-2} yr^{-1} in Nahuelbuta (Table 3) which is

hat gelöscht: – 5

hat gelöscht: .

hat gelöscht: impacting

hat gelöscht: . A

hat gelöscht: but not in Santa Gracia.

hat gelöscht: and in

hat gelöscht: in spite of

hat gelöscht: The

hat gelöscht: become effectively decoupled from

hat gelöscht: ultimate

hat gelöscht: .

hat gelöscht: empirical evidence provided here

hat gelöscht: solid

hat gelöscht: counterbalance

hat gelöscht: biomass growth

7 Conclusions

While the EarthShape study sites define a north-south gradient in precipitation and biomass production, no such gradient is apparent for weathering rates and weathering intensity between the study sites situated in semi-arid, mediterranean, and humid-temperate climate.

At all four sites we locate the primary mineral nutrient source to plants in the bio-available fraction. This pool of mineral nutrients is initially fed by geogenic sources, which comprise the weathering of primary minerals. It is further fed from organic sources, which involves recycling of nutrients from leaf litter. The size of the bio-available nutrient pool decreases from north to south and while pedogenic properties (e.g. pH) likely contribute to set its size, we attribute its decrease mainly to an increase in the below-ground water flow. To fulfill their nutrient demand at increasing NPP but decreasing pool size, ecosystems increase nutrient recycling rather than enhancing biogenic weathering. We consequently find that the organic nutrient cycle intensifies, whereas the geogenic nutrient pathway is steady despite increasing MAP and NPP.

In fact, the presence of plants might even counteract a potential weathering increase along the gradient by inducing secondary mineral formation rather than nutrient-acquisition through weathering. Due to nutrient buffering by recycling and a potential biological dampening of weathering, any additional contribution to weathering by NPP is unresolvable in our data and is certainly smaller than abiotic controls like denudation, rainfall, or bedrock mineralogy. The global silicate-weathering cycle may thus not be as sensitive to plant growth as commonly thought and cannot be simulated in a straightforward manner in weathering models. This non-linear behavior is of relevance for models of the global weathering and the linked carbon cycle, of which accelerated weathering by land plants since the Ordovician is a common component.

hat gelöscht: 6

hat gelöscht: We found that even though

hat gelöscht: four

hat gelöscht: feature

hat gelöscht: steep

hat gelöscht: MAP

hat gelöscht: NPP, none

hat gelöscht: a

hat gelöscht: was

hat gelöscht: Thus, the ecosystems with high NPP maintain their nutrient supply by increasing recycling rather than increasing weathering. We consequently find that the "organic nutrient pathway" intensifies, whereas the "geogenic nutrient pathway" stays steady despite increasing MAP and NPP.

hat gelöscht: Ecological stoichiometry in plants and Sr isotopes reflects the bio-available fraction in saprolite and soil. At the sites with high NPP, the bio-available fraction approaches a plant-dominated ecological stoichiometry signature by intense recycling. Besides nitrogen, the first mineral nutrient to be limit plant growth might be K rather than P. However, we found that deep-rooting plants can bypass this shortage K in the upper regolith by deep K-uptake from beneath the regolith profiles. ¶

hat gelöscht: compensate

hat gelöscht: downward by regulating the hydrological cycle, fostering…

hat gelöscht: , and a microbial community specializing on nutrient-recycling

hat gelöscht: this

hat gelöscht: , higher plants today may not be a big driver

hat gelöscht: silicate-weathering cycle.

8 Appendices

Appendix A: Calculation of fluxes and inventories in terrestrial ecosystems

Weathering indices (CDF & τ)

Zr, Ti, and Nb are commonly used to estimate mass losses to the dissolved form during weathering (Eqs. 5 & 6) as they are presumed to be the least mobile elements during weathering (Chadwick et al., 1990; White et al., 1998). The suitability of these elements for the EarthShape study sites has been evaluated and thoroughly discussed on a site to site basis in Oeser et al. (2018). Based on possible Ti-mobility in some samples and the fact that Zr is used as a reference element in the majority of weathering and soil production studies worldwide (e.g. Fisher et al., 2017; Green et al., 2006; Hewawasam et al., 2013; Riebe and Granger, 2013; Riebe et al., 2001; Schuessler et al., 2018; Uhlig et al., 2017), Zr was taken as immobile reference element in this study.

The calculations of these weathering indices rely on a good approximation of the chemical composition of the initial bedrock from which regolith formed. To this end, any regolith sample with a Zr concentration that was lower than the mean of unweathered bedrock by more than one standard deviation (1SD) was excluded from further consideration. Because a lower Zr concentration cannot be due to weathering, such regolith samples likely originate from chemically distinct bedrock or small-scale bedrock heterogeneities (e.g. a pegmatitic vein). Saprolite samples were also excluded from our data set if Cr and Ti concentrations were twice those of unweathered bedrock (+ 1SD). Elevated concentrations of these elements imply the presence of mafic precursor rock such as commonly present in bedrocks' mafic enclaves. All such excluded samples are marked in grey color in Figs. 3 & A1, and mainly affect only the lower section of the south-facing Nahuelbuta profile.

The concentration of K throughout the entire regolith profiles in Santa Gracia is three-fold higher than K contained in local bedrock samples (Oeser et al., 2018). We thus assume that the K concentration in the bedrock samples of Santa Gracia as determined by Oeser et al. (2018) underestimates the actual occurring K concentration of local bedrock. Thus, τ^{K} has been calculated using published values for K and Zr concentration from a study nearby (Miralles González, 2013).

hat gelöscht: ¶
7

hat gelöscht: Oeser et al. (2018)

hat gelöscht: regolith profiles' initial substrate (i.e.

hat gelöscht: bedrock

hat gelöscht:). Thus

hat gelöscht: These

hat gelöscht: potentially

hat gelöscht: a

hat gelöscht: highlight another type of substrate heterogeneity

hat gelöscht:) as a lower Zr concentration cannot be due to weathering….

hat gelöscht: .

hat gelöscht: (Oeser et al., 2018)

hat gelöscht: Oeser et al. (2018)

hat gelöscht: actually

hat gelöscht: on

Weathering fluxes

To estimate elemental release fluxes from regolith (Eq. 3) for each study site, the most negative τ-values from the shallowest mineral-soil sample of each regolith profile were used (red-circled symbols in Fig. A1). This practice is common in eroding regolith, where the loss indicators τ and CDF represent the integrated mass loss over the time and depth interval that a given sample moved from bedrock reference level to its present position (Brantley and Lebedeva, 2011; Ferrier et al., 2010; Hewawasam et al., 2013; Uhlig and von Blanckenburg, 2019). The elemental chemical weathering flux ($W^{X}_{regolith}$) at each study site has been averaged. Because not all of this flux might not be within reach of plant roots (e.g. if a fraction is lost into deep groundwater), this is an upper estimate of the nutrient supply from rock into vegetation. $W^{X}_{regolith}$ is reported in Table 3.

Ecosystem nutrient uptake fluxes

Total ecosystem nutrient uptake fluxes (U^{X}_{total}) have been evaluated using Eq. 4 and are reported in Table 3. Because we compare these to the weathering fluxes that integrate over several millennia, we estimate uptake fluxes that are representative for the Holocene. Net primary productivity (NPP), has been derived from a dynamic vegetation model (LPJ-GUESS) simulating vegetation cover and composition during the Holocene (Werner et al., 2018) and is reported in Table 1. Biomass production was estimated from NPP(C) by assuming that dry biomass consists of 50 wt% carbon. To obtain the element-specific uptake rate U^{X}_{total}, NPP is multiplied with the bulk concentration of X in the plants $[X]_{Plant}$.

The sampling and analyses of roots was not done in this study, because of the difficulties in obtaining entire roots or representative root segments from a specific tree or shrub including fine roots. For elemental analysis this difficulty is compounded by the need to remove any remaining soil particles or attached precipitates that might bias measured concentrations. To nevertheless estimate bulk plant elemental composition, we applied the dimensionless organ growth quotients GL/GS (leaf growth relative to stem growth) and GL/GR (leaf growth relative to root growth) in accordance with Niklas and Enquist (2002). This estimation invokes several assumptions: (1) Roots biomass growth contributes little to total plant growth, namely 9% in angiosperms and 17% in gymnosperms (Niklas and Enquist, 2002). We thus

hat gelöscht:), resulting
hat gelöscht: an
hat gelöscht: net-elemental release
hat gelöscht: each entire regolith profile. Ultimately, the
hat gelöscht: some fraction
hat gelöscht: in the
hat gelöscht: the plants'
hat gelöscht:)
hat gelöscht: fluxes
hat gelöscht: results
hat gelöscht: ¶
hat gelöscht: U^{X} $GrowthRate_{Plant}$
hat gelöscht: To estimate an
hat gelöscht: ecosystem
hat gelöscht: Niklas and Enquist (2002)
hat gelöscht: However, the sampling and analyses of roots was excluded in this study, because of the difficulties that arose in associating roots to a specific tree or shrub. For elemental analysis this difficulty is compounded by the difficulties encountered during the roots' purification from soil particles.

treat roots and stem/ twig as one plant compartment. In total, the pooled growth of root, stem, and twig amounts to 68% and 52% of relative growth in angiosperms and gymnosperms, respectively. (2) Differences in biomass allocation are relevant only between angiosperms and gymnosperms and not between single plant species of a given class. (3) The pattern of relative growth and standing biomass allocation holds true across a minimum of eight orders of magnitude of species size (Niklas and Enquist, 2002). We thus adapted the organ growth quotients from the work of Niklas and Enquist (2002), such that we only differentiate between the growth rate of leaves and stem, respectively, and the adapt these quotients between angiosperms and gymnosperms. The bulk elemental ecosystem composition (Table 5) has been determined by weighting the averaged elemental composition for each sampled plant for their relative abundance in the respective ecosystem.

Inventories

The inventories for the bio-available fraction ($I^X_{bio\text{-}av.}$) and in bulk regolith (I^X_{bulk}) have been calculated using Eq. 8 and are reported in Table 4. $I^X_{bio\text{-}av.}$ was determined for both the bio-available fraction in soil (comprised of the A and B horizon; $I^X_{bio\text{-}av,\,soil}$) and saprolite of 1m thickness ($I^X_{bio\text{-}av,\,sap}$). For the calculation of all inventories we used the soils' bulk density determined by Bernhard et al. (2018). I^X_{bulk} is comprised of elements contained in fine-earth material and in fragmented rocks and coarse material (e.g. core stones). We derive the relative amount of coarse material of each depth increment from Bernhard et al. (2018) and allocate them the bedrocks' chemical composition (Table S1). If information on either bulk density or the relative amount of coarse material was unavailable, the respective horizons' average has been used for the calculation of $I^X_{i,j}$. In none of the eight regolith profiles is the depth to unweathered bedrock known. Thus, for comparison purposes, we calculated the inventories of the bio-available fraction in saprolite ($I^X_{bio\text{-}av,\,sap}$) and in bulk regolith ($I^X_{bulk}$) to the depth of the respective regolith profile and normalized this value to the arbitrary value of 1 m.

hat gelöscht: Niklas and Enquist (2002)

hat gelöscht: differences of

hat gelöscht: Ultimately,

hat gelöscht: bulk

hat gelöscht: ¶

hat gelöscht: not available

hat gelöscht: ¶
Ultimately, we do not know how far the saprolite extents to depth in each…

Nutrient recycling factor

We call the ratio of nutrient uptake to nutrient supply by weathering the "nutrient recycling factor" Rec^X which was calculated using Eq. 7 and is reported in Table 7. Importantly, as defined, this factor ratios fluxes between entire regolith and total uptake into the entire vegetation cover (the same rationale as used by Cleveland et al., 2013 for the inverse; the "new" fraction of P). Rec^X represents a minimum estimate as some fraction of $W^X_{regolith}$ will bypass nutrient uptake by plants if it is drained directly via groundwater into streams. Rec^X might represent an underestimate for some elements that are returned to soil by stem-flow or throughfall. According to e.g. Wilcke et al. (2017), these fluxes are generally highest for K compared to other plant-essential elements. Rec^X might also be an overestimate, if a substantial fraction of nutrient is eroded by leaf litter and other plant debris after uptake, rendering it unavailable for recycling. In Pan de Azúcar, where atmospheric deposition (Dep^X_{dry} and Dep^X_{wet}) is known to be an important component of ecosystem element budgets (e.g. increasing τ-values towards the profiles top in absence of bio-lifting of elements and field observation; Oeser et al., 2018) we need to consider these inputs in addition to the weathering release fluxes ($W^X_{regolith}$). Thus, to account for all potential sources of elements available for plant uptake, the nutrient recycling factor in Pan de Azúcar is given as:

$$Rec^X = \frac{U^X_{total}}{W^X_{regolith} + Dep^X_{wet} + Dep^X_{dry}}$$

Atmospheric deposition fluxes have been estimated by determining the absolute difference between the lowest τ-value in the shallowest mineral-soil sample and the highest τ-value in the soil profile above it. Further, we assume that elemental gains (i.e. increasing τ-values) in the regolith profiles are attributed solely to atmospheric deposition. We test these estimates for atmospheric depositional fluxes by placing the elemental gains in proportion to the initially determined weathering release fluxes ($W^X_{regolith}$, Eq. 3; Table 3).

Uncertainty estimation of nutrient fluxes

The analytical uncertainty of measured samples and certified international reference materials are reported in section "Analytical methods" and in Oeser and von Blanckenburg (2020).

hat gelöscht: ¶

hat gelöscht: The

hat gelöscht: This

hat gelöscht: , however, might represent an underestimate as it is parameterized with $W^X_{regolith}$

hat gelöscht: which

hat gelöscht: Moreover,

hat gelöscht: also be underrated

hat gelöscht: as it does not account for

hat gelöscht: fluxes and

hat gelöscht: Wilcke et al. (2017)

hat gelöscht: has been reported

hat gelöscht: despite

hat gelöscht: has been determined using

hat gelöscht: *DepwetX+ DepdryX*

hat gelöscht: on

The uncertainties on the nutrient fluxes of $W^X_{regolith}$ and U^X_{total} were estimated by Monte Carlo simulations in which 20 000 random data sets were sampled within the standard deviation of all input parameters using a Box-Muller transformation (Box and Muller, 1958). The simulation of each regolith profiles' $W^X_{regolith}$ incorporates the SD of the average soil denudation rate D (Table 1), the SD of the concentration of the element of interest in bedrock (Table S1), and 3% relative uncertainty on the element concentration in regolith samples. In the case of U^X_{total} the SD of the respective study sites' NPP and the SD of the chemical composition of the weighted plants (Table 5) were used. The resultant uncertainties on both fluxes are reported in Table 3.

hat gelöscht: performing

hat gelöscht:

hat gelöscht: (Box and Muller, 1958)

hat gelöscht: uncertainties used for the

hat gelöscht: were the SD

hat gelöscht: , the respective regolith profile's

hat gelöscht: (

hat gelöscht: , Table 1),

hat gelöscht: bedrocks' element

hat gelöscht: ,

hat gelöscht: site's

Appendix B: Data presentation and Statistical analyses

hat gelöscht: 8

Replication

We present our results on nutrient fluxes, inventories, and turnover times as study-site averages for synthesis reasons only. Indeed, at each study site four replicate regolith profiles have been analyzed in previous studies. Within a given site, these profiles show no significant differences in chemistry and pedogenic properties (Bernhard et al., 2018; Oeser et al., 2018). In this study we focused on two regolith profiles situated on opposing slopes (north- and south facing midslope profiles) to account for the variations in substrate and/ or the effects of insolation and microclimate on weathering and nutrient uptake by plants. However, these profiles are natural replicates.

Statistical analysis

An analysis of variance (ANOVA) was performed to evaluate how denudation rate (D), the chemical depletion fraction (CDF), soil weathering rate (W), and the elemental weathering rates for Ca, K, Na, P, and Si ($W^X_{regolith}$) vary among sites. Variance homogeneity was tested using Levene's Test before applying ANOVAs and pair-wise differences were assessed using Tukey's HSD test. In these, p values ≤ 0.05 were considered as significant. The correlations between D, MAP, NPP, and the degree (CDF, τ^X) and rate (W, $W^X_{regolith}$) of weathering were evaluated using Pearson's correlation coefficients. To test for the significance of D on these weathering parameters, Pearson's correlation coefficients were evaluated twice:

with (Table A1) and without La Campana (Table A2). This test is possible because of the high denudation rate of this site which originates from the steepest relief of all sites (Oeser et al., 2018; Schaller et al., 2018b; van Dongen et al., 2019). The sample set includes study site average values from all tested parameters and those of the single regolith profiles. Statistical analyses were conducted using the statistics packages included in the software OriginPro (Version 2020).

Equal variances could be assumed throughout and all weathering patterns differed among sites on the total population (Table A3). However, post-hoc comparisons indicated that sites did not always differ, and that differences between sites varied for the different weathering parameters (Table A3). Particularly, few statistically significant differences exist between the semi-arid Santa Gracia and humid-temperate Nahuelbuta. In these two sites the weathering release fluxes for K ($W^{K}_{regolith}$), Na ($W^{Na}_{regolith}$), P ($W^{P}_{regolith}$), and Si ($W^{Si}_{regolith}$) do not differ significantly (Table A3) despite massive differences in D, MAP, and NPP (Table 1).

9 Sample availability

All sample metadata are already available on a public server using unique sample identifiers in form of the “International Geo Sample Number” (IGSN).

10 Author contributions

hat gelöscht: 9

R.A. Oeser conducted field sampling, analyzed samples, interpreted data, and wrote text. F. von Blanckenburg designed the study, selected the study sites, interpreted data, and wrote text.

11 Competing financial interests

hat gelöscht: 10

The authors declare no competing financial interests.

12 Additional information

Supplementary data tables are available at GFZ data services (Oeser and von Blanckenburg, 2020).

13 Acknowledgements

We acknowledge CONAF in Chile for providing us with the opportunity to work in the national parks of Pan de Azúcar, La Campana, and Nahuelbuta. We also thank CEAZA for facilitating access to the Reserva Natural Santa Gracia. We are grateful to J. Boy (Soil Sciences, Leibniz Universität Hannover, Germany) for discussions, and D. Uhlig (Institute of Bio- and Geosciences, Forschungszentrum Jülich, Germany), Michaela Dippold (Department of Crop Sciences, Georg-August University Goettingen, Germany), Matthew Winnick (Department of Geosciences, University of Massachusetts, USA), and Patrick Frings (Section "Earth Surface Geochemistry", GFZ German Research Centre for Geosciences, Germany) for informal reviews of the text. We thank the three anonymous referees and Marjin van de Broeck and his MSc students for their detailed critique of our work which led us to revise the manuscript with the aim of attempting to avoiding the pitfalls emerging when working across disciplines. R.A. Oeser and F. von Blanckenburg are grateful for funding by the German National Science Foundation Priority Program DFG-SPP 1803 (EarthShape; http://www.earthshape.net). We thank Leandro Paulino (Departamento de Suelos y Recursos Naturales, Universitad de Concepción, Chile) and Kirstin Übernickel for managing the priority program and Todd Ehlers (both Institute for Geosciences, Universität Tübingen, Germany) for its co-coordination.

hat gelöscht: 11

hat gelöscht: 12

hat gelöscht: and

hat gelöscht: an earlier

hat gelöscht: version.

hat gelöscht: www.earthshape.net).

hat verschoben (Einfügung) [3]

14 References

Amundson, R., Richter, D. D., Humphreys, G. S., Jobbágy, E. G., and Gaillardet, J. r. m.: Coupling between Biota and Earth Materials in the Critical Zone, Elements, 3, 327-332, doi:10.2113/gselements.3.5.327, 2007.

Andrino, A., Boy, J., Mikutta, R., Sauheitl, L., and Guggenberger, G.: Carbon Investment Required for the Mobilization of Inorganic and Organic Phosphorus Bound to Goethite by an Arbuscular Mycorrhiza (Solanum lycopersicum x Rhizophagus irregularis), Frontiers in Environmental Science, 7, doi:10.3389/fenvs.2019.00026, 2019.

Armesto, J. J., Vidiella, P. E., and Gutiérrez, J. R.: Plant communities of the fog-free coastal desert of Chile: plant strategies in a fluctuating environment., Rev. Chil. Hist. Nat., 66, 271-282, 1993.

Arunachalam, J., Emons, H., Krasnodebska, B., and Mohl, C.: Sequential extraction studies on homogenized forest soil samples, The Science of the Total Environment, 181, 147-159, doi:10.1016/0048-9697(95)05005-1, 1996.

Bahre, C. J.: Destruction of the natural vegetation of north-central Chile, Univ of California Press, 1979.

Balogh-Brunstad, Z., Keller, C. K., Gill, R. A., Bormann, B. T., and Li, C. Y.: The effect of bacteria and fungi on chemical weathering and chemical denudation fluxes in pine growth experiments., Biogeochemistry, 88, 153-167, doi:10.1007/s10533-008-9202-y, 2008a.

Balogh-Brunstad, Z., Kent Keller, C., Thomas Dickinson, J., Stevens, F., Li, C. Y., and Bormann, B. T.: Biotite weathering and nutrient uptake by ectomycorrhizal fungus, Suillus tomentosus, in liquid-culture experiments, Geochim. Cosmochim. Acta, 72, 2601-2618, doi:10.1016/j.gca.2008.04.003, 2008b.

Beerling, D. J., and Berner, R. A.: Feedbacks and the coevolution of plants and atmospheric CO2, Proc Natl Acad Sci U S A, 102, 1302-1305, doi:10.1073/pnas.0408724102, 2005.

Berg, K., and Breitkreuz, C.: Mesozoische Plutone in der nordchilenischen Küstenkordillere: petrogenese, geochronologie, Geochemie und Geodynamik mantelbetonter Magmatite, Geotectonic Research, 66, Schweizerbart Science Publishers, 1983.

Berg, K., and Baumann, A.: Plutonic and metasedimentary rocks from the Coastal Range of northern Chile: Rb-Sr and U-Pb isotopic systematics, Earth, Planet. Sci. Lett., 75, 101-115, doi:10.1016/0012-821X(85)90093-7, 1985.

Berner, E. K., Berner, R. A., and Moulton, K. L.: Plants and Mineral Weathering: Present and Past, in: Treatise on Geochemistry, 169-188, doi:10.1016/b0-08-043751-6/05175-6, 2003.

Bernhard, N., Moskwa, L.-M., Schmidt, K., Oeser, R. A., Aburto, F., Bader, M. Y., Baumann, K., von Blanckenburg, F., Boy, J., van den Brink, L., Brucker, E., Canessa, R., Dippold, M. A., Ehlers, T. A., Fuentes, J. P., Godoy, R., Köster, M., Kuzyakov, Y., Leinweber, P., Neidhard, H., Matus, F., Mueller, C. W., Oelmann, Y., Oses, R., Osses, P., Paulino, L., Schaller, M., Schmid, M., Spielvogel, S., Spohn, M., Stock, S., Stroncik, N., Tielbörger, K., Übernickel, K., Scholten, T., Seguel, O., Wagner, D., and Kühn, P.: Pedogenic and microbial interrelations to regional climate and local topography: new insights from a climate gradient (arid to humid) along the Coastal Cordillera of Chile, Catena, 170, doi:10.1016/j.catena.2018.06.018, 2018.

Blanco-Chao, R., Pedoja, K., Witt, C., Martinod, J., Husson, L., Regard, V., Audin, L., Nexer, M., Delcaillau, B., Saillard, M., Melnick, D., Dumont, J. F., Santana, E., Navarrete, E., Martillo, C., Pappalardo, M., Ayala, L., Araya, J. F., Feal-Perez, A., Correa, D., and Arozarena-Llopis, I.: The rock coast of South and Central America, in: Rock Coast Geomorphology: A Global Synthesis., 1, The Geological Society, London, 155-191, doi:10.1144/m40.10, 2014.

Blum, J. D., Klaue, A., Nezat, C. A., Driscoll, C. T., Johnson, C. E., Siccama, T. G., Eagar, C., Fahey, T. J., and Likens, G. E.: Mycorrhizal weathering of apatite as an important calcium source in base-poor forest ecosystems, Nature, 417, 729-731, doi:10.1038/nature00793, 2002.

Blum, J. D., Hamburg, S. P., Yanai, R. D., and Arthur, M. A.: Determination of foliar Ca/Sr discrimination factors for six tree species and implications for Ca sources in northern hardwood forests, Plant Soil, 356, 303-314, doi:10.1007/s11104-011-1122-2, 2012.

Bonneville, S., Morgan, D. J., Schmalenberger, A., Bray, A., Brown, A., Banwart, S. A., and Benning, L. G.: Tree-mycorrhiza symbiosis accelerate mineral weathering: Evidences from nanometer-scale elemental fluxes at the hypha–mineral interface, Geochim. Cosmochim. Acta, 75, 6988-7005, doi:10.1016/j.gca.2011.08.041, 2011.

Bormann, F., Likens, G., and Eaton, J.: Biotic regulation of particulate and solution losses from a forest ecosystem, Bioscience, 19, 600-610, doi:10.2307/1294934, 1969.

Box, G. E. P., and Muller, M. E.: A note on the generation of random normal deviates, Ann. Math. Statist., 29, 610-611, doi:10.1214/aoms/1177706645, 1958.

Boy, J., and Wilcke, W.: Tropical Andean forest derives calcium and magnesium from Saharan dust, Global Biogeochem. Cycles, 22, GB1027, doi:10.1029/2007gb002960, 2008.

Brantley, S. L., and Lebedeva, M.: Learning to Read the Chemistry of Regolith to Understand the Critical Zone, Annual Review of Earth and Planetary Sciences, 39, 387-416, doi:10.1146/annurev-earth-040809-152321, 2011.

Brantley, S. L., Megonigal, J. P., Scatena, F. N., Balogh-Brunstad, Z., Barnes, R. T., Bruns, M. A., Van Cappellen, P., Dontsova, K., Hartnett, H. E., Hartshorn, A. S., Heimsath, A., Herndon, E., Jin, L., Keller, C. K., Leake, J. R., McDowell, W. H., Meinzer, F. C., Mozdzer, T. J., Petsch, S., Pett-Ridge, J., Pregitzer, K. S., Raymond, P. A., Riebe, C. S., Shumaker, K., Sutton-Grier, A., Walter, R., and Yoo, K.: Twelve testable hypotheses on the geobiology of weathering, Geobiology, 9, 140-165, doi:10.1111/j.1472-4669.2010.00264.x, 2011.

Brantley, S. L., Lebedeva, M., and Heimshath, E. H.: A Geobiological View of Weathering and Erosion, in: Fundamentals of Geobiology, edited by: Knoll, A. H., Blackwell Publishing, doi:10.1002/9781118280874.ch12, 2012.

hat gelöscht: 13

hat gelöscht: Revista Chilena de Historia Natural,

hat gelöscht: Baskaran, P., Hyvonen, R., Berglund, S. L., Clemmensen, K. E., Agren, G. I., Lindahl, B. D., and Manzoni, S.: Modelling the influence of ectomycorrhizal decomposition on plant nutrition and soil carbon sequestration in boreal forest ecosystems, New Phytol, 213, 1452-1465, 10.1111/nph.14213, 2017.¶

hat gelöscht: and Planetary Science Letters,

hat gelöscht: 2003.

hat gelöscht: and

hat gelöscht: Cy

hat gelöscht: n/a-n/a,

Brantley, S. L., Eissenstat, D. M., Marshall, J. A., Godsey, S. E., Balogh-Brunstad, Z., Karwan, D. L., Papuga, S. A., Roering, J., Dawson, T. E., Evaristo, J., Chadwick, O., McDonnell, J. J., and Weathers, K. C.: Reviews and syntheses: on the roles trees play in building and plumbing the critical zone, Biogeosciences, 14, 5115-5142, doi:10.5194/bg-14-5115-2017, 2017.

Brucker, E., and Spohn, M.: Formation of soil phosphorus fractions along a climate and vegetation gradient in the Coastal Cordillera of Chile, Catena, 180, 203-211, doi:10.1016/j.catena.2019.04.022, 2019.

Buendía, C., Kleidon, A., and Porporato, A.: The role of tectonic uplift, climate, and vegetation in the long-term terrestrial phosphorous cycle, Biogeosciences, 7, 2025-2038, doi:10.5194/bg-7-2025-2010, 2010.

Bullen, T. D., and Chadwick, O.: Ca, Sr and Ba stable isotopes reveal the fate of soil nutrients along a tropical climosequence in Hawaii, Chem. Geol., 422, 25-45, doi:10.1016/j.chemgeo.2015.12.008, 2016.

Buss, H. L., Bruns, M. A., Schultz, D. J., Moore, J., Mathur, C. F., and Brantley, S. L.: The coupling of biological iron cycling and mineral weathering during saprolite formation, Luquillo Mountains, Puerto Rico, Geobiology, 3, 247-260, doi:10.1111/j.1472-4669.2006.00058.x, 2005.

Calmels, D., Gaillardet, J., and François, L.: Sensitivity of carbonate weathering to soil CO2 production by biological activity along a temperate climate transect, Chem. Geol., 390, 74-86, doi:10.1016/j.chemgeo.2014.10.010, 2014.

Canadell, J., Jackson, R., Ehleringer, J., Mooney, H., Sala, O., and Schulze, E.-D.: Maximum rooting depth of vegetation types at the global scale, Oecologia, 108, 583-595, 1996.

Chadwick, K. D., and Asner, G. P.: Tropical soil nutrient distributions determined by biotic and hillslope processes, Biogeochemistry, 127, 273-289, doi:10.1007/s10533-015-0179-z, 2016.

Chadwick, O. A., Brimhall, G. H., and Hendricks, D. M.: From a black to a gray box — a mass balance interpretation of pedogenesis, Geomorphology, 3, 369-390, doi:10.1016/0169-555x(90)90012-f, 1990.

Chadwick, O. A., Derry, L. A., Vitousek, P. M., Huebert, B. J., and Hedin, L. O.: Changing sources of nutrients during four million years of ecosystem development, Nature, 397, 491-497, doi:10.1038/17276, 1999.

Chapin III, F. S.: The mineral nutrition of wild plants, Annu. Rev. Ecol. Syst., 11, 233-260, 1980.

Chapin III, F. S., Matson, P. A., and Vitousek, P. M.: Principles of Terrestrial Ecosystem Ecology, 2nd ed., 2011.

Chaudhuri, S., Clauer, N., and Semhi, K.: Plant decay as a major control of river dissolved potassium: A first estimate, Chem. Geol., 243, 178-190, doi:10.1016/j.chemgeo.2007.05.023, 2007.

Cleveland, C. C., Houlton, B. Z., Smith, W. K., Marklein, A. R., Reed, S. C., Parton, W., Del Grosso, S. J., and Running, S. W.: Patterns of new versus recycled primary production in the terrestrial biosphere, Proc Natl Acad Sci U S A, 110, 12733-12737, doi:10.1073/pnas.1302768110, 2013.

Dal Bo, I., Klotzsche, A., Schaller, M., Ehlers, T. A., Kaufmann, M. S., Fuentes Espoz, J. P., Vereecken, H., and van der Kruk, J.: Geophysical imaging of regolith in landscapes along a climate and vegetation gradient in the Chilean coastal cordillera, Catena, 180, 146-159, doi:10.1016/j.catena.2019.04.023, 2019.

Day, T. A., Guénon, R., and Ruhland, C. T.: Photodegradation of plant litter in the Sonoran Desert varies by litter type and age, Soil Biol. Biochem., 89, 109-122, doi:10.1016/j.soilbio.2015.06.029, 2015.

Delhaize, E., and Ryan, P. R.: Aluminum Toxicity and Tolerance in Plants, Plant Physiol., 107, 315-321, doi:10.1104/pp.107.2.315, 1995.

Dere, A. L., White, T. S., April, R. H., Reynolds, B., Miller, T. E., Knapp, E. P., McKay, L. D., and Brantley, S. L.: Climate dependence of feldspar weathering in shale soils along a latitudinal gradient, Geochim. Cosmochim. Acta, 122, 101-126, doi:10.1016/j.gca.2013.08.001, 2013.

Dixon, J. L., Heimsath, A. M., Kaste, J., and Amundson, R.: Climate-driven processes of hillslope weathering, Geology, 37, 975-978, doi:10.1130/g30045a.1, 2009.

Dixon, J. L., Hartshorn, A. S., Heimsath, A. M., DiBiase, R. A., and Whipple, K. X.: Chemical weathering response to tectonic forcing: A soils perspective from the San Gabriel Mountains, California, Earth Planet. Sci. Lett., 323-324, 40-49, doi:10.1016/j.epsl.2012.01.010, 2012.

Dixon, J. L., Chadwick, O. A., and Vitousek, P. M.: Climate-driven thresholds for chemical weathering in postglacial soils of New Zealand, Journal of Geophysical Research: Earth Surface, 121, 1619-1634, doi:10.1002/2016jf003864, 2016.

Dosseto, A., Buss, H. L., and Suresh, P. O.: Rapid regolith formation over volcanic bedrock and implications for landscape evolution, Earth Planet. Sci. Lett., 337-338, 47-55, doi:10.1016/j.epsl.2012.05.008, 2012.

Doughty, C. E., Taylor, L. L., Girardin, C. A. J., Malhi, Y., and Beerling, D. J.: Montane forest root growth and soil organic layer depth as potential factors stabilizing Cenozoic global change, Geophys. Res. Lett., 41, 983-990, doi:10.1002/2013gl058737, 2014.

Drever, J. I., and Zobrist, J.: Chemical weathering of silicate rocks as a function of elevation in the southern Swiss Alps, Geochim. Cosmochim. Acta, 56, 3209-3216, doi:10.1016/0016-7037(92)90298-w, 1992.

Drever, J. I.: The effect of land plants on weathering rates of silicate minerals, Geochim. Cosmochim. Acta, 58, 2325-2332, doi:10.1016/0016-7037(94)90013-2, 1994.

Eger, A., Yoo, K., Almond, P. C., Boitt, G., Larsen, I. J., Condron, L. M., Wang, X., and Mudd, S. M.: Does soil erosion rejuvenate the soil phosphorus inventory?, Geoderma, 332, 45-59, doi:10.1016/j.geoderma.2018.06.021, 2018.

Egli, M., Mirabella, A., Sartori, G., and Fitze, P.: Weathering rates as a function of climate: results from a climosequence of the Val Genova (Trentino, Italian Alps). Geoderma, 111, 99-121, doi:10.1016/S0016-7061(02)00256-2, 2003.

hat gelöscht: Chemical Geology,

hat gelöscht: 2005.

hat gelöscht: Chemical Geology,

hat gelöscht: Capek, P., Manzoni, S., Kastovska, E., Wild, B., Diakova, K., Barta, J., Schnecker, J., Biasi, C., Martikainen, P. J., Alves, R. J. E., Guggenberger, G., Gentsch, N., Hugelius, G., Palmtag, J., Mikutta, R., Shibistova, O., Urich, T., Schleper, C., Richter, A., and Santruckova, H.: A plant-microbe interaction framework explaining nutrient effects on primary production, Nat Ecol Evol, 10.1038/s41559-018-0662-8, 2018.¶

hat gelöscht: Annual review of ecology and systematics,

hat gelöscht: Chemical Geology,

hat gelöscht: Cleveland, C. C., and Liptzin, D.: C:N:P stoichiometry in soil: is there a "Redfield ratio" for the microbial biomass?, Biogeochemistry, 85, 235-252, 10.1007/s10533-007-9132-0, 2007.¶

hat gelöscht: Biology and Biochemistry,

hat gelöscht: Physiology,

hat gelöscht: Geochimica et Cosmochimica

hat gelöscht: and Planetary Science Letters,

hat gelöscht: and Planetary Science Letters,

hat gelöscht: Geophysical Research Letters,

hat gelöscht: Geochimica et Cosmochimica

hat gelöscht: Geochimica et Cosmochimica

hat gelöscht: 2003.

Fabian, J., Zlatanovic, S., Mutz, M., and Premke, K.: Fungal-bacterial dynamics and their contribution to terrigenous carbon turnover in relation to organic matter quality, ISME J, 11, 415-425, doi:10.1038/ismej.2016.131, 2017.
Fan, Y., Miguez-Macho, G., Jobbagy, E. G., Jackson, R. B., and Otero-Casal, C.: Hydrologic regulation of plant rooting depth, Proc Natl Acad Sci U S A, 114, 10572-10577, doi:10.1073/pnas.1712381114, 2017.
Faure, G., and Powell, J. L.: Strontium Isotope Geology, Isotopes in Geology, 1972.
Faure, G., and Mensing, T. M.: Isotopes: principles and applications, Wiley-Blackwell, 2005.
Ferrier, K. L., Kirchner, J. W., and Finkel, R. C.: Erosion rates over millennial and decadal timescales at Caspar Creek and Redwood Creek, Northern California Coast Ranges, Earth Surface Processes and Landforms, 30, 1025-1038, doi:10.1002/esp.1260, 2005.
Ferrier, K. L., Kirchner, J. W., Riebe, C. S., and Finkel, R. C.: Mineral-specific chemical weathering rates over millennial timescales: Measurements at Rio Icacos, Puerto Rico, Chem. Geol., 277, 101-114, doi:10.1016/j.chemgeo.2010.07.013, 2010.
Ferrier, K. L., Kirchner, J. W., and Finkel, R. C.: Weak influences of climate and mineral supply rates on chemical erosion rates: Measurements along two altitudinal transects in the Idaho Batholith, Journal of Geophysical Research: Earth Surface, 117, F02026, doi:10.1029/2011jf002231, 2012.
Finlay, R. D., Mahmood, S., Rosenstock, N., Bolou-Bi, E. B., Köhler, S. J., Fahad, Z., Rosling, A., Wallander, H., Belyazid, S., Bishop, K., and Lian, B.: Reviews and syntheses: Biological weathering and its consequences at different spatial levels – from nanoscale to global scale, Biogeosciences, 17, 1507-1533, doi:10.5194/bg-17-1507-2020, 2020.
Fisher, B. A., Rendahl, A. K., Aufdenkampe, A. K., and Yoo, K.: Quantifying weathering on variable rocks, an extension of geochemical mass balance: Critical zone and landscape evolution, Earth Surface Processes and Landforms, 42, 2457-2468, doi:10.1002/esp.4212, 2017.
Gallo, M. E., Sinsabaugh, R. L., and Cabaniss, S. E.: The role of ultraviolet radiation in litter decomposition in arid ecosystems, Applied Soil Ecology, 34, 82-91, doi:10.1016/j.apsoil.2005.12.006, 2006.
Gerrits, R., Pokharel, R., Breitenbach, R., Radnik, J., Feldmann, I., Schuessler, J. A., von Blanckenburg, F., Gorbushina, A. A., and Schott, J.: How the rock-inhabiting fungus K. petricola A95 enhances olivine dissolution through attachment, Geochim. Cosmochim. Acta, 282, 76-97, doi:10.1016/j.gca.2020.05.010, 2020.
Giehl, R. F., and von Wiren, N.: Root nutrient foraging, Plant Physiol., 166, 509-517, doi:10.1104/pp.114.245225, 2014.
Godoy, R., and Mayr, R.: Caracterización morfológica de micorrizas vesículo-arbusculares en coníferas endémicas del sur de Chile., Bosque, 10, 89-98, 1989.
Godsey, S. E., Hartmann, J., and Kirchner, J. W.: Catchment chemostasis revisited: Water quality responds differently to variations in weather and climate, Hydrological Processes, 33, 3056-3069, doi:10.1002/hyp.13554, 2019.
Green, E., Dietrich, W., and Banfield, J.: Quantification of chemical weathering rates across an actively eroding hillslope, Earth, Planet. Sci. Lett., 242, 155-169, doi:10.1016/j.epsl.2005.11.039, 2006.
Hahm, W. J., Riebe, C. S., Lukens, C. E., and Araki, S.: Bedrock composition regulates mountain ecosystems and landscape evolution, Proc Natl Acad Sci U S A, 111, 3338-3343, doi:10.1073/pnas.1315667111, 2014.
Hasenmueller, E. A., Gu, X., Weitzman, J. N., Adams, T. S., Stinchcomb, G. E., Eissenstat, D. M., Drohan, P. J., Brantley, S. L., and Kaye, J. P.: Weathering of rock to regolith: The activity of deep roots in bedrock fractures, Geoderma, 300, 11-31, doi:10.1016/j.geoderma.2017.03.020, 2017.
Hattenschwiler, S., Coq, S., Barantal, S., and Handa, I. T.: Leaf traits and decomposition in tropical rainforests: revisiting some commonly held views and towards a new hypothesis, New Phytol., 189, 950-965, doi:10.1111/j.1469-8137.2010.03483.x, 2011.
He, X. T., Logan, T. J., and Traina, S. J.: Physical and chemical characteristics of selected US municipal solid waste composts., Journal of Environmental Quality, 24, 543-552, doi:10.2134/jeq1995.00472425002400030022x, 1995.
Heartsill Scalley, T., Scatena, F. N., Moya, S., and Lugo, A. E.: Long-term dynamics of organic matter and elements exported as coarse particulates from two Caribbean montane watersheds, J. Trop. Ecol., 28, 127-139, doi:10.1017/s0266467411000733, 2012.
Heimsath, A. M., Dietrich, W. E., Nishiizumi, K., and Finkel, R. C.: The soil production function and landscape equilibrium, Nature, 388, 358-361, doi:10.1038/41056, 1997.
Hervé, F., Munizaga, F., Mantovani, M., and Hervé, M.: Edades Rb/Sr neopaleozoicas del basamento cristallino de la Cordillera de Nahuelbuta, Primer Congresso Geologico Chileno, Santiago, 1976.
Hervé, F.: Petrology of the crystalline basement of the Nahuelbuta Mountains, south-central Chile, Comparative studies on the Geology of the Circum-Pacific orogenic belt in Japan and Chile, edited by: Ishikava, I., and Aguirre, L., Japan Society for the Promotion of Science, 1977.
Hewawasam, T., von Blanckenburg, F., Bouchez, J., Dixon, J. L., Schuessler, J. A., and Maekeler, R.: Slow advance of the weathering front during deep, supply-limited saprolite formation in the tropical Highlands of Sri Lanka, Geochim. Cosmochim. Acta, 118, 202-230, doi:10.1016/j.gca.2013.05.006, 2013.
Ibarra, D. E., Caves, J. K., Moon, S., Thomas, D. L., Hartmann, J., Chamberlain, C. P., and Maher, K.: Differential weathering of basaltic and granitic catchments from concentration–discharge relationships, Geochim. Cosmochim. Acta, 190, 265-293, doi:10.1016/j.gca.2016.07.006, 2016.
Ibarra, D. E., Rugenstein, J. K. C., Bachan, A., Baresch, A., Lau, K. V., Thomas, D. L., Lee, J.-E., Boyce, C. K., and Chamberlain, C. P.: Modeling the consequences of land plant evolution on silicate weathering, Am. J. Sci., 319, 1-43, doi:10.2475/01.2019.01, 2019.

hat gelöscht: Elser, J. J., Fagan, W. F., Kerkhoff, A. J., Swenson, N. G., and Enquist, B. J.: Biological stoichiometry of plant production: metabolism, scaling and ecological response to global change, The New phytologist, 186, 593-608, 10.1111/j.1469-8137.2010.03214.x, 2010.¶

hat gelöscht: n/a-n/a,

hat gelöscht: Finlay, R., Wallander, H., Smits, M., Holmstrom, S., van Hees, P., Lian, B., and Rosling, A.: The role of fungi in biogenic weathering in boreal forest soils, Fungal Biology Reviews, 23, 101-106, 10.1016/j.fbr.2010.03.002, 2009.¶

hat gelöscht: Geider, R. J., and La Roche, J.: Redfield revisited: variability of C [ratio] N [ratio] P in marine microalgae and its biochemical basis, European Journal of Phycology, 37, 1-17, 10.1017/S0967026201003456, 2002.¶

hat gelöscht: ,

hat gelöscht: and Planetary Science Letters,

hat gelöscht: Journal of Tropical Ecology,

hat gelöscht: Geochimica et Cosmochimica

hat gelöscht: Hillebrand, H., Cowles, J. M., Lewandowska, A., Van de Waal, D. B., and Plum, C.: Think ratio! A stoichiometric view on biodiversity–ecosystem functioning research, Basic and Applied Ecology, 15, 465-474, 10.1016/j.baae.2014.06.003, 2014.¶

hat gelöscht: American Journal of Science,

Jobbágy, E. G., and Jackson, R. B.: The uplift of soil nutrients by plants: Biogeochemical consequences across scales., Ecology, 85, 2380-2389, 2004.
Jobbágy, E. G. a. J., Robert B: The distribution of soil nutrients with depth: global patterns and the imprint of plants, Biogeochemistry, 53, 51-77, doi:10.1023/A:1010760720215, 2001.
Joos, O., Hagedorn, F., Heim, A., Gilgen, A. K., Schmidt, M. W. I., Siegwolf, R. T. W., and Buchmann, N.: Summer drought reduces total and litter-derived soil CO2 effluxes in temperate grassland – clues from a 13C litter addition experiment, Biogeosciences, 7, 1031-1041, doi:10.5194/bg-7-1031-2010, 2010.
Jung, M., Reichstein, M., Margolis, H. A., Cescatti, A., Richardson, A. D., Arain, M. A., Arneth, A., Bernhofer, C., Bonal, D., Chen, J., Gianelle, D., Gobron, N., Kiely, G., Kutsch, W., Lasslop, G., Law, B. E., Lindroth, A., Merbold, L., Montagnani, L., Moors, E. J., Papale, D., Sottocornola, M., Vaccari, F., and Williams, C.: Global patterns of land-atmosphere fluxes of carbon dioxide, latent heat, and sensible heat derived from eddy covariance, satellite, and meteorological observations, Journal of Geophysical Research, 116, doi:10.1029/2010jg001566, 2011.
Kalinowski, B. E., Liermann, L. J., Givens, S., and Brantley, S. L.: Rates of bacteria-promoted solubilization of Fe from minerals: a review of problems and approaches, Chem. Geol., 169, 357-370, doi:10.1016/s0009-2541(00)00214-x, 2000.
Kelly, A. E., and Goulden, M. L.: A montane Mediterranean climate supports year-round photosynthesis and high forest biomass, Tree Physiol, 36, 459-468, doi:10.1093/treephys/tpv131, 2016.
Kelly, E. F., Chadwick, O. A., and Hilinski, T. E.: The effect of plants on mineral weathering, Biogeochemistry, 42, 21-53, doi:10.1023/a:1005919306687, 1998.
Kleidon, A., Fraedrich, K., and Heimann, M.: A Green Planet Versus a Desert World: Estimating the Maximum Effect of Vegetation on the Land Surface Climate, Clim. Change, 44, 471-493, doi:10.1023/a:1005559518889, 2000.
Kronzucker, H. J., and Britto, D. T.: Sodium transport in plants: a critical review, New Phytol., 189, 54-81, doi:10.1111/j.1469-8137.2010.03540.x, 2011.
Kump, L. R., Brantley, S. L., and Arthur, M. A.: Chemical Weathering, Atmospheric CO2, and Climate, Annual Review of Earth and Planetary Sciences, 28, 611-667, doi:10.1146/annurev.earth.28.1.611, 2000.
Laliberte, E., Grace, J. B., Huston, M. A., Lambers, H., Teste, F. P., Turner, B. L., and Wardle, D. A.: How does pedogenesis drive plant diversity?, Trends Ecol. Evol., 28, 331-340, doi:10.1016/j.tree.2013.02.008, 2013.
Lambers, H., Raven, J. A., Shaver, G. R., and Smith, S. E.: Plant nutrient-acquisition strategies change with soil age, Trends Ecol. Evol., 23, 95-103, doi:10.1016/j.tree.2007.10.008, 2008.
Lambers, H., Brundrett, M. C., Raven, J. A., and Hopper, S. D.: Plant mineral nutrition in ancient landscapes: high plant species diversity on infertile soils is linked to functional diversity for nutritional strategies, Plant Soil, 348, 7-27, doi:10.1007/s11104-011-0977-6, 2011.
Lang, F., Bauhus, J., Frossard, E., George, E., Kaiser, K., Kaupenjohann, M., Krüger, J., Matzner, E., Polle, A., Prietzel, J., Rennenberg, H., and Wellbrock, N.: Phosphorus in forest ecosystems: New insights from an ecosystem nutrition perspective, J. Plant Nutr. Soil Sci., 179, 129-135, doi:10.1002/jpln.201500541, 2016.
Lang, F., Krüger, J., Amelung, W., Willbold, S., Frossard, E., Bünemann, E. K., Bauhus, J., Nitschke, R., Kandeler, E., Marhan, S., Schulz, S., Bergkemper, F., Schloter, M., Luster, J., Guggisberg, F., Kaiser, K., Mikutta, R., Guggenberger, G., Polle, A., Pena, R., Prietzel, J., Rodionov, A., Talkner, U., Meesenburg, H., von Wilpert, K., Hölscher, A., Dietrich, H. P., and Chmara, I.: Soil phosphorus supply controls P nutrition strategies of beech forest ecosystems in Central Europe, Biogeochemistry, 136, 5-29, doi:10.1007/s10533-017-0375-0, 2017.
Lee, J.-E., and Boyce, K.: Impact of the hydraulic capacity of plants on water and carbon fluxes in tropical South America, Journal of Geophysical Research, 115, doi:10.1029/2010jd014568, 2010.
Lenton, T. M., Crouch, M., Johnson, M., Pires, N., and Dolan, L.: First plants cooled the Ordovician, Nature Geoscience, 5, 86-89, doi:10.1038/ngeo1390, 2012.
Liang, Y., Sun, W., Zhu, Y. G., and Christie, P.: Mechanisms of silicon-mediated alleviation of abiotic stresses in higher plants: a review, Environ. Pollut., 147, 422-428, doi:10.1016/j.envpol.2006.06.008, 2007.
Lin, H.: Linking principles of soil formation and flow regimes, Journal of Hydrology, 393, 3-19, doi:10.1016/j.jhydrol.2010.02.013, 2010.
Lucas, Y.: The Role of Plants in Controlling Rates and Products of Weathering: Importance of Biological Pumping, Annual Review of Earth and Planetary Sciences, 29, 135-163, doi:10.1146/annurev.earth.29.1.135, 2001.
Luebert, F., and Pliscoff, P.: Sinópsis bioclimática y vegetacional de Chile., Editorial Universitaria, Santiago de Chile, 2006.
Ma, J. F., and Yamaji, N.: Functions and transport of silicon in plants, Cell. Mol. Life Sci., 65, 3049-3057, doi:10.1007/s00018-008-7580-x, 2008.
Maher, K.: The dependence of chemical weathering rates on fluid residence time, Earth. Planet. Sci. Lett., 294, 101-110, doi:10.1016/j.epsl.2010.03.010, 2010.
Maher, K., and Chamberlain, C. P.: Hydrologic regulation of chemical weathering and the geologic carbon cycle, Science, 343, 1502-1504, doi:10.1126/science.1250770, 2014.
Marschner, H.: General introduction to the mineral nutrition of plants, Inorganic plant nutrition, 5-60, 1983.
McCulley, R. L., Jobbágy, E. G., Pockman, W. T., and Jackson, R. B.: Nutrient uptake as a contributing explanation for deep rooting in arid and semi-arid ecosystems, Oecologia, 141, 620-628, doi:10.1007/s00442-004-1687-z, 2004.

hat gelöscht: Jobbágy, E. G. a.
hat gelöscht: Climatic
hat gelöscht: ,
hat gelöscht: ,
hat gelöscht: Journal of
hat gelöscht: Nutrition and
hat gelöscht: Science,
hat gelöscht: J Geophys Res
hat gelöscht: ,
hat gelöscht: 2001.

Melnik, D.: Rise of the central Andean coast by Earthquakes straddling the Moho., Nature Geoscience, 9, 401-407, doi:10.1038/ngeo2683, 2016.
Información Oficial Hidrometeorológica y de Calidad de Aguas en Línea: http://snia.dga.cl/BNAConsultas/reportes, access: 12.06.2017, 2017.
Minyard, M. L., Bruns, M. A., Liermann, L. J., Buss, H. L., and Brantley, S. L.: Bacterial Associations with Weathering Minerals at the Regolith-Bedrock Interface, Luquillo Experimental Forest, Puerto Rico, Geomicrobiol. J., 29, 792-803, doi:10.1080/01490451.2011.619640, 2012.
Miralles González, C.: Evaluación de los factores que controllan la geoquímica de sedimentos fluviales de la cuenca del Río Elqui, Región de Coquimbo, Chile, Depeartamento de Geología, Universidad de Chile, 2013.
Molina, P. G., Parada, M. A., Gutiérrez, F. J., Ma, C., Li, J., Yuanyuan, L., Reich, M., and Aravena, Á.: Protracted late magmatic stage of the Caleu pluton (central Chile) as a consequence of heat redistribution by diking: Insights from zircon data and thermal modeling, Lithos, 227, 255-268, doi:10.1016/j.lithos.2015.04.008, 2015.
Mooney, H. A., Gulmon, S. L., Ehleringer, J., and Rundel, P. W.: Atmospheric water uptake by an Atacama Desert shrub, Science, 209, 693-694, 1980.
Moscoso, R., Nasi, C., and Salinas, P.: Hoja Vallenar y parte norte de La Serena: regiones de Atacama y Coquimbo: carta geológica de Chile 1: 250.000, Servicio Nacional de Geología y Minería Chile, 1982.
Moulton, K. L., West, J., and Berner, R. A.: Solute flux and mineral mass balance approaches to the quantification of plant effects on silicate weathering, Am. J. Sci., 300, 539-570, doi:10.2475/ajs.300.7.539, 2000.
Nier, A. O.: The Isotopic Constitution of Strontium, Barium, Bismuth, Thallium and Mercury, Physical Review, 54, 275-278, doi:10.1103/PhysRev.54.275, 1938.
Niklas, K. J., and Enquist, B. J.: Canonical rules for plant organ biomass partitioning and annual allocation., Am. J. Bot., 89, 812-819, 2002.
Oelkers, E. H., Benning, L. G., Lutz, S., Mavromatis, V., Pearce, C. R., and Plümper, O.: The efficient long-term inhibition of forsterite dissolution by common soil bacteria and fungi at Earth surface conditions, Geochim. Cosmochim. Acta, 168, 222-235, doi:10.1016/j.gca.2015.06.004, 2015.
Oelmann, Y., Richter, A. K., Roscher, C., Rosenkranz, S., Temperton, V. M., Weisser, W. W., and Wilcke, W.: Does plant diversity influence phosphorus cycling in experimental grasslands?, Geoderma, 167-168, 178-187, doi:10.1016/j.geoderma.2011.09.012, 2011.
Oeser, R. A., Stroncik, N., Moskwa, L.-M., Bernhard, N., Schaller, M., Canessa, R., van den Brink, L., Köster, M., Brucker, E., Stock, S., Fuentes, J. P., Godoy, R., Matus, F. J., Oses Pedraza, R., Osses McIntyre, P., Paulino, L., Seguel, O., Bader, M. Y., Boy, J., Dippold, M. A., Ehlers, T. A., Kühn, P., Kuzyakov, Y., Leinweber, P., Scholten, T., Spielvogel, S., Spohn, M., Übernickel, K., Tielbörger, K., Wagner, D., and von Blanckenburg, F.: Chemistry and Microbiology of the Critical Zone along a steep climate and vegetation gradient in the Chilean Coastal Cordillera., Catena, 170, 183-203, doi:10.1016/j.catena.2018.06.002, 2018.
Oeser, R. A., and von Blanckenburg, F.: Dataset for evaluation element fluxes released by weathering and taken up by plants along the EarthShape climate and vegetation gradient, GFZ Data Services, doi:10.5880/GFZ.3.3.2020.003, 2020.
OriginPro, OriginLab Corporation, Northampton, MA, USA, Version 2020.
Pagani, M., Caldeira, K., Berner, R., and Beerling, D. J.: The role of terrestrial plants in limiting atmospheric CO(2) decline over the past 24 million years, Nature, 460, 85-88, doi:10.1038/nature08133, 2009.
Parada, M. A., and Larrondo, P.: Thermochronology of the Lower Cretaceous Caleu Pluton in the coastal range of central Chile: tectonostratigraphic implications, Abstracts, 4th International Symposium of Andean Geodynamics, Göttingen, 1999, 563-566,
Parada, M. A., Larrondo, P., Guiresse, C., and Roperch, P.: Magmatic Gradients in the Cretaceous Caleu Pluton (Central Chile): Injections of Pulses from a Stratified Magma Reservoir, Gondwana Research, 5, 307-324, doi:10.1016/s1342-937x(05)70725-5, 2002.
Parada, M. A., López-Escobar, L., Oliveros, V., Fuentes, F., Morata, D., Calderón, M., Aguirre, L., Féraud, G., Espinoza, F., Moreno, H., Figueroa, O., Muñoz Bravo, J., Vásquez, R. T., and Stern, C. R.: Andean magmatism, in: The Geology of Chile, edited by: Moreno, T., and Gibbons, W., The Geological Society of London, 115-146, doi:10.1144/GOCH.4, 2007.
Pearce, C. R., Parkinson, I. J., Gaillardet, J., Chetelat, B., and Burton, K. W.: Characterising the stable (δ 88/86 Sr) and radiogenic (87 Sr/ 86 Sr) isotopic composition of strontium in rainwater, Chem. Geol., 409, 54-60, doi:10.1016/j.chemgeo.2015.05.010, 2015.
Perez-Fodich, A., and Derry, L. A.: Organic acids and high soil CO2 drive intense chemical weathering of Hawaiian basalts: Insights from reactive transport models, Geochim. Cosmochim. Acta, 249, 173-198, doi:10.1016/j.gca.2019.01.027, 2019.
Porada, P., Lenton, T. M., Pohl, A., Weber, B., Mander, L., Donnadieu, Y., Beer, C., Poschl, U., and Kleidon, A.: High potential for weathering and climate effects of non-vascular vegetation in the Late Ordovician, Nat Commun, 7, 12113, doi:10.1038/ncomms12113, 2016.
Porder, S., Vitousek, P. M., Chadwick, O. A., Chamberlain, C. P., and Hilley, G. E.: Uplift, Erosion, and Phosphorus Limitation in Terrestrial Ecosystems, Ecosystems, 10, 159-171, doi:10.1007/s10021-006-9011-x, 2007.
Porder, S., and Chadwick, O. A.: Climate and soil-age constraints on nutrient uplift and retention by plants, Ecology, 90, 623-636, doi:10.1890/07-1739.1, 2009.
Porder, S.: How Plants Enhance Weathering and How Weathering is Important to Plants, Elements, 15, 241-246, doi:10.2138/gselements.15.4.241, 2019.

hat gelöscht: https://doi.org/10.1038/ngeo2683,

hat gelöscht: Geomicrobiology Journal,

hat gelöscht: Moore, C. M., Mills, M. M., Arrigo, K. R., Berman-Frank, I., Bopp, L., Boyd, P. W., Galbraith, E. D., Geider, R. J., Guieu, C., Jaccard, S. L., Jickells, T. D., La Roche, J., Lenton, T. M., Mahowald, N. M., Marañón, E., Marinov, I., Moore, J. K., Nakatsuka, T., Oschlies, A., Saito, M. A., Thingstad, T. F., Tsuda, A., and Ulloa, O.: Processes and patterns of oceanic nutrient limitation, Nature Geoscience, 6, 701-710, 10.1038/ngeo1765, 2013.¶
Moore, T. R., Trofymow, J. A., Siltanen, M., Prescott, C., and Group, C. W.: Patterns of decomposition and carbon, nitrogen, and phosphorus dynamics of litter in upland forest and peatland sites in central Canada, Canadian Journal of Forest Research, 35, 133-142, 10.1139/x04-149, 2005.¶

hat gelöscht: American Journal of Science,

hat gelöscht: American Journal of Botany,

hat gelöscht: Chemical Geology,

Poszwa, A., Dambrine, E., Ferry, B., Pollier, B., and Loubet, M.: Do deep tree roots provide nutrients to the tropical rainforest, Biogeochemistry, 60, 97-118, doi:10.1023/A:1016548113624, 2002.
Powers, J. S., Becklund, K. K., Gei, M. G., Iyengar, S. B., Meyer, R., O'Connell, C. S., Schilling, E. M., Smith, C. M., Waring, B. G., and Werden, L. K.: Nutrient addition effects on tropical dry forests: a mini-review from microbial to ecosystem scales, Frontiers in Earth Science, 3, doi:10.3389/feart.2015.00034, 2015.
Quirk, J., Andrews, M. Y., Leake, J. R., Banwart, S. A., and Beerling, D. J.: Ectomycorrhizal fungi and past high CO2 atmospheres enhance mineral weathering through increased below-ground carbon-energy fluxes., Biol. Lett., 10, doi:10.1098/rsbl.2014.0375, 2014.
Rempe, D. M., and Dietrich, W. E.: Direct observations of rock moisture, a hidden component of the hydrologic cycle, Proceedings of the National Academy of Sciences, doi:10.1073/pnas.1800141115, 2018.
Riebe, C. S., Kirchner, J. W., Granger, D. E., and Finkel, R. C.: Strong tectonic and weak climatic control of long-term chemical weathering rates, Geology, 29, 511-514, doi:10.1130/0091-7613, 2001.
Riebe, C. S., and Granger, D. E.: Quantifying effects of deep and near-surface chemical erosion on cosmogenic nuclides in soils, saprolite, and sediment, Earth Surface Processes and Landforms, 38, 523-533, doi:10.1002/esp.3339, 2013.
Rundel, P. W., Ehleringer, J., Mooney, H. A., and Gulmon, S. L.: Patterns of drought response in leaf-succulent shrubs of the coastal Atacama Desert in Northern Chile, Oecologia, 46, 196-200, doi:10.1007/BF00540126, 1980.
Schaller, J., Turner, B. L., Weissflog, A., Pino, D., Bielnicka, A. W., and Engelbrecht, B. M. J.: Silicon in tropical forests: large variation across soils and leaves suggests ecological significance, Biogeochemistry, 140, 161-174, doi:10.1007/s10533-018-0483-5, 2018a.
Schaller, M., Ehlers, T. A., Lang, K. A. H., Schmid, M., and Fuentes-Espoz, J. P.: Addressing the contribution of climate and vegetation cover on hillslope denudation, Chilean Coastal Cordillera (26°–38°S), Earth Planet. Sci. Lett., 489, 111-122, doi:10.1016/j.epsl.2018.02.026, 2018b.
Schuessler, J. A., Kämpf, H., Koch, U., and Alawi, M.: Earthquake impact on iron isotope signatures recorded in mineral spring water, Journal of Geophysical Research: Solid Earth, 121, 1-21, doi:10.1002/2016JB013408, 2016.
Schuessler, J. A., von Blanckenburg, F., Bouchez, J., Uhlig, D., and Hewawasam, T.: Nutrient cycling in a tropical montane rainforest under a supply-limited weathering regime traced by elemental mass balances and Mg stable isotopes, Chem. Geol., 497, 74-87, doi:10.1016/j.chemgeo.2018.08.024, 2018.
The Geobiology of Weathering: a 13th Hypothesis, https://arxiv.org/pdf/1509.04234.pdf, 2015.
Smeck, N. E., Runge, E., and Mackintosh, E.: Dynamics and genetic modeling of soil systems., in: Pedogenesis and soil taxonomy, edited by: Wilding, L. P., Elsevier, 51 - 81, 1983.
Smits, M. M., Bonneville, S., Benning, L. G., Banwart, S. A., and Leake, J. R.: Plant-driven weathering of apatite - the role of an ectomycorrhizal fungus., Geobiology, 10, 445-456, 2012.
Sohrt, J., Uhlig, D., Kaiser, K., von Blanckenburg, F., Siemens, J., Seeger, S., Frick, D. A., Krüger, J., Lang, F., and Weiler, M.: Phosphorus Fluxes in a Temperate Forested Watershed: Canopy Leaching, Runoff Sources, and In-Stream Transformation, Frontiers in Forests and Global Change, 2, doi:10.3389/ffgc.2019.00085, 2019.
Spohn, M., and Sierra, C. A.: How long do elements cycle in terrestrial ecosystems?, Biogeochemistry, 139, 69-83, doi:10.1007/s10533-018-0452-z, 2018.
Sprenger, M., Stumpp, C., Weiler, M., Aeschbach, W., Allen, S. T., Benettin, P., Dubbert, M., Hartmann, A., Hrachowitz, M., Kirchner, J. W., McDonnell, J. J., Orlowski, N., Penna, D., Pfahl, S., Rinderer, M., Rodriguez, N., Schmidt, M., and Werner, C.: The Demographics of Water: A Review of Water Ages in the Critical Zone, Rev. Geophys., 57, 800-834, doi:10.1029/2018rg000633, 2019.
Tessier, A., Campbell, P. G. C., and Bisson, M.: Sequential Extraction Procedure for the Speciation of Particulate Trace Metals, Anal. Chem., 51, 844-851, 1979.
Tielbörger, K., Bilton, M. C., Metz, J., Kigel, J., Holzapfel, C., Lebrija-Trejos, E., Konsens, I., Parag, H. A., and Sternberg, M.: Middle-Eastern plant communities tolerate 9 years of drought in a multi-site climate manipulation experiment, Nature Communications, 5, doi:10.1038/ncomms6102, 2014.
Tiessen, H., and Moir, J. O.: Characterization of available P by sequential extraction, in: Soil sampling and methods of analysis, Lewis Publishers Boca Raton, FL, USA, 5-229, 1993.
Tipping, E., Woof, C., Rigg, E., Harrison, A., Ineson, P., Taylor, K., Benham, D., Poskitt, J., Rowland, A., and Bol, R.: Climatic influences on the leaching of dissolved organic matter from upland UK moorland soils, investigated by a field manipulation experiment, Environ. Int., 25, 83-95, doi:10.1016/s0160-4120(98)00098-1, 1999.
Uhlig, D., Schuessler, J. A., Bouchez, J. L., Dixon, J., and von Blanckenburg, F.: Quantifying nutrient uptake as driver of rock weathering in forest ecosystems by magnesium stable isotopes, Biogeosci. Disc., 1-28, doi:10.5194/bg-2016-521, 2017.
Uhlig, D., and von Blanckenburg, F.: How Slow Rock Weathering Balances Nutrient Loss During Fast Forest Floor Turnover in Montane, Temperate Forest Ecosystems, Frontiers in Earth Science, 7, doi:10.3389/feart.2019.00159, 2019.
van der Heijden, M. G. A., Klironomos, J. N., Ursic, M., Moutoglis, P., Streitwolf-Engel, R., Boller, T., Wiemken, A., and Sanders, I. R.: Mycorrhizal fungal diversity determines plant biodiversity, ecosystem variability and productivity, Nature, 396, 69-72, doi:10.1038/23932, 1998.

hat gelöscht: Taylor, L. L.,

hat gelöscht: Weathering by tree-root-associating

hat gelöscht: diminishes under simulated Cenozoic atmospheric CO₂ decline, Biogeosciences, 11, 321-331,

hat gelöscht: .5194/bg-11-321-

hat gelöscht: Redfield, A. C.: On the proportions of organic derivatives in sea water and their relation to the composition of plankton, James Johnstone memorial volume, 176-192, 1934.¶

hat gelöscht: Rosenstock, N. P.: Can ectomycorrhizal weathering activity respond to host nutrient demands?, Fungal Biology Reviews, 23, 107-114, 10.1016/j.fbr.2009.11.003, 2009.¶
Rosling, A., Lindahl, B. r. D., Taylor, A. F. S., and Finlay, R. D.: Mycelial growth and substrate acidification of ectomycorrhizal fungi in response to different minerals, FEMS Microbiology Ecology, 47, 31-37, 10.1016/s0168-6496(03)00222-8, 2004.¶

hat gelöscht: Sardans

hat gelöscht: Rivas-Ubach

hat gelöscht: Peñuelas,

hat gelöscht: The elemental stoichiometry of aquatic

hat gelöscht: terrestrial ecosystems and its relationships with organismic lifestyle and ecosystem structure and function: a review and perspectives

hat gelöscht: 111, 1-39,

hat gelöscht: 011-9640-9, 2011.¶
Scatena, F. N., and Lugo, A. E.: Geomorphology, disturbance, and the soil and vegetation of two subtropical wet steepland watersheds of Puerto Rico, Geomorphology, 13, 199-213, 10.1016/0169-555x(95)00021-v, 1995

hat gelöscht: and Planetary Science Letters,

hat gelöscht: 2018

hat gelöscht: Chemical Geology,

hat gelöscht: Schwartzmann, D.:

hat gelöscht: , arXiv preprint arXiv:1509.04234,

hat gelöscht: Silver, W. L., and Miya, R. K.: Global patterns in root decomposition: comparisons of climate and litter quality effects, Oecologia, 129, 407-419, 10.1007/s004420100740, 2001.¶

hat gelöscht: Sterner, R. W., and Elser, J. J.: Ecological Stoichiometry: The Biology of Elements from Molecules to the Biosphere, 2003.¶
Stock, S. C., Köster, M., Dippold, M. A., Nájera, F., Matus, F., Merino, C., Boy, J., Spielvogel, S., Gorbushina, A., and Kuzyakov, Y.: Environmental drivers and stoichiometric constraints on enzyme activities in soils from rhizosphere to continental scale, Geoderma, 337, 973-982, 10.1016/j.geoderma.2018.10.030, 2019.¶

hat gelöscht: Analytical Chemistry,

hat gelöscht: Biogeosciences Discussions,

van Dongen, R., Scherler, D., Wittmann, H., and von Blanckenburg, F.: Cosmogenic 10Be in river sediment: where grain size matters and why, Earth Surface Dynamics, 7, 393-410, doi:10.5194/esurf-7-393-2019, 2019.
van Schöll, L., Kuyper, T. W., Smits, M. M., Landeweert, R., Hoffland, E., and Breemen, N. v.: Rock-eating mycorrhizas: their role in plant nutrition and biogeochemical cycles, Plant Soil, 303, 35-47, doi:10.1007/s11104-007-9513-0, 2007.
Vitousek, P., Chadwick, O., Matson, P., Allison, S., Derry, L., Kettley, L., Luers, A., Mecking, E., Monastra, V., and Porder, S.: Erosion and the Rejuvenation of Weathering-derived Nutrient Supply in an Old Tropical Landscape, Ecosystems, 6, 762-772, doi:10.1007/s10021-003-0199-8, 2003.
Vitousek, P. M., and Reiners, W. A.: Ecosystem Succession and Nutrient Retention: A Hypothesis, Bioscience, 25, 376-381, doi:10.2307/1297148, 1975.
Vitousek, P. M., and Farrington, H.: Nutrient limitation and soil development: Experimental test of a biogeochemical theory, Biogeochemistry, 37, 63-75, doi:10.1023/a:1005757218475, 1997.
Vitousek, P. M., Hedin, L. O., Matson, P. A., Fownes, J. H., and Neff, J.: Within-System Element Cycles, Input-Output Budgets, and Nutrient Limitation, in: Successes, Limitations, and Frontiers in Ecosystem Science, Springer, New York, 432-451, doi:10.1007/978-1-4612-1724-4_18, 1998.
Vitousek, P. M.: Nutrient Cycling and Limitation: Hawai'i as a Model System, PRINCETON ENVIRONMENT AL INSTITUTE SERIES, 2004.
Vitousek, P. M., Porder, S., Houlton, B. Z., and Chadwick, O. A.: Terrestrial phosphorus limitation: mechanisms, implications, and nitrogen–phosphorus interactions, Ecol. Appl., 20, 5-15, doi:10.1890/08-0127.1, 2010.
Vitousek, P. M., and Chadwick, O. A.: Pedogenic Thresholds and Soil Process Domains in Basalt-Derived Soils, Ecosystems, 16, 1379-1395, doi:10.1007/s10021-013-9690-z, 2013.
von Blanckenburg, F., Wittmann, H., and Schuessler, J. A.: HELGES: Helmholtz Laboratory for the Geochemistry of the Earth Surface, Journal of large-scale research facilities JLSRF, 2, doi:10.17815/jlsrf-2-141, 2016.
Werner, C., Schmid, M., Ehlers, T. A., Fuentes-Espoz, J. P., Steinkamp, J., Forrest, M., Liakka, J., Maldonado, A., and Hickler, T.: Effect of changing vegetation and precipitation on denudation – Part 1: Predicted vegetation composition and cover over the last 21 thousand years along the Coastal Cordillera of Chile, Earth Surface Dynamics, 6, 829-858, doi:10.5194/esurf-6-829-2018, 2018.
White, A. F., Blum, A. E., Schulz, M. S., Vivit, D. V., Stonestrom, D. A., Larsen, M., Murphy, S. F., and Eberl, D.: Chemical Weathering in a Tropical Watershed, Luquillo Mountains, Puerto Rico: I. Long-Term Versus Short-Term Weathering Fluxes, Geochim. Cosmochim. Acta, 62, 209-226, doi:10.1016/s0016-7037(97)00335-9, 1998.
White, A. F., and Brantley, S. L.: The effect of time on the weathering of silicate minerals: why do weathering rates differ in the laboratory and field?, Chem. Geol., 202, 479-506, doi:10.1016/j.chemgeo.2003.03.001, 2003.
Wilcke, W., Yasin, S., Abramowski, U., Valarezo, C., and Zech, W.: Nutrient storage and turnover in organic layers under tropical montane rain forest in Ecuador, Eur. J. Soil Sci., 53, 15-27, 2002.
Wilcke, W., Velescu, A., Leimer, S., Bigalke, M., Boy, J., and Valarezo, C.: Biological versus geochemical control and environmental change drivers of the base metal budgets of a tropical montane forest in Ecuador during 15 years, Biogeochemistry, 136, 167-189, doi:10.1007/s10533-017-0386-x, 2017.
Winnick, M. J., and Maher, K.: Relationships between CO2, thermodynamic limits on silicate weathering, and the strength of the silicate weathering feedback, Earth Planet. Sci. Lett., 485, 111-120, doi:10.1016/j.epsl.2018.01.005, 2018.

hat gelöscht: and

hat gelöscht: Ecological Applications,

hat gelöscht: Wang, F., Michalski, G., Seo, J.-h., and Ge, W.: Geochemical, isotopic, and mineralogical constraints on atmospheric deposition in the hyper-arid Atacama Desert, Chile, Geochimica et Cosmochimica Acta, 135, 29-48, 10.1016/j.gca.2014.03.017, 2014.¶

hat gelöscht: White, A. E., Spitz, Y. H., Karl, D. M., and Letelier, R. M.: Flexible elemental stoichiometry in Trichodesmium spp. and its ecological implications, Limnology and Oceanography, 51, 1777-1790, 10.4319/lo.2006.51.4.1777, 2006.¶

hat gelöscht: Geochimica et Cosmochimica

hat gelöscht: European Journal of

hat gelöscht: Science,

hat gelöscht: and Planetary Science Letters,

hat gelöscht: ¶

15 Figures

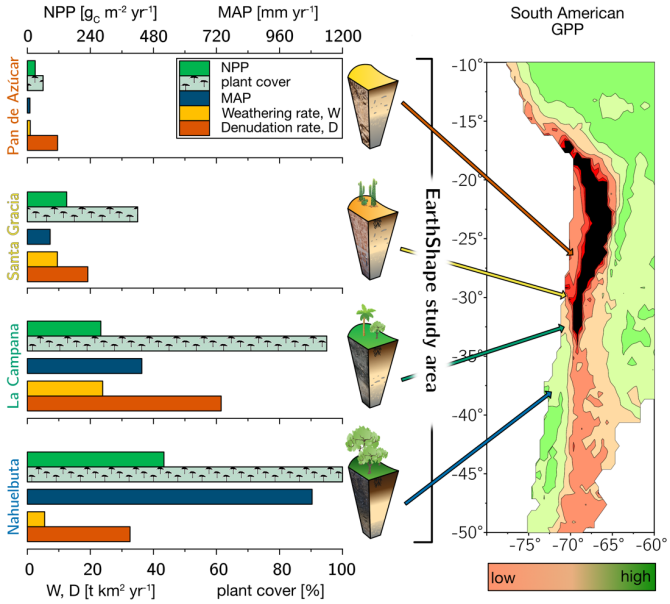

Figure 1 The climate and vegetation gradient of the four EarthShape study sites (from arid to humid: Pan de Azúcar, Santa Gracia, La Campana, and Nahuelbuta). Left: Net primary productivity (NPP), plant cover, annual precipitation (MAP). Denudation rate (D) and weathering rate (W) were determined with cosmogenic ^{10}Be. Right: Position of the four study sites in South America and their respective gross primary productivity (GPP) derived from the FLUXNET data base (Jung et al., 2011). Black colour refers to very low GPP in the Atacama Desert. The uncertainties are not shown for clarity. They are provided in Table 1.

hat nach oben verschoben [3]: Seitenumbruch

14

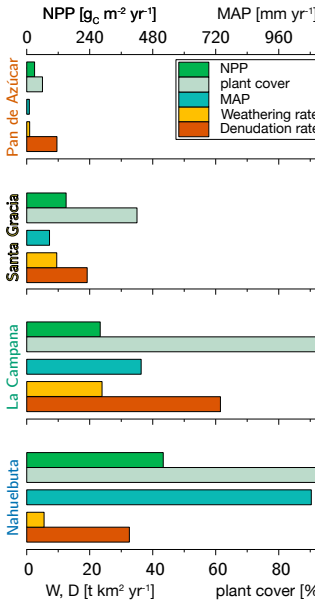

hat gelöscht:

hat gelöscht: (Jung et al., 2011)

hat gelöscht: ... [10]

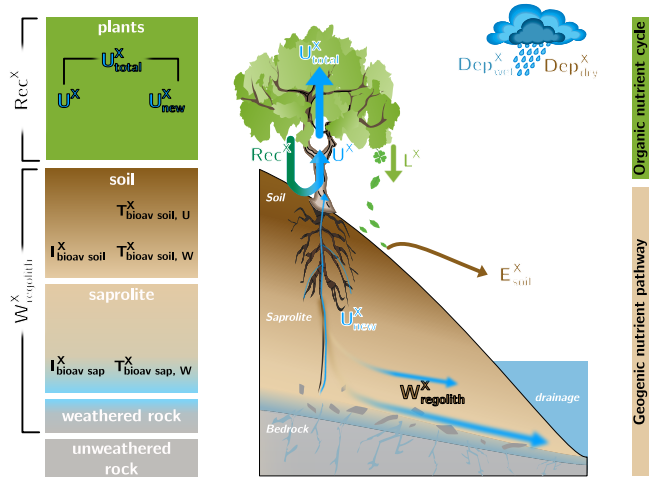

Figure 2 Conceptual framework of an ecosystem comprising the "geogenic nutrient pathway" and the "organic nutrient cycle" (modified after Uhlig and von Blanckenburg, 2019). Whereas the former is mainly set by mineral nutrient release by weathering ($W^X_{regolith}$) and to a minor extent by atmospheric wet- (Dep^X_{wet}) and dry deposition (Dep^X_{dry}), the organic nutrient cycle is mainly affected by nutrient re-utilization (i.e. recycling; Rec^X) from organic matter. Left: The different compartments (i.e. rock, saprolite, soil, and plants) are shown as boxes. They include the metrics used to quantify their properties such as the inventory I^X_{bulk} and turnover time $T^X_{i,j}$ of element X in compartment j. Right: The compartments are linked by fluxes (arrows) with the thickness of them denoting to their relative proportions. E^X_{soil} denotes to erosion of soil.

hat gelöscht: (modified after Uhlig and von Blanckenburg, 2019)....

hat gelöscht:)

hat gelöscht: (Rec^X).

hat gelöscht: the litter layer,

hat gelöscht: biota

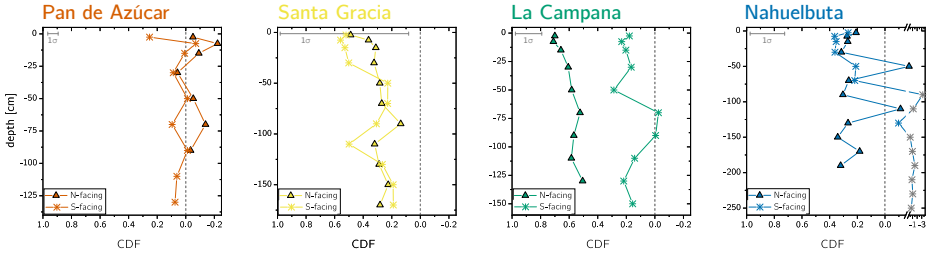

Figure 3 Chemical depletion fraction (CDF) for each study sites' north- and south- facing profile. The accuracy of the absolute CDF values is limited by the variability in the bedrocks' Zr concentration in the respective study sites and are indicated as grey 1 σ bar

(Table S1). The grey symbols correspond mainly to saprolite samples in the south-facing regolith profile in Nahuelbuta and are excluded from further consideration. Note that in Nahuelbuta a different scaling compared to the other study sites applies after the axis break.

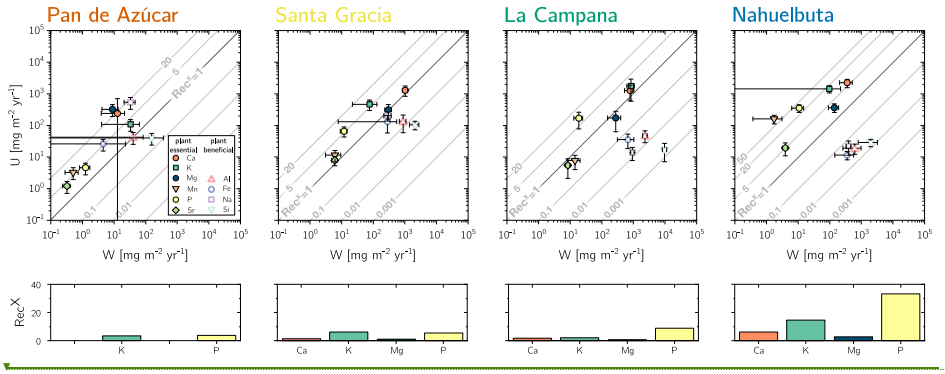

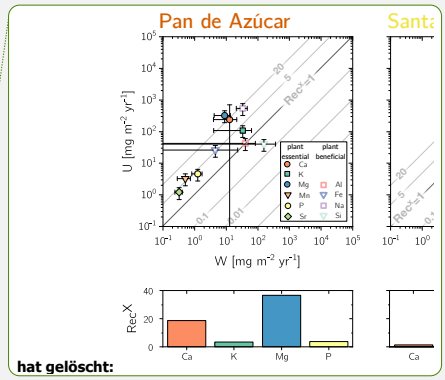

Figure 4 Chemical weathering flux ($W^X_{regolith}$) and plant nutrient-uptake fluxes (U^X_{total}) for Pan de Azúcar, Santa Gracia, La Campana, and Nahuelbuta (from left to right) for plant-essential and plant-beneficial elements. Grey contour lines emphasize the nutrient recycling factor (Rec^X), which is the ratio of U^X_{total} to $W^X_{regolith}$. Uncertainty bars show 1SD. Differences in nutrient recycling factors for the plant essential elements Ca, K, Mg, and P among the four study sites are highlighted in the lower panels. Note that here we use the Rec^X calculated for $W^X_{regolith}$ from silicate weathering only. In Table 7 and Fig. A4 we also show Rec^X including atmospheric inputs. Because Pan de Azúcar Ca and Mg inputs are exclusively atmospheric their Rec^X are overestimated and thus not plotted on the lower left panel.

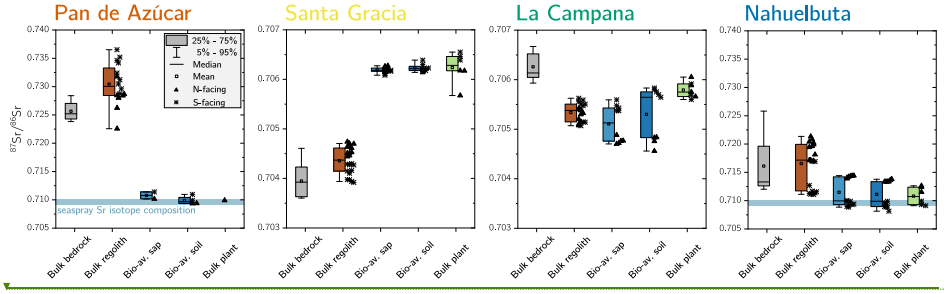

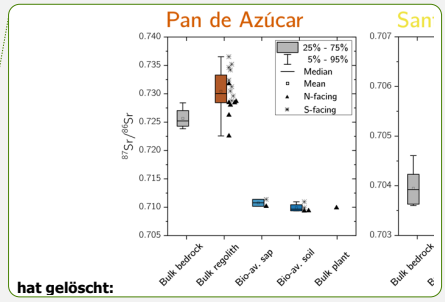

Figure 5 Average $^{87}Sr/^{86}Sr$ isotope composition of bedrock, bulk regolith, and the bio-available fraction in saprolite, soil, and plants in Pan de Azúcar, Santa Gracia, La Campana, and Nahuelbuta. The $^{87}Sr/^{86}Sr$ isotope ratios of bulk plant (green) are weighted according to the single species' organs relative growth rate (see Table 5 for weighting parameters). Whiskers span 90% of the respective data set. On the boxes' right-hand site, the differences between north- and south-facing regolith profiles are depicted. Note that bulk regolith samples in Nahuelbuta with anomalously low Zr concentrations have been excluded from this analysis as

they are suspected to comprise a different parent rock. Y-axis covers broader range in Pan de Azúcar and Nahuelbuta than in Santa Gracia and La Campana.

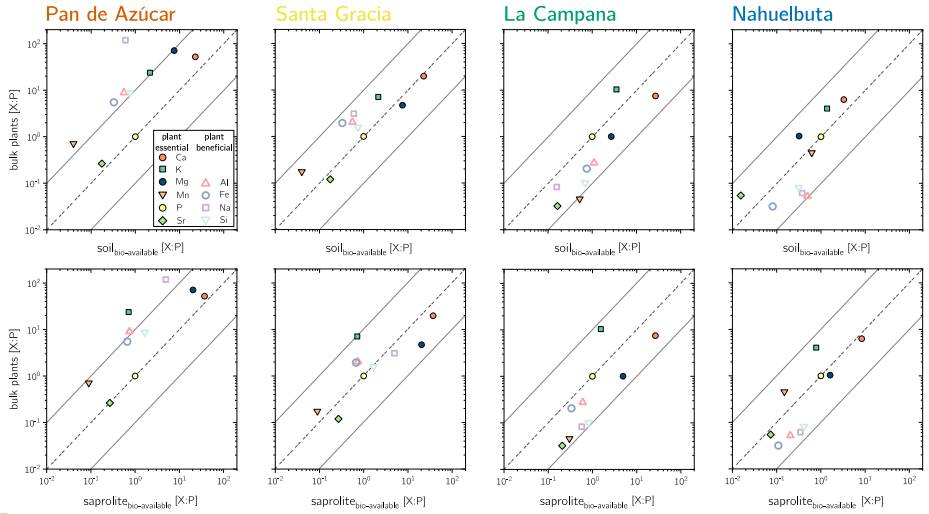

675 **Figure 6 P-normalized element composition for bulk plants and the bio-available fraction in soil and saprolite. Solid grey lines reflect the 10-x P and 0.1-x P concentration, respectively. Note that with increasing recycling from Santa Gracia to Nahuelbuta, the bio-available fractions' X:P successively approaches X:P in vegetation.**

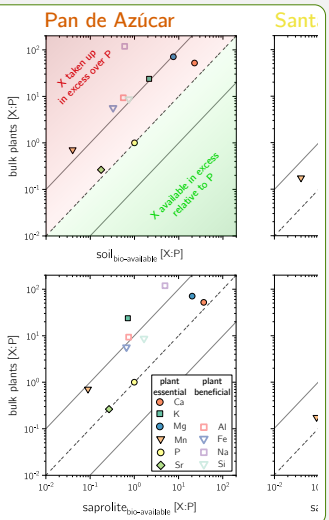

hat gelöscht:

hat gelöscht: in Pan de Azúcar, Santa Gracia, La Campana, and Nahuelbuta….

hat gelöscht: -

hat gelöscht: -fold

hat gelöscht: Elements

hat gelöscht: within this envelope are believed

hat gelöscht: set the ecosystems' ecological stoichiometry. Elements above the dashed grey line are taken up in excess over P, below the line they exist in surplus in

hat gelöscht: soil fraction

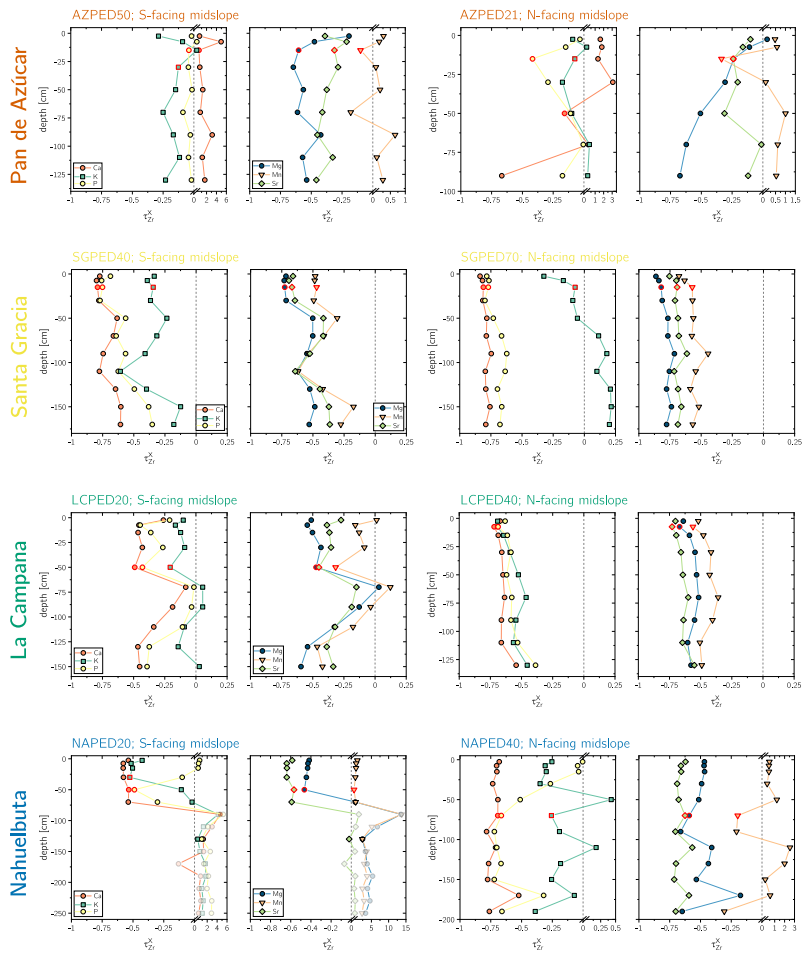

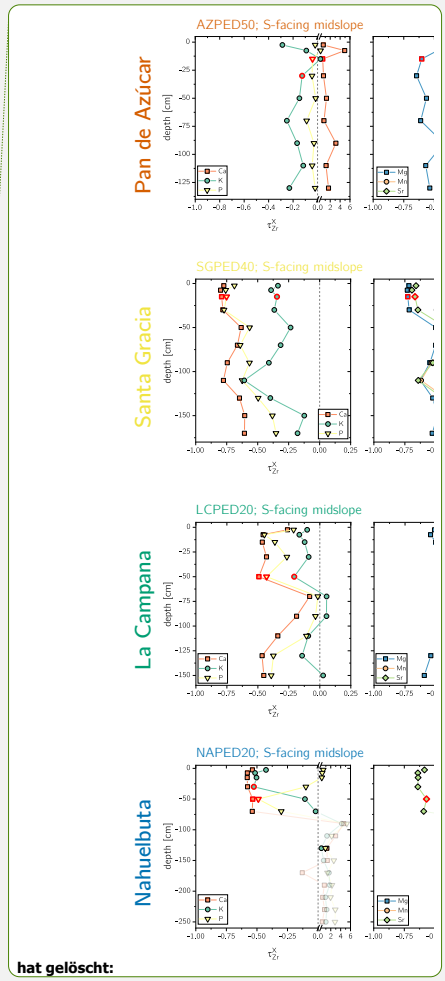

hat gelöscht:

Figure A1. Depth distribution of the elemental loss and gain fractions (i.e. elemental mass transfer coefficient, τ). The vertical dashed line indicates $\tau_{Zr}^{X} = 0$ and represents unweathered parent bedrock. τ-values corresponding to the shallowest mineral soil samples are highlighted with a red rim. Grey symbols in Nahuelbuta are discarded due to the samples' anomalous low Zr concentration. Note that these τ-values deviate from those reported in Oeser et al., 2018, such that in this work they have been calculated relative to the bedrocks' initial chemical composition.

hat gelöscht: **) for Pan de Azúcar, Santa Gracia, La Campana, and Nahuelbuta.**

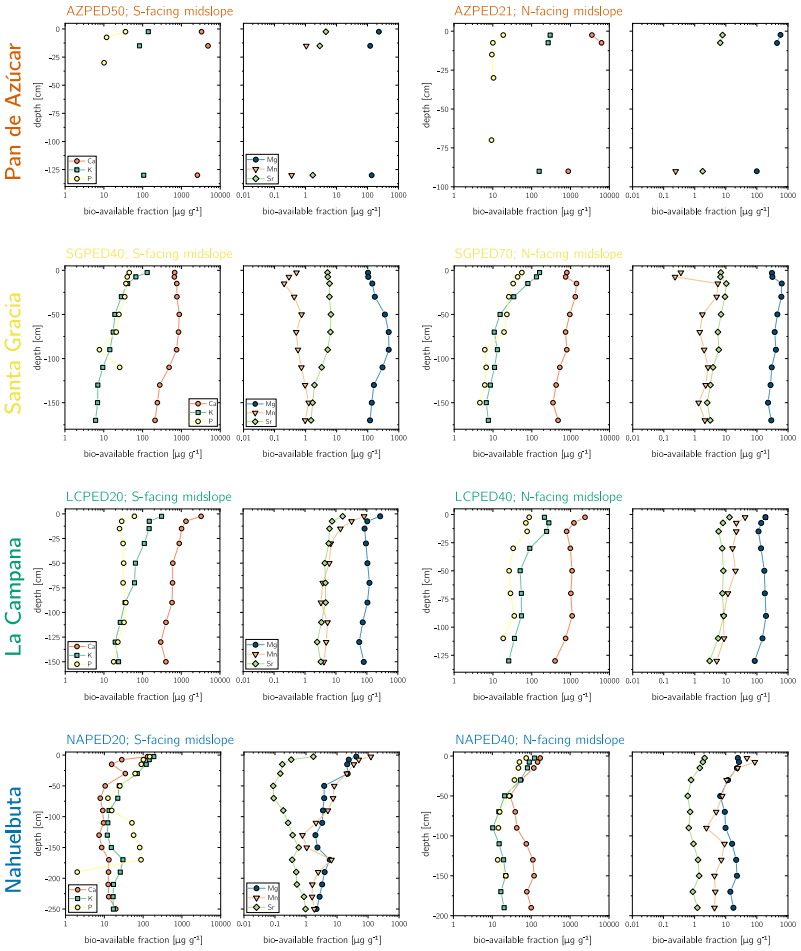

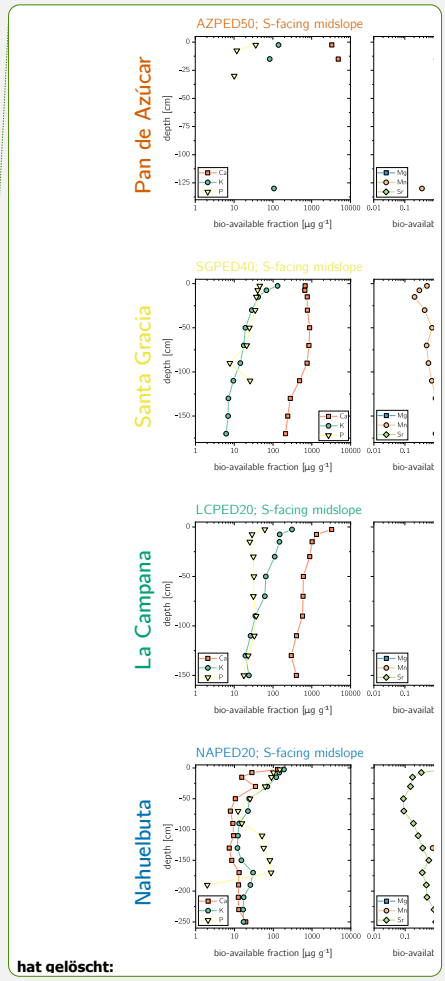

Figure A2. Depth distribution of the concentration of sequentially extracted bio-available fraction of plant-essential elements including Sr, comprised of the water soluble (18 MΩ Milli-Q H_2O) and the exchangeable (1 M NH_4OAc) fraction. P-accessibility in the bio-available fraction has been determined by Brucker and Spohn (2019) using a modified Hedley sequential P fractionation method. Note that in Pan de Azúcar the acquisition of the bio-available fraction was only possible on three samples per site. Data gaps do occur if both extractions of one sample were below limit of detection.

hat gelöscht: at Pan de Azúcar, Santa Gracia, La Campana, and Nahuelbuta.

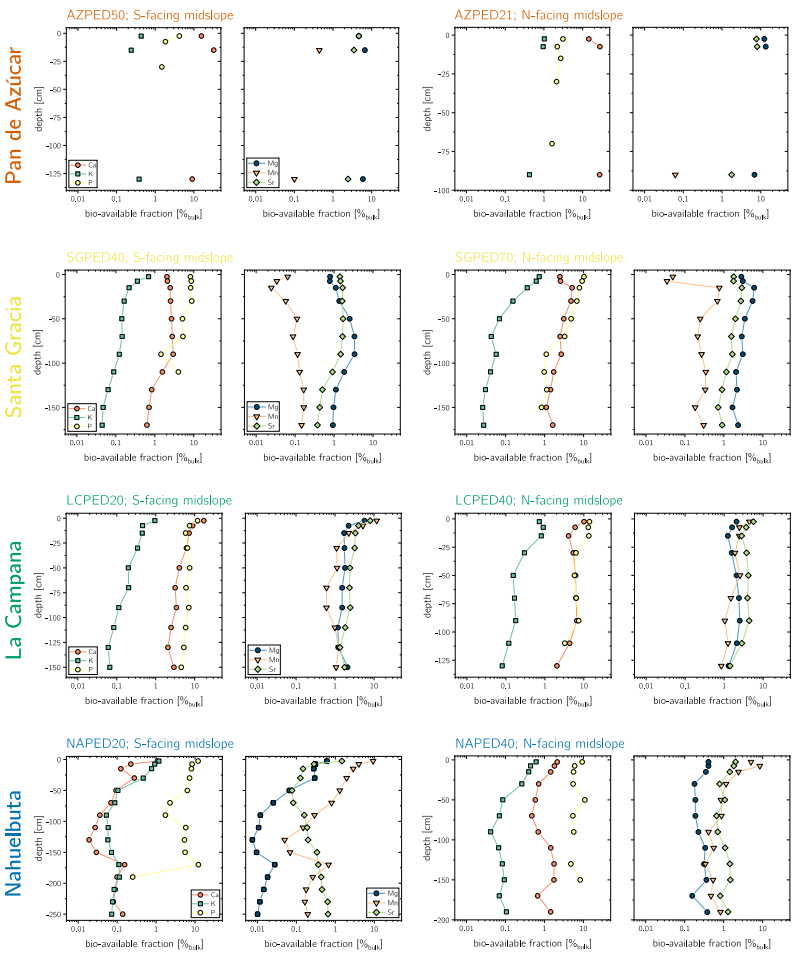

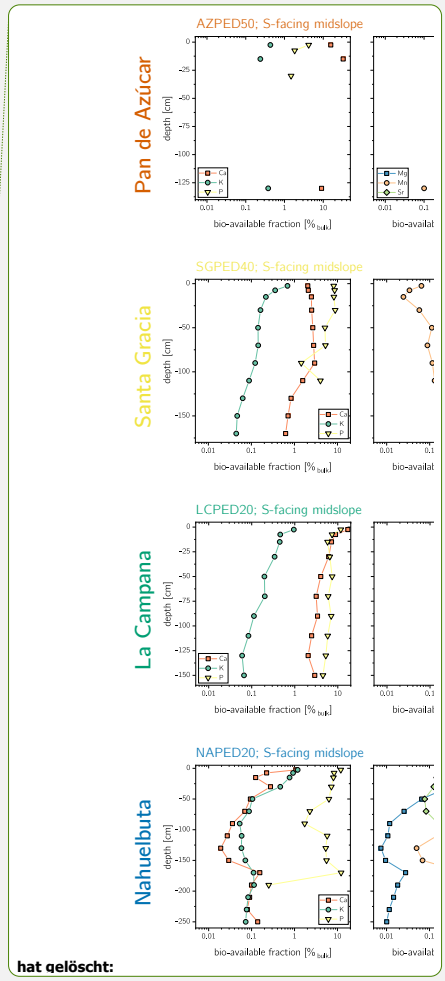

hat gelöscht:

Figure A3. Depth distribution of the sequentially extracted bio-available fraction of plant-essential elements relative to their respective amount contained in bulk regolith including Sr, comprised of the water soluble (18 MΩ Milli-Q H_2O) and the exchangeable (1 M NH_4OAc) fraction. P-accessibility in the bio-available fraction has been determined by Brucker and Spohn (2019) using a modified Hedley sequential P fractionation method. Note that in Pan de Azúcar the acquisition of the bio-available fraction was only possible on three samples per site. Data gaps do occur if both extractions of one sample were below limit of detection.

hat gelöscht: samples at Pan de Azúcar, Santa Gracia, La Campana, and Nahuelbuta.

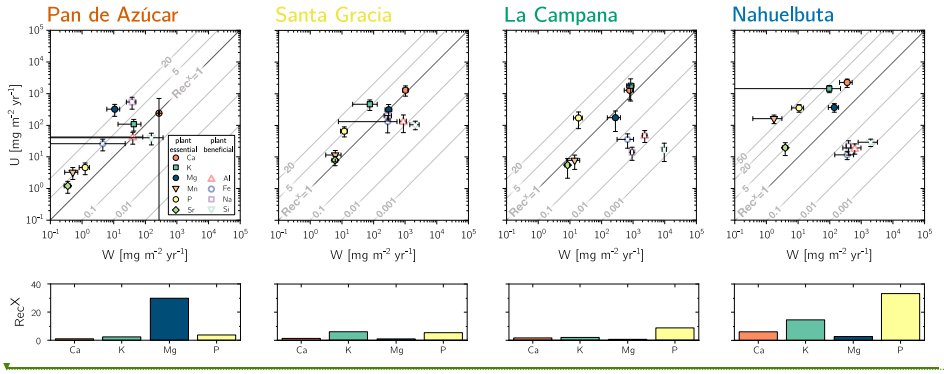

Figure A4. Chemical weathering flux ($W^X_{regolith}$) and ecosystem nutrient-uptake fluxes (U^X_{total}) for Pan de Azúcar, Santa Gracia, La Campana, and Nahuelbuta (from left to right) for plant-essential (closed symbols) and plant-beneficial elements (open symbols). Weathering-release fluxes for Ca, K, Mg, Na, and Sr in Pan de Azúcar have been complemented by atmospheric depositional fluxes such that the total amount of available nutrients increase by 95, 22, 18, 12, and 10%, respectively. Grey contour lines emphasize the nutrient recycling factor (Rec^X), which is the ratio of U^X_{total} to $W^X_{regolith}$. Uncertainty bars show 1SD. Differences in nutrient recycling factors for the plant essential elements Ca, K, Mg, and P among the four study sites are highlighted in the lower panels.

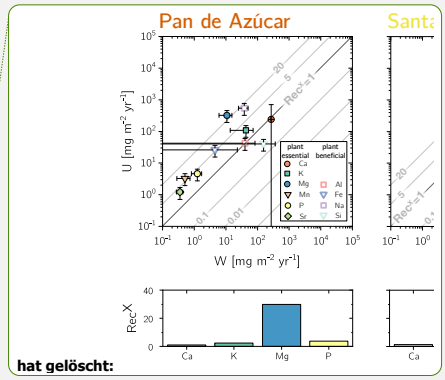

hat gelöscht:

16 Tables

hat gelöscht: 15

Table 1 Characteristics of the four EarthShape study sites and soil profile names in Pan de Azúcar, Santa Gracia, La Campana, and Nahuelbuta.

		Pan de Azúcar		Santa Gracia		La Campana		Nahuelbua		
		AZPED21	*AZPED50*	*SGPED70*	*SGPED40*	*LCPED40*	*LCPED20*	*NAPED40*	*NAPED20*	*Reference*
Latitude		26.1093 S	26.1102 S	29.7612 S	29.7574 S	32.9573 S	32.9559 S	37.8090 S	37.8077 S	†
Longitude		70.5491 W	70.5493 W	71.1656 W	71.1664 W	71.0643 W	71.0635 W	73.0138 W	73.0135 W	†
Altitude	[m a.s.l.]	343	330	690	682	734	730	1219	1239	*
Slope	[°]	25	40	15	25	12	23	13	15	‡
Aspect		N-facing	S-facing	N-facing	S-facing	N-facing	S-facing	N-facing	S-facing	†, ‡
Mean annual temperature (MAT)	[°C]	18.1		16.1		14.9		14.1		§
Mean annual precipitation (MAP)	[mm yr^{-1}]	10		87		436		1084		§
Lithology		granite		diorite		granodiorite		granodiorite		†
Mineralogy*	[Vol%]	Quartz xxx, Plagioclase x, K-feldspar xxx, Pyroxene -, Biotite x, Amphibole -		Quartz x, Plagioclase xx, K-feldspar xxx, Pyroxene xx, Biotite -, Amphibole x		Quartz xx, Plagioclase x, K-feldspar xxx, Pyroxene -, Biotite x, Amphibole -		Quartz xx, Plagioclase xx, K-feldspar xxx, Pyroxene x, Biotite x, Amphibole -		†
Soil type		Regosol	Regosol	Cambisol	Leptosol	Cambisol	Cambisol	umbric Podzol	orthodystric Umbrisol	‡
Soil thickness	[cm]	20	20	35	45	35	60	60	70	†
Soil pH**		8.1 ± 0.1	8.1 ± 0.1	6.0 ± 0.3	6.1 ± 0.3	5.2 ± 0.3	5.0 ± 0.3	4.7 ± 0.1	4.3 ± 0.2	‡
Cation exchange capacity (CEC)**	[µmole g^{-1}]	-	-	108.5 ± 50.2	64.6 ± 23.4	86.4 ± 43.1	72.7 ± 62.1	21.0 ± 15.4	38.2 ± 24.7	‡
Catchment-wide denudation rate (D)	[t km^{-2} yr^{-1}]	7.7 ± 0.7		9.2 ± 0.8		200 ± 22		27.2 ± 2.4		‖
Soil denudation rate (D_{soil})	[t km^{-2} yr^{-1}]	8.2 ± 0.5	11.0 ± 0.7	15.9 ± 0.9	22.4 ± 1.5	69.2 ± 4.6	53.7 ± 3.4	17.7 ± 1.1	47.5 ± 3.0	†, #
Soil weathering rate (W)	[t km^{-2} yr^{-1}]	-1.0 ± 0.1***	0.9 ± 0.2	7.2 ± 4.7	11.9 ± 7.6	45.9 ± 8.0	20.0 ± 3.1	3.5 ± 0.9	7.5 ± 3.1	†, #
Soil erosion rate (E)	[t km^{-2} yr^{-1}]	9.1 ± 0.5	10.1 ± 0.7	8.7 ± 4.8	10.5 ± 7.7	23.4 ± 9.2	33.8 ± 4.6	14.2 ± 1.4	40.0 ± 4.3	†, #
Chemical depletion fraction (CDF)		-0.1 ± 0.0	0.1 ± 0.0	0.5 ± 0.3	0.5 ± 0.3	0.7 ± 0.1	0.4 ± 0.1	0.2 ± 0.1	0.2 ± 0.1	†, #
Vegetation cover	[%]	<5		30 – 40		95		100		‡
Vegetation types		*Cristaria integerrima, Nolana mollis, Perityle* sp., *Stipa plumosa, Tetragonia maritima*		*Adesmia* sp., *Cordia decandra, Cumulopuntia sphaerica, Eulychnia acida, Proustia cuneifolia, Senna cumingii*		*Aristeguietia salvia, Colliguaja odorifera, Cryptocarya alba, Jubaea chilensis, Lithraea caustica*		*Araucaria araucana, Chusquea culeou, Nothofagus antarctica*		‡
Net primary production (NPP)	[g_C m^{-2} yr^{-1}]	30 ± 10		150 ± 40		280 ± 50		520 ± 130		¶

* Estimation of mineral abundances based on thin section microscopy: -: absence, x: presence (<10 Vol%), xx: abundant (10-35 Vol%), xxx: very abundant (>35 Vol%)

** Denoting to regolith-profile averages

*** N-facing slope in Pan de Azúcar yield negative CDF and hence weathering rates due to the input of seaspray

† Oeser et al. (2018); ‡ Bernhard et al. (2018); § Ministerio de Obras Públicas (2017); ‖ van Dongen et al. (2019); # Schaller et al. (2018); ¶ Werner et al. (2018)

Table 2 Glossary of metrics for the parameterization of the geogenic nutrient pathway and organic nutrient cycle in terrestrial ecosystems after Uhlig and von Blanckenburg (2019).

Total mass fluxes (in e.g. t km^{-2} yr^{-1})		
Eq. (1)	$D = E + W$	denudation rate; the sum of chemical weathering and physical erosion
	E	physical erosion; physical removal of primary and secondary minerals along with biogenic material
Eq. (2)	$W = D \times CDF$	chemical weathering rate; net-chemical release flux from minerals as some fraction of which is being incorporated into secondary minerals and pedogenic (hydr-)oxides
	GPP	gross primary production; gross carbon input into biomass
	NPP	net primary productivity; net-carbon fixation by biomass
Elemental fluxes (in e.g. mg m^2 yr^{-1})		
Eq. (3)	$W^X_{regolith} = D \times [X]_{parent} \times (-\tau^X_{Xi})$	Chemical weathering flux of element X; release flux of X from minerals minus the flux of incorporation of X into secondary minerals and oxides
Eq. (4)	$U^X_{total} = \frac{NPP \times [X]_{plant}}{[C]_{plant}}$	Total nutrient uptake flux of element X; uptake of X by trees at the ecosystem scale, where $[C]_{plant}$ denotes the carbon concentration in dry mass, typically 50 weight%
	Dep^X_{dry}	Atmospheric dry deposition of element X
	Dep^X_{wet}	Atmospheric wet deposition of element X as rainfall
Elemental mass fractions and flux ratios (dimensionless)		
Eq. (5)	$CDF = 1 - \frac{[X_i]_{parent}}{[X_i]_{weathered}}$	chemical depletion fraction; fractional mass loss by dissolution of elements from the regolith
Eq. (6)	$\tau^X = \frac{[X]_{weathered}}{[X]_{parent}} \times \frac{[X_i]_{parent}}{[X_i]_{weathered}} - 1$	elemental mass transfer coefficient; elemental loss or gain relative to unweathered bedrock
Eq. (7)	$Rec^X = \frac{U^X_{total}}{W^X_{regolith}}$	nutrient recycling factor; number of times, element X is re-utilized from plant litter after its initial release from rock weathering
Elemental inventories (in e.g. g m^{-2} or kg m^{-2})		
Eq. (8)	$I_j = \int_{z=a}^{z=b} [X_j] \times \rho \, dz$	Inventory of element X in compartment j
	$I^X_{bio\text{-}av.\ soil}$	Inventory of element X in the bio-available fraction in soil
	$I^X_{bio\text{-}av.\ sap}$	Inventory of element X in the bio-available fraction in saprolite
	I^X_{bulk}	Inventory of element X in bulk regolith
Elemental turnover times (in e.g. yr)		
Eq. (9)	$T^X_{i,j} = \frac{I^X_i}{j}$	Turnover time of element X in compartment i with respect to input or output flux j; the ratio of total stock of element X in i to input or output flux j
	$T^X_{bio\text{-}av,\ U}$	Turnover time of element X in the forest floor with respect to uptake into trees; mean time a nutrient rest in the forest floor before re-utilization by forest trees
	$T^X_{bio\text{-}av,\ W}$	Turnover time of element X in the bio-available fraction in regolith with respect to adsorption onto clay minerals; mean time over which the inventory of the bio-available fraction is replenished by chemical silicate weathering in the absence of other gains or losses

hat gelöscht: τ_X

Table 3 Elemental weathering fluxes ($W^{X}_{regolith}$) and ecosystem nutrient uptake fluxes (U^{X}_{total}) in Pan de Azúcar, Santa Gracia, La Campana, and Nahuelbuta along with the respective study site's average soil denudation rate (D) and net primary productivity (NPP).

Study site	D [t km^{-2} yr^{-1}]	NPP [g$_C$ m^{-2} yr^{-1}]	Al	Ca	Fe	K	Mg	Mn	Na	P	Si	Sr
			[mg m^{-2} yr^{-1}]									
Pan de Azúcar												
$W^{X}_{regolith}$	9.6		40	13*	5	30	9	0.5	33	1.3	160	0.3
SD	*0.6*		*43*	*9*	*18*	*30*	*5*	*0.2*	*13*	*0.4*	*210*	*0.1*
U^{X}_{total}	-	30	40	200	30	110	300	3	500	5	40	1.2
SD	-	*10*	*20*	*500*	*10*	*40*	*100*	*1*	*200*	*2*	*20*	*0.5*
Santa Gracia												
$W^{X}_{regolith}$	19.2		870	1030	280	80	300	6	290	12	2100	6.1
SD	*1.2*		*200*	*200*	*270*	*50*	*70*	*3*	*80*	*3*	*680*	*1.3*
U^{X}_{total}	-	150	140	1300	130	500	300	12	200	70	100	8
SD	-	*40*	*80*	*500*	*70*	*200*	*100*	*5*	*60*	*20*	*30*	*3*
La Campana												
$W^{X}_{regolith}$	61.5		2330	770	670	840	280	14	930	19	9700	8.5
SD	*4.0*		*370*	*250*	*350*	*220*	*120*	*6*	*110*	*6*	*1500*	*1.5*
U^{X}_{total}	-	280	50	1300	40	2000	200	8	14	170	17	6
SD	-	*50*	*20*	*600*	*20*	*1000*	*100*	*4*	*6*	*90*	*10*	*3*
Nahuelbuta												
$W^{X}_{regolith}$	32.6		620	360	360	100	140	1	400	11	2000	4.0
SD	*2.1*		*360*	*150*	*210*	*120*	*50*	*3*	*70*	*4*	*1200*	*0.7*
U^{X}_{total}	-	520	19	2200	12	1400	400	160	22	350	30	19
SD	-	*130*	*7*	*700*	*3*	*400*	*100*	*50*	*11*	*100*	*10*	*9*

* $W^{X}_{regolith}$ only includes information from AZPED21 (N-facing slope regolith profile) as atmospheric deposition of Ca in the S-facing slope led to (theoretically) negative weathering fluxes.

Uncertainties on weathering fluxes are estimated by Monte-Carlo simulations, where the SD of the respective profile's denudation rate, the SD of the bedrocks' element concentration of interest, and 3% relative uncertainty on the element concentration in regolith samples have been used.

Uncertainties on nutrient uptake fluxes are estimated by Monte-Carlo simulations, where the SD of the respective study site's net primary productivity (NPP) and the SD of the chemical composition of the weighted above-ground living ecosystem have been used (Table 5)

Table 4 Inventories of plant-essential and plant-beneficial elements in bulk regolith and the bio-available fraction in soil and saprolite. Apart from phosphorus, the accessibility of these elements was determined using a sequential extraction method described by Arunachalam et al. (1996); Tessier et al. (1979); He et al. (1995). P-accessibility in the bio-available fraction has been determined by Brucker and Spohn (2019) using a modified Hedley sequential P fractionation method. Supplementary Tables S3 & S4 include depth-dependent concentration of the bio-available fraction (pooled) and the Milli-Q and NH4OAc extractions used for calculation of the inventories (Oeser and von Blanckenburg, 2020).

Study site		Extent* [m]	Al	Ca	Fe	K	Mg	Mn	Na	P	Si	Sr	Σ
Pan de Azúcar													
$I^X_{bio\text{-}av,\ soil}$	[g m^{-2}]	0.2	0.3	1440	n.c.	53	92	0.1	493	3.3	19	1.5	2100
$I^X_{bio\text{-}av,\ sap}$	[g m^{-2}]	1.0	1.7	3833	n.c.	253	244	0.6	682	0.0	75	3.5	5100
I^X_{bulk}	[kg m^{-2}]	1.0	136	21	44	65	8.6	0.5	39	1.3	636	0.2	950
Santa Gracia													
$I^X_{bio\text{-}av,\ soil}$	[g m^{-2}]	0.4	12	616	7.2	38	221	1.4	18	22	19	4.6	960
$I^X_{bio\text{-}av,\ sap}$	[g m^{-2}]	1.0	23	1179	21	23	651	2.9	159	21	53	8.5	2100
I^X_{bulk}	[kg m^{-2}]	1.0	183	130	75	29	42	1.5	61	1.6	532	1.0	1100
La Campana													
$I^X_{bio\text{-}av,\ soil}$	[g m^{-2}]	0.5	37	673	24	90	79	11	6.7	28	34	4.5	1000
$I^X_{bio\text{-}av,\ sap}$	[g m^{-2}]	1.0	51	1026	23	70	191	12	31	39	142	8.0	1600
I^X_{bulk}	[kg m^{-2}]	1.0	118	26	49	46	10	0.9	31	0.7	456	0.3	740
Nahuelbuta													
$I^X_{bio\text{-}av,\ soil}$	[g m^{-2}]	0.9	14	60	1.8	39	9.9	15	17	31	14	0.5	200
$I^X_{bio\text{-}av,\ sap}$	[g m^{-2}]	1.0	1.5	52	< 0.5	19	11	3.9	13	23	12	0.8	140
I^X_{bulk}	[kg m^{-2}]	1.0	95	15	47	22	13	1.0	10	0.7	309	0.1	510

$I^X_{bio\text{-}av,\ soil}$ = inventory of element X in the soil bio-available fraction; extent amounts to maximum soil depth

$I^X_{bio\text{-}av,\ sap}$ = inventory of element X in the saprolite bio-available fraction;

I^X_{bulk} = inventory of element X in bulk regolith

* the extent of the saprolite and regolith inventory have been scaled to 1.0 m for purposes of comparisons between the four study sites and the lack of an absolute measure of the depth of saprolite.

n.c. = not calculated as the respective bio-available fraction (Table S4) was below the limit of calibration of ICP-OES measurements

hat gelöscht: $I^X_{bio\text{-}av,\ soil}$
hat gelöscht: $I^X_{bio\text{-}av,\ sap}$
hat gelöscht: I^X_{bulk}
hat gelöscht: $I^X_{bio\text{-}av,\ soil}$
hat gelöscht: $I^X_{bio\text{-}av,\ sap}$
hat gelöscht: I^X_{bulk}
hat gelöscht: $I^X_{bio\text{-}av,\ soil}$
hat gelöscht: $I^X_{bio\text{-}av,\ sap}$
hat gelöscht: I^X_{bulk}
hat gelöscht: $I^X_{bio\text{-}av,\ soil}$
hat gelöscht: $I^X_{bio\text{-}av,\ sap}$
hat gelöscht: I^X_{bulk}

765 **Table 5 Chemical composition of the above ground living plants. Plant organs have been weighted according to Niklas and Enquist (2002), using the plant organs' relative growth rate (see Appendix A). Relative growth rates and relative abundance of the different plant species can be found in this table's footnotes. The unweighted chemical composition of each plant organ is listed in Table S5 (Oeser and von Blanckenburg, 2020).**

Study site	Al	Ca	Fe	K	Mg	Mn	Na	P	Si	Sr
					[µg g^{-1}]					
Pan de Azúcar[†]										
mean	2700	15200	1700	6900	20700	210	34600	290	2500	80
SD	*300*	*1500*	*200*	*700*	*2100*	*20*	*3500*	*30*	*300*	*10*
Santa Gracia[‡]										
mean	1880	17800	1800	6400	4200	160	2800	900	1400	110
SD	*920*	*4400*	*900*	*1600*	*1700*	*50*	*500*	*220*	*300*	*20*
SE (n=15)	*650*	*2900*	*600*	*1100*	*1000*	*30*	*400*	*140*	*200*	*20*
La Campana[§]										
mean	340	8900	250	12300	1200	50	100	1200	120	40
SD	*120*	*4100*	*110*	*8000*	*700*	*20*	*40*	*600*	*70*	*20*
SE (n=16)	*70*	*2300*	*70*	*5300*	*400*	*20*	*20*	*400*	*40*	*10*
Nahuelbuta[¶]										
mean	70	8500	40	5400	1400	610	80	1300	110	70
SD	*20*	*1400*	*10*	*500*	*250*	*110*	*30*	*200*	*10*	*30*
SE (n=10)	*10*	*1000*	*10*	*300*	*180*	*80*	*20*	*100*	*10*	*20*

Standard deviation and standard error relate to the variability within the data set of each ecosystem. Where natural replicates were not available (i.e. in Pan de Azúcar), 10% relative uncertainty has been assumed.

[†] Pan de Azúcar ecosystem composition: 100% Nolona mollis; 32% and 68% relative leaf and stem growth, respectively, accounting for 5% leaf and 95% stem standing biomass

[‡] Santa Gracia ecosystem composition: 25% each of Asterasia sp., Cordia decandra, Cumulopuntia sphaerica, Proustia cuneifolia; 32% and 68% relative leaf and stem growth assumed for all species, respectively, accounting for 5% leaf and 95% stem standing biomass

[§] La Campana ecosystem composition: 5% each for Aristeguieta salvia and Colliguaja odorifera and 45% each for Cryptocaria alba and Lithraea caustica; 32% and 68% relative leaf and stem growth assumed for all species, respectively, accounting for 5% leaf and 95% stem standing biomass

[¶] Nahuelbuta ecosystem composition: 60% Araucaria araucana, 10% Chusquea culeou, and 30% Nothofagus antarctica; 48% and 52% relative leaf and stem growth assumed for Araucaria araucana, respectively, accounting for 16% leaf and 84% stem standing biomass, 32% and 68% relative leaf and stem growth assumed for Chusquea culeou and Nothofagus antarctica, respectively, accounting for 5% leaf and 95% stem standing biomass.

hat gelöscht: Niklas and Enquist (2002), using the plant organs' relative growth rate (see Appendix A).

Table 6 Average $^{87}Sr/^{86}Sr$ ratio for bulk bedrock, bulk regolith, and the bio-available fraction in saprolite and soil. $^{87}Sr/^{86}Sr$ in bulk plants are weighted by the plant organs' relative growth rate and relative species abundance in the respective ecosystem (see Table 5). Radiogenic Sr composition for each single specimen are reported in Tables S2 (bulk regolith samples), S3 (bio-available fraction of saprolite and soil), and S5 (plant samples), respectively (Oeser and von Blanckenburg, 2020).

	bulk samples		bio-available samples		bulk living plants†	Seaspray input‡
	$^{87}Sr/^{86}Sr_{rock}$	$^{87}Sr/^{86}Sr_{regolith}$	$^{87}Sr/^{86}Sr_{sap}$	$^{87}Sr/^{86}Sr_{soil}$	$^{87}Sr/^{86}Sr_{plant}$	
		h				
Pan de Azúcar	0.7257	0.7305	0.7108	0.7099	0.7099	93%
SD	*0.0020*	*0.0036*	*0.0009*	*0.0007*		
Santa Gracia	0.7039	0.7044	0.7062	0.7062	0.7062	43%
SD	*0.0004*	*0.0003*	*0.0001*	*0.0001*	*0.0003*	
La Campana	0.7063	0.7053	0.7051	0.7053	0.7059	
SD	*0.0003*	*0.0002*	*0.0004*	*0.0005*	*0.0002*	
Nahuelbuta	0.7161	0.7162	0.7115	0.7111	0.7111	
SD	*0.0065*	*0.0036*	*0.0025*	*0.0023*	*0.0016*	
Seaspray*				0.7092		

* Seaspray composition from Pearce et al. (2015)

† Standard deviation corresponds to species-to-species differences in $^{87}Sr/^{86}Sr$

‡ Potential seaspray input into the bio-available fraction derived from a simple two-component mixing equation using bulk bedrock and seaspray as end-members. Substantial seaspray incorporation into the bio-available fraction in La Campana and Nahuelbuta is very unlikely (see text for discussion), therefore not shown.

775

Table 7 Nutrient recycling factors in Pan de Azúcar, Santa Gracia, La Campana, and Nahuelbuta. Shown in brackets are the Rec^X prior correction for atmospheric deposition.

	Rec^{Al}	Rec^{Ca}	Rec^{Fe}	Rec^{K}	Rec^{Mg}	Rec^{Mn}	Rec^{Na}	Rec^{P}	Rec^{Si}	Rec^{Sr}
Pan de Azúcar	1.1	1 (19)*	5.8	3 (3)*	30 (36)*	6	15 (16)*	4	0.26	3 (4)*
SD	*0.4*	*2*	*0.6*	*1*	*20*	*6*	*15*	*4*	*0.08*	*5*
Santa Gracia	0.1	1	0.4	6	1	1	1	5	0.04	1
SD	*0.5*	*4*	*0.5*	*3*	*3*	*3*	*1*	*13*	*0.07*	*3*
La Campana	0	2	0.1	2	1	0.5	0	9	0	1
SD	*0.1*	*2*	*0*	*5*	*1*	*0.6*	*0.1*	*15*	*0.01*	*2*
Nahuelbuta	0	6	0	15	3	190†	0.1	30	0.01	5
SD	*0*	*4*	*0*	*3*	*2*	*70*	*0.2*	*20*	*0.01*	*12*

* Rec^X in Pan de Azúcar has been corrected for atmospheric deposition of seaspray, ultimately decreases the recycling rates of weathering-derived nutrients by 95, 22, 18, 12, and 10% for Ca, K, Mg, Na, and Sr, respectively (see supporting information for further explanation and Fig. A6).

† values not being considered in the discussion as $W^{Mn}_{regolith}$ is potentially biased by high bedrock heterogeneities

780

Table 8 Turnover times for the soil and saprolite bio-available fraction with respect to the release by weathering and turnover times for bio-available fraction in soil with respect to uptake into plants.

study site	Al	Ca	Fe	K	Mg	Mn [yr]	Na	P	Si	Sr
Pan de Azúcar										
$T^X_{bio-av.soil,U}$	10	6040	0	490	280	40	910	710	480	1250
$T^X_{bio-av.soil,W}$	10	n.d.	0	1590	10300	280	14800	2570	120	4670
$T^X_{bio-av.sap,W}$	40	n.d.	0	7570	27400	1240	20400	n.d.	490	10870
Santa Gracia										
$T^X_{bio-av.soil,U}$	90	480	50	80	710	120	90	330	180	590
$T^X_{bio-av.soil,W}$	10	600	30	510	730	230	60	1850	10	760
$T^X_{bio-av.sap,W}$	30	1150	80	300	2160	470	540	1760	30	1400
La Campana										
$T^X_{bio-av.soil,U}$	780	530	660	50	460	1420	480	160	1970	820
$T^X_{bio-av.soil,W}$	20	870	40	110	290	770	10	1470	3	530
$T^X_{bio-av.sap,W}$	20	1330	30	80	690	830	30	2050	10	950
Nahuelbuta										
$T^X_{bio-av.soil,U}$	760	30	160	30	30	90	790	90	490	20
$T^X_{bio-av.soil,W}$	20	170	10	400	70	17400	40	2900	10	120
$T^X_{bio-av.sap,W}$	0	150	0	190	80	4750	30	2130	10	210

$T^X_{bio-av.soil,U}$ = turnover time of element X in the soil bio-available fraction with respect to uptake into the ecosystem

$T^X_{bio-av.soil,W}$ = turnover time of element X in the soil bio-available fraction with respect to supply from dissolution of primary minerals and secondary precipitates

$T^X_{bio-av.sap,W}$ = turnover time of element X in the saprolite bio-available fraction with respect to supply from dissolution of primary minerals and secondary precipitates

n.d. = not determined; not determined turnover times because the respective inventory (Table 4) could not be determined

hat gelöscht: $T^X_{bioav,\ soil,\ U}$
hat gelöscht: $T^X_{bioav,\ soil,\ W}$
hat gelöscht: $T^X_{bioav,\ sap.,\ W}$
hat gelöscht: $T^X_{bioav,\ soil,\ U}$
hat gelöscht: $T^X_{bioav,\ soil,\ W}$
hat gelöscht: $T^X_{bioav,\ sap.,\ W}$
hat gelöscht: $T^X_{bioav,\ soil,\ U}$
hat gelöscht: $T^X_{bioav,\ soil,\ W}$
hat gelöscht: $T^X_{bioav,\ sap.,\ W}$
hat gelöscht: $T^X_{bioav,\ soil,\ U}$
hat gelöscht: $T^X_{bioav,\ soil,\ W}$
hat gelöscht: $T^X_{bioav,\ sap.,\ W}$

Table A1 Correlation matrix with Pearson's correlation coefficients and significance (: p < 0.01, *: p < 0.05) for net primary productivity (NPP), denudation rate (D), mean annual precipitation (MAP), and indices of total and elemental degree and rate of weathering. Correlation coefficients involve the entire EarthShape study area.**

	D	MAP	NPP	CDF	W	$W^{Ca}_{regolith}$	$W^{K}_{regolith}$	$W^{Na}_{regolith}$	$W^{P}_{regolith}$	$W^{Si}_{regolith}$	τ^{Ca}	τ^{K}	τ^{Na}	τ^{P}	τ^{Si}
D		0.40	**0.48***	0.56	**0.88****	0.44	**0.83****	**0.95****	**0.87****	**0.88****	0.35	**0.72****	**0.60***	0.24	**0.59***
MAP			**0.98****	-0.16	0.06	-0.09	0.08	0.31	0.30	0.13	0.29	0.11	**0.66***	0.21	-0.06
NPP				0.01	0.16	0.09	0.15	0.40	0.43	0.21	0.45	0.19	**0.76****	0.36	0.10

CDF = chemical depletion fraction; W = soil weathering rate; $W^{X}_{regolith}$ = elemental weathering flux; τ^{X} = elemental mass transfer coefficient

Note that because CDF and τ^{X} are per definition different in sign (i.e. a CDF of +1 denote entire depletion, whereas a τ^{X} of -1 denote entire depletion), τ^{X} was multiplied by -1 for presentation purposes.

Table A2 Correlation matrix with Pearson's correlation coefficients and significance (: p < 0.01, *: p < 0.05) for net primary productivity (NPP), denudation rate (D), mean annual precipitation (MAP), and indices of total and elemental degree and rate of weathering. Correlation coefficients involve the study sites Pan de Azúcar, Santa Gracia, and Nahuelbuta. La Campana has been excluded because it features the steepest relief of all sites which causes elevated denudation rates.**

	D	MAP	NPP	CDF	W	$W^{Ca}_{regolith}$	$W^{K}_{regolith}$	$W^{Na}_{regolith}$	$W^{P}_{regolith}$	$W^{Si}_{regolith}$	τ^{Ca}	τ^{K}	τ^{Na}	τ^{P}	τ^{Si}
D		**0.74***	**0.78***	0.05	**0.51***	0.29	**0.59***	**0.94****	**0.76***	**0.80***	0.40	0.14	0.66	0.29	0.19
MAP			**0.99****	-0.24	0.09	-0.11	0.47	**0.67***	0.43	0.44	0.29	0.18	**0.73***	0.22	-0.11
NPP				-0.07	0.25	0.05	0.53	**0.76***	**0.56***	**0.56***	0.45	0.27	**0.83****	0.37	0.06

CDF = chemical depletion fraction; W = soil weathering rate; $W^{X}_{regolith}$ = elemental weathering flux; τ^{X} = elemental mass transfer coefficient

Note that because CDF and τ^{X} are per definition different in sign (i.e. a CDF of +1 denote entire depletion, whereas a τ^{X} of -1 denote entire depletion), τ^{X} was multiplied by -1 for presentation purposes.

Table A3 ANOVAs evaluating variations in denudation rate (D), the chemical depletion fraction (CDF), soil weathering rate (W), and the elemental weathering rates for Ca, K, Na, P, and Si ($W^{Ca}_{regolith}$, $W^{K}_{regolith}$, $W^{Na}_{regolith}$, $W^{P}_{regolith}$, $W^{Si}_{regolith}$) among sites. The Tukey HSD test for site comparison is shown below. Sig = 1 indicates significant differences between the sites. The comparison between Santa Gracia and Nahuelbuta is highlighted in bold because of their importance in the discussion.

		D		*CDF*		*W*		$W^{Ca}_{regolith}$		$W^{K}_{regolith}$		$W^{Na}_{regolith}$		$W^{P}_{regolith}$		$W^{Si}_{regolith}$	
		F ratio	***p > F***	***F ratio***	***p > F***	***F ratio***	***p > F***	***F ratio***	***p > F***	***F ratio***	***p > F***	***F ratio***	***p > F***	***F value***	***p > F***	***F value***	***p > F***
Homogeneity of variance		*1.96*	*0.20*	*2.90*	*0.10*	*3.08*	*0.09*	*1.52*	*0.28*	*3.51*	*0.07*	*2.37*	*0.15*	*1.38*	*0.32*	*1.38*	*0.32*
Overall ANOVA		*20.75*	*0.00*	*24.22*	*0.00*	*13.74*	*0.00*	*23.59*	*0.00*	*6.67*	*0.01*	*10.88*	*0.00*	*10.57*	*0.00*	*10.57*	*0.00*
Site 1	**Site 2**	***p value***	***Sig***	***p value***	***Sig***	***p value***	***Sig***	***p value***	***Sig***	***p value***	***Sig***	***p value***	***Sig***	***p value***	***Sig***	***p value***	***Sig***
Santa Gracia	Pan de Azúcar	0.55	0	0.00	1	0.44	0	0.00	1	1.00	0	0.43	0	0.04	1	0.04	1
La Campana	Pan de Azúcar	0.00	1	0.00	1	0.00	1	0.00	1	0.02	1	0.00	1	0.00	1	0.00	1
La Campana	Santa Gracia	0.00	1	0.98	0	0.01	1	0.28	0	0.03	1	0.02	1	0.20	0	0.20	0
Nahuelbuta	Pan de Azúcar	0.04	1	0.50	0	0.83	0	0.11	0	0.99	0	0.19	0	0.07	0	0.07	0
Nahuelbuta	**Santa Gracia**	**0.29**	**0**	**0.00**	**1**	**0.88**	**0**	**0.00**	**1**	**1.00**	**0**	**0.91**	**0**	**0.98**	**0**	**0.98**	**0**
Nahuelbuta	La Campana	0.01	1	0.00	1	0.00	1	0.05	0	0.03	1	0.04	1	0.12	0	0.12	0

F ratio = ratio of two mean square values.
P value ≤ 0.05 = Populations have significant different mean values
Sig = significance; 0: not significant, 1: significant

Seite 5: [1] hat gelöscht	**author**	**25.06.20 11:47:00**
Seite 16: [2] hat gelöscht	**author**	**25.06.20 11:47:00**
Seite 19: [3] hat gelöscht	**author**	**25.06.20 11:47:00**
Seite 20: [4] hat gelöscht	**author**	**25.06.20 11:47:00**
Seite 23: [5] hat gelöscht	**author**	**25.06.20 11:47:00**
Seite 23: [6] hat gelöscht	**author**	**25.06.20 11:47:00**
Seite 28: [7] hat gelöscht	**author**	**25.06.20 11:47:00**
Seite 28: [8] hat gelöscht	**author**	**25.06.20 11:47:00**
Seite 28: [9] hat gelöscht	**author**	**25.06.20 11:47:00**
Seite 45: [10] hat gelöscht	**author**	**25.06.20 11:47:00**